Investigating Pharmaceutical 3D Printing: From Process Assessment to Product Characteristics

Dissertation

der Mathematisch-Naturwissenschaftlichen Fakultät

der Eberhard Karls Universität Tübingen

zur Erlangung des Grades eines

Doktors der Naturwissenschaften

(Dr. rer. nat.)

vorgelegt von

Thomas Rainer Pflieger

aus Straubing

Tübingen

2024

Gedruckt mit Genehmigung der Mathematisch-Naturwissenschaftlichen Fakultät der Eberhard Karls Universität Tübingen.

Tag der mündlichen Qualifikation:	31.10.2024
Dekan:	Prof. Dr. Thilo Stehle
1. Berichterstatter/-in:	Prof. Dr. Dominique Lunter
2. Berichterstatter/-in:	Prof. Dr. Stefan Laufer
3. Berichterstatter/-in:	Prof. Dr. Karl Wagner

Acknowledgements

First and foremost, I want to express my heartfelt gratitude to my supervisor, Prof. Dr. Dominique Jasmin Lunter, for granting me the invaluable opportunity to undertake this dissertation. I am sincerely thankful for her generous investment of time and effort in guiding me through this endeavor. I am fortunate to have received unwavering respect, encouragement, and support from her. I am deeply indebted to her for her boundless patience in proofreading my publications and posters, as well as for acquainting me with suitable methodologies. Moreover, she has played a crucial role in bolstering my confidence and expanding my knowledge base, for which I am immensely grateful.

My sincere appreciation also goes to Prof. Dr. Stefan Laufer, my second supervisor, for his guidance, his always respectful treatment of me and constructive feedback throughout this journey. His insightful recommendations and engaging discussions during progress reports have been instrumental in shaping this work. Additionally, I am grateful for his support in revising and evaluating this dissertation.

Furthermore, I would like to express my gratitude to *DiHeSys Digital Health Systems*, my company, and all the colleagues who have accompanied me over the years. I am appreciative of the time spent together in the lab, at conferences, and during social activities. On top of that, I am thankful not only for the financial support provided by the company, but also for the access to the infrastructure that facilitated my work. Special recognition goes to my direct mentors, Dr. Markus Dachtler, Prof. Dr. Gerald Huber, and especially Dr. Rakesh Venkatesh, for their steady support. Their guidance has set me on the right path, involving me in collaborative projects and international scientific programs, and offering help both in professional and personal matters during challenging times. I am happy to be able to call my colleagues and people I met friends.

I also wish to thank my current and former colleagues at *Gen-Plus*. Their assistance in familiarizing me with new instruments and sharing their expertise has been invaluable. They were always patient with me and invested their time in helping me realize my goals.

My heartfelt thanks extend to my partner and friend, whose unwavering support and encouragement have been my source of strength throughout these challenging years. Her presence has been a source of comfort and inspiration, and I am profoundly grateful for her unwavering belief in me.

I am deeply grateful to my beloved parents and brother for their constant support and encouragement. Their love and encouragement have been my pillars of strength, and I am truly fortunate to have such a loving and supportive family. This journey would not have been possible without their unwavering emotional support. Their constant belief in me and their sacrifices have been the foundation upon which I have built my success.

Table of contents

Abbreviations III
Zusammenfassung VI
Abstract VIII
List of Publications X
Personal Contribution XI
1. Introduction 1
1.1 Introduction to Personalized Medicine 1
1.2 Benefits of 3D Printed Pharmaceuticals 2
1.2.1 Tailored Doses 2
1.2.2 Tailored Release Profiles 2
1.2.3 Drug Co-Administration 3
1.2.4 Elevated Patient Compliance by Tablet Design 3
1.2.5 Bioavailability Enhancement via Amorphous Solid Dispersions 4
1.3 Challenges of Pharmaceutical 3D Printing 5
1.4 Model Drugs 7
1.4.1 Metoprolol 8
1.4.2 Theophylline 8
1.4.3 Prednisolone 9
1.5 Technological Background of Pharmaceutical 3D Printing 9
1.5.1 Market Review: State-Of-The-Art Technologies 9
1.5.2 The Flexdose™ 3D Printer 12
1.5.2.1 Hardware Setup 12
1.5.2.2 Operation and Software Setup 13
1.5.3 From Granules to 3D Printed Products 13
1.5.3.1 Production Process Flow 13
1.5.3.2 Benefits of Granule Feeding 17
1.6 Analytical Background 18
1.6.1 Thermogravimetric Analysis 18
1.6.1 Differential Scanning Calorimetry 19
1.6.2 Small Amplitude Oscillatory Shear Rheology 20
1.6.3 Tests According to the European Pharmacopoeia 22
1.6.4 In-Vitro Dissolution 23
1.6.5 Quality by Design and Design of Experiments 25
1.6.6 Physiologically Based Pharmacokinetic Modeling 26
1.7 References 28

2. Objectives 38

3. Novel Approach to Pharmaceutical 3D-Printing Omitting the Need for Filament — Investigation of Materials, Process, and Product Characteristics 39

4. Influence of Design Parameters on Sustained Drug Release Properties of 3D-Printed Theophylline Tablets 56

5. An Investigation of the Drug Release Kinetics of 3D-Printed Two Compartment Theophylline and Prednisolone Tablets 68

Abbreviations

%	Percentage
% w/w	Mass concentration expressed by weight per weight
°C	Celsius degree
.gcode	G-code (also RS-274)
1/s	Per second; Herz
3D	Three-dimensional
3DP	Three-dimensional printing
A	Absorbance
ACE	Angiotensin converting enzyme
ADME	Absorption, distribution, metabolism and excretion
AMG	German medicines act; Arzneimittelgesetz
API	Active pharmaceutical ingredient
ARB	Angiotensin II receptor blockers
AV	Acceptance value
BCS	Biopharmaceutics classification system
c	Concentration
C_0	Initial drug concentration
CAD	Computer aided design
CE	Conformité européenne
cm	Centimeter
COPD	Chronic obstructive pulmonary disease
COVID	Corona virus disease
C_p	Heat capacity
CQA	Critical quality attributes
C_R	Reference heat capacity
C_S	Sample heat capacity
C_s	Drug solubility in matrix
CU	Content uniformity
ΔT	Temperature difference
D	Diffusivity
DiHeSys	DiHeSys Digital Health Systems GmbH
DPE	Direct powder extrusion
DSC	Differential scanning calorimetry
EPO	Eudragit® E PO
ε	Molar absorptivity
ERL	Eudragit® RL
η	Dynamic viscosity
η*	Complex viscosity
et al.	Et alia, and others
FDA	Food and drug administration
FDM	Fused deposition modeling
FDP	Flexdose printer
g	Gram
G’	Storage modulus
G’’	Loss modulus
γ_0	Maximum strain amplitude
g/cm^3	Gram per cubic centimeter
GMP	Good manufacturing practice

h	Height
h	Hour
HDAC	Histone deacetylase
HME	Hot-melt extrusion
HPLC	High performance liquid chromatography
HTN	Hypertension
IPC	In-process control
IR	Immediate release
k	Number of factor levels
k	Release rate constant
k_H	Higuchi release constant
KP	Korsmeyer-Peppas
KVA64	Kollidon® VA 64
L	Liter
l	Length
l	Number of Levels
LOD	Limit of detection
LOQ	Limit of quantification
LVR	Linear viscoelastic region
M	Molar
MED	Melt extrusion deposition
min	Minute
mg	Milligram
mL	Milliliter
mm	Millimeter
MSN	Metoprolol Succinate
M_t/M_{max}	Fraction of drug released at timepoint t
MV	Mass variation
n	Number
n	Number of repetitions
n	Diffusion exponent
n_{runs}	Number of experimental runs
NIR	Near infrared
nm	Nanometer
N·m	Newton meter
NTW	Narrow therapeutic window
ω	Angular frequency
p	Number of generators
Pa·s	Pascal seconds
PEG	Polyethylene glycol
Ph. Eur.	European Pharmacopoeia
pH	Negative log of activity of hydrogen ions
p. m.	Physical mixture
PSL	Prednisolone
Q	Heat flow
Q	Amount of drug released at given timepoint by area
QBD	Quality by design
r	Radius
R^2	Coefficient of determination
rad	radian

R_T	Thermal resistance
ρ	Density
r_n	Nozzle outlet radius
rpm	Revolutions per minute
s	Second
SAOS	Small amplitude oscillatory shear
SA/V	Surface area to volume ratio
SLA	Stereolithography
σ	Shear stress
γ	Shear rate
γ_{nw}	Apparent nozzle wall shear rate
SR	Sustained release
SSE	Semi-solid extrusion
t	Time
tan(δ)	Loss factor
T_c	Crystallization temperature
T_g	Glass transition temperature
TGA	Thermogravimetric analysis
TM	Trademark
T_m	Melting point
TPH	Theophylline
USP	United States Pharmacopoeia
UV	Ultraviolet
V	Volume
$\dot{V}$	Volumetric flow rate

Zusammenfassung

In den letzten Jahren konnte sich der pharmazeutische 3D-Druck (3DP) als revolutionäre Technologie für die Entwicklung personalisierter Arzneimittel beweisen. Dieses additive Fertigungsverfahren ermöglicht die Herstellung oraler Darreichungsformen mit maßgeschneiderten Eigenschaften. Ein individualisiertes Anpassen der Freisetzungsverhalten, Formen und Maße einer Tablette ist mit konventionellen Methoden nicht vergleichbar umsetzbar. Im Gegensatz zu konventionellen und generalisierten Behandlungsansätzen birgt das Eingehen auf patientenspezifische Bedürfnisse das Potenzial, die Effektivität, die Adhärenz und folglich die Therapie zu verbessern. Während sich das Feld des pharmazeutischen 3DP stetig weiterentwickelt, werden neue Möglichkeiten für Innovationen in der Pharmaindustrie geschaffen.

Das übergeordnete Ziel dieser Arbeit war es, die Eignung der Technologie 3DP zur Umsetzung personalisierter Therapien im pharmazeutischen Bereich zu erforschen. Dazu wurde eine umfassende Betrachtung durchgeführt, die sowohl die Analyse der grundlegenden wissenschaftlichen Prozesse als auch die Untersuchung von Produkt-Eigenschaften beinhaltete. Einer der Hauptaspekte dieser Arbeit beinhaltete die Anwendung von Oszillationsrheologie (SAOS) zur Evaluierung der Schmelzeigenschaften pharmazeutischer Granulate. Es konnten Korrelationen zwischen der Schmelzviskosität der Granulate und deren Verdruckbarkeit für ein neuartiges 3DP Setup gefunden werden. Die Neuheit liegt dabei im technischen Design des Druckkopfs, da ein mit Granulaten gespeister Einzel-Schnecken-Extruder Druckkopf zur Herstellung der Tabletten verwendet wurde. Die Ergebnisse heben die zentrale Bedeutung der Drucktemperatur für das erfolgreiche Verdrucken einer Formulierung hervor, die aber wiederum durch Prozessparameter, welche die Scherbelastung an der Düse beeinflussen, und den Abbau des Wirkstoffs begrenzt wird. Materialcharakterisierung durch Dynamische Differenzkalorimetrie (DSC) und Thermogravimetrische Analyse (TGA) erlaubten zu verstehen, bei welchen Temperaturen und Formulierungszusammensetzungen thermische Stabilität und Komponenten-Mischbarkeit gegeben sind. Die Gleichförmigkeit einzeldosierter Arzneiformen entsprach außerdem den Standards des Europäischen Arzneibuchs (Ph. Eur.).

Im Anschluss wurde das retardierte Freisetzungsverhalten 3D gedruckter Tabletten mit Theophyllin (TPH), einem Wirkstoff mit enger therapeutischer Breite (NTW), präzise untersucht. Durch einen teil-faktoriellen statistischen Versuchsplan (DOE) nach Taguchi wurden die Designparameter der Tabletten für Prozessstabilität und maßgeschneiderte Dosierungen optimiert. Die Auswertung umfasst dabei statistische Effektgrößen, Signal zu Rausch (S/N) Verhältnisse und faktorbezogene Standardabweichungen (SDs). Die verschiedenen Freisetzungsprofile wurden mit mathematischen Modellen gefittet, um eine Beziehung zwischen gedruckten Dosierungen und verzögerter Wirkstofffreisetzung herzustellen. In vitro-in vivo Korrelation (IVIVC) und physiologisch-basierte pharmakokinetische (PBPK) Simulationen bestätigten die Wirksamkeit der Tabletten für eine beispielhafte Patientenpopulation.

Darüber hinaus wurde untersucht, inwiefern die Technologie des 3DP für die Herstellung personalisierter Kombinationspräparate geeignet ist, indem zweischichtige

Tabletten mit den Wirkstoffen TPH und Prednisolon (PSL) gedruckt wurden. Die Zielsetzung umfasste, die gegenseitige Einflussnahme der einzelnen Tablettenkompartimente auf deren individuelle Wirkstofffreisetzung zu verstehen. Gemäß einem voll faktoriellen statistischen Versuchsdesign wurden verschiedene Kombinationen produziert und ihre Freisetzungsprofile verglichen. Die Ergebnisse zeigten, dass die Addition eines zweiten Kompartiments die verzögerte Freisetzung von TPH nicht signifikant beeinflusste, während die sofortige Freisetzung von PSL beeinflusst wurde, jedoch immer noch die erforderlichen Freisetzungsraten erreichte. Eine Dosisindividualisierung mit dieser Darreichungsform ohne Veränderung der proportionalen Wirkstofffreisetzung konnte bestätigt werden.

Diese Thesis hilft einen weiteren Schritt in Richtung präziser Dosierungen, gezielter Freisetzungsprofile und effektiver Kombinationstherapien durch pharmazeutischen 3DP zu gehen, die auf die individuellen Bedürfnisse der Patienten zugeschnitten werden können.

Abstract

In recent years, pharmaceutical 3D printing (3DP) has emerged as a revolutionary technology with profound importance for personalized drug manufacturing. By employing additive manufacturing principles, this innovative technology enables the production of pharmaceutical oral dosage forms with tailored properties, such as release kinetics, and shapes previously unattainable by conventional methods. Unlike the conventional “one size fits all” approach, the convergence of pharmaceuticals to patient needs holds potential for enhancing drug efficacy, patient compliance, and therefore therapeutic outcomes. As the field continues to advance, pharmaceutical 3DP offers unprecedented opportunities for innovation in the pharmaceutical industry, but also raises new research questions.

The main goal of this thesis was to explore the use of 3DP as a pharmaceutical tool for personalized therapy. This involved a thorough assessment, covering everything from analyzing the fundamental scientific processes to examining the characteristics of the final products. One objective included employing small amplitude shear oscillatory (SAOS) rheology to investigate pharmaceutical granules of two polymers, establishing correlations between polymer viscosity and printability for a novel 3DP setup. The novelty lies in the technical design of the printhead, as granules-fed single screw extrusion was used to produce tablets. The findings highlight the critical importance of the printing temperature for successful printability of a formulation, constrained by process parameters and API decomposition. Material characterization through differential scanning calorimetry (DSC) and thermogravimetric analyses (TGA) helped to understand at which temperatures and formulation compositions thermal stability and component miscibility is given. Uniformity of mass and dosage were tested and conformed to European Pharmacopoeia (Ph. Eur.) standards.

Also, the sustained release properties of 3D printed tablets containing theophylline (TPH), a drug with a narrow therapeutic window (NTW), were precisely explored. Through a Taguchi orthogonal array design of experiments (DOE), tablet design parameters were optimized for process stability and tailored dosages in terms of statistical effect sizes, signal-to-noise ratios (S/N) and factor level related standard deviations (SDs). Release profiles were analyzed with various mathematical models, establishing a predictable relationship between printed doses and sustained drug release kinetics. In-vivo/in-vitro correlation (IVIVC) and physiologically based pharmacokinetic (PBPK) modeling confirmed the tablets' efficacy for a selected patient group.

Additionally, the potential of 3DP for combination therapy, printing bi-layered tablets with the drugs TPH and prednisolone (PSL), was investigated. This study aimed to understand the interaction between separate distinctive tablet compartments on individual drug dissolution release profiles. Employing a full factorial statistical experimental design, various doses were produced and analyzed for their drug release profiles. The results indicated that the addition of a second compartment did not significantly influence TPH's sustained release, while PSL's immediate release was influenced but still reached the required release rates. The bi-layered tablets showed high release curve similarity to mono-tablets, confirming the feasibility of dose individualization in combination therapies without altering proportional drug release.

Overall, this thesis helps to take another step towards precise dosages, targeted release profiles, and effective combination therapies through pharmaceutical 3DP.

List of Publications

Publication 1

Thomas Pflieger, Rakesh Venkatesh, Markus Dachtler, Karin Eggenreich and Dominique Lunter. Novel Approach to Pharmaceutical 3D-Printing Omitting the Need for Filament — Investigation of Materials, Process, and Product Characteristics. Pharmaceutics. 2022; 14(11):2488.
DOI: https://doi.org/10.3390/pharmaceutics14112488

Publication 2

Thomas Pflieger, Rakesh Venkatesh, Markus Dachtler, Karin Cooke, Stefan Laufer and Dominique Lunter. Influence of design parameters on sustained drug release properties of 3D-printed theophylline tablets. International Journal of Pharmaceutics. 2024;124207.
DOI: https://doi.org/10.1016/j.ijpharm.2024.124207

Publication 3

Thomas Pflieger, Rakesh Venkatesh, Markus Dachtler, Stefan Laufer and Dominique Lunter. An Investigation of the Drug Release Kinetics of 3D-Printed Two Compartment Theophylline and Prednisolone Tablets. SSRN.
DOI: https://doi.org/10.2139/ssrn.4932428

Personal Contribution

Publication 1

Novel Approach to Pharmaceutical 3D-Printing Omitting the Need for Filament — Investigation of Materials, Process, and Product Characteristics. Pharmaceutics. 2022; 14(11):2488. DOI: 10.3390/pharmaceutics14112488

Thomas Pflieger, Rakesh Venkatesh, Markus Dachtler, Karin Eggenreich, Stefan Laufer and Dominique Lunter*

Thomas Pflieger: validation, investigation, writing - original draft preparation, visualization

Rakesh Venkatesh: methodology, writing - review and editing, supervision

Markus Dachtler: resources, writing - review and editing

Karin Eggenreich: methodology, writing - review and editing, supervision

Stefan Laufer: methodology, writing - review and editing, supervision

Dominique Lunter*: methodology, writing - review and editing, supervision

* Corresponding author

Publication 2

Thomas Pflieger, Rakesh Venkatesh, Markus Dachtler, Karin Cooke, Stefan Laufer and Dominique Lunter. Influence of design parameters on sustained drug release properties of 3D-printed theophylline tablets. International Journal of Pharmaceutics. 2024; 124207. DOI: 10.1016/j.ijpharm.2024.124207

Thomas Pflieger, Rakesh Venkatesh, Markus Dachtler, Karin Cooke, Stefan Laufer and Dominique Lunter*

Thomas Pflieger: conceptualization, methodology, validation, investigation, data curation, writing - original draft preparation, visualization

Rakesh Venkatesh: conceptualization, methodology, writing - review and editing, supervision

Markus Dachtler: conceptualization, writing - review and editing

Karin Eggenreich: writing - review and editing

Stefan Laufer: conceptualization, methodology, writing - review and editing, supervision

Dominique Lunter*: conceptualization, methodology, writing - review and editing, supervision

* Corresponding author

Publication 3

Thomas Pflieger, Rakesh Venkatesh, Markus Dachtler, Stefan Laufer and Dominique Lunter. An Investigation of the Drug Release Kinetics of 3D-Printed Two Compartment Theophylline and Prednisolone Tablets. SSRN.
DOI: https://doi.org/10.2139/ssrn.4932428

Thomas Pflieger, Rakesh Venkatesh, Markus Dachtler, Stefan Laufer and Dominique Lunter*

Thomas Pflieger: conceptualization, methodology, validation, investigation, data curation, writing - original draft preparation, visualization

Rakesh Venkatesh: conceptualization, methodology, writing - review and editing, supervision

Markus Dachtler: conceptualization, writing - review and editing

Stefan Laufer: conceptualization, methodology, writing - review and editing, supervision

Dominique Lunter*: conceptualization, methodology, writing - review and editing, supervision

* Corresponding author

List of poster and plenary presentations

Poster and plenary presentations in academic conferences during the period of this thesis are separately listed.

Poster presentation 1

Markus Dachtler, Karin Eggenreich and Thomas Pflieger. Digital health — digital 2D/3D printing of personalized medication. 4th International Symposium on Pharmaceutical Engineering Research (SPhERe), 2021, Braunschweig.

Poster presentation 2

Thomas Pflieger, Rakesh Venkatesh, Markus Dachtler, Karin Eggenreich, Stefan Laufer and Dominique Lunter. Granule-Fed 3D Printing for Personalized Pharmaceuticals — A Comprehensive Investigation of Material Characteristics from Physical Mixture to Final Product. Annual Meeting of the German Pharmaceutical Society (DPhG), 2023, Tübingen.

Poster presentation 3

Thomas Pflieger, Rakesh Venkatesh, Markus Dachtler, Karin Cooke, Stefan Laufer and Dominique Lunter. Effects of Design Parameters on Drug Release from 3D-Printed Tablets for Patient-Tailored Pulmonary Disease Therapy. 14th World Meeting on Pharmaceutics, Biopharmaceutics and Pharmaceutical Technology (PBP), 2024, Vienna.

Plenary presentation 1

Thomas Pflieger. The Future of Health Care – Personalized Medication Delivered By 2D/3D Printing. International Conference on Global Advanced Nursing and Healthcare, 2023, Online.

Plenary presentation 2

Thomas Pflieger and Benjamin Huber. Vision to Application — The Future of Digital Health Care Through Personalized Medication Delivered By 2D/3D Printing. Enterprise Management Track Hackathon: Developing Platform Businesses Facilitating Independent Living for Older Adults to Age Gracefully in Place, 2023, Boston.

Plenary presentation 3

Thomas Pflieger. Personalized Medicine for Drug Products Via 3D Printing Technology. Conscio Science Day, 2023, Munich.

1. Introduction

1.1 Introduction to Personalized Medicine

Historically, there in fact have been various dosages and forms of administration available for many drugs on the market [1, 2], but physicians had to rely on empirical knowledge, with little consideration for variability in patients throughout the past [1]. The concept of personalized medicine began to gain traction in the last quarter of the 20th century, made possible by breakthroughs in pharmaceutical research and advancements in computer science [1]. As the complexities of the variations in disease courses and drug response were investigated, the limitations of the one-size-fits-all approach became increasingly evident. One size does not fit all, every patient is unique.

The term “personalized medicine” refers to an approach in medicine that tailors healthcare decisions, practices, and treatments to each individual patient [3-8]. It recognizes that people differ in their physiology, disease history, lifestyle, and their response to treatment [3-8]. The aim is to provide the most effective and precise treatment for each patient. The term is not solely limited to pharmaceuticals but needs to be considered a concept relying on multiple contributors from various fields [4, 9, 10]. The approach often involves using advanced technologies such as pharmaceutical 3DP to optimize patient care [7-10]. Today, there is still a long way to go for personalized medicine to be fully implemented in mainstream health care [7-11]. The realization is a gradual process that depends on several steps as shown in Figure 1 [7-11].

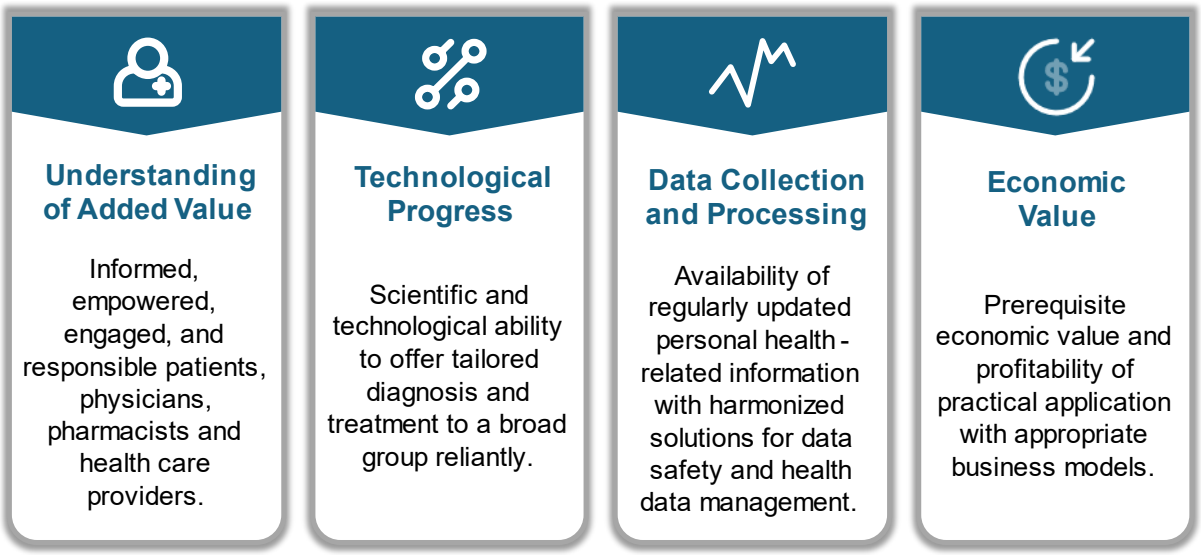

Figure 1. Different requirements to realize the mainstream establishment of personalized medicine [7-11].

1.2 Benefits of 3D Printed Pharmaceuticals

1.2.1 Tailored Doses

Several groups greatly benefit from personalized doses, particularly pediatric, geriatric, obesity, rare-disease and oncologic patients, due to their particularly high diversity [12, 13]. Traditionally, there are only insufficient methods for dose individualization, with superficial approaches to addressing the diverse needs of these patient groups, such as manually splitting dosage forms or time-intensively producing personalized oral formulations by pharmacists [14, 15]. These methods also are tightly limited in terms of dose incrementation and precision [14, 15]. Risks include high variability in actual doses and disruption of intended release profiles due to breaking coatings or unintended modification of the dosage forms [14-16].

Furthermore, certain medications already require personalized doses, even though a highly effective and economic infrastructure often does not exist yet [14-16]. In fields like oncology and neurology, many medications are classified as NTW drugs, where the difference between the minimum effective dose and the minimum toxic dose is minimal [17, 18]. Close monitoring is essential to avoid under or overdosing, which could result in ineffective treatment or severe adverse effects [17, 18]. The manual production of dosage forms is considered tedious among the pharmaceutical community making technologies like 3DP ideal for this purpose [19]. By application of such tools, the production of tailored doses can be digitized, accelerated, streamlined, and standardized. Regulations under the German law permit individual compounding production of pharmaceuticals based on medical prescriptions utilizing appropriate technology, such as additive manufacturing [20]. Pharmacists ensure quality assurance, and production complies with strict regulations overseen by local health authorities [21].

1.2.2 Tailored Release Profiles

The release profile of 3D printed tablets depends not only on a variety of parameters but can also be controlled and predicted through deliberate design [22-35]. Parameters whose direct influence on release can be designed fall into the following two main groups:

- **Formulation design**: The release kinetics can be predetermined through the pharmaceutical formulation [27]. This involves combinations of various excipients such as carrier polymers of different chemical structures and molecular weights, plasticizers, pore formers, flow agents and more [27, 28]. The drug content of the formulation also influences the subsequent release properties, as diffusion speed is significantly dependent on the concentration gradient as well as many other factors [22]. The formulation design also dictates the general mechanism of tablet disintegration, whether erosion or diffusion [27, 28]. Additionally, the formulation affects tablet hardness, friability, and the morphology in which the drug is present [29, 30]. In 3DP, solid dispersions, containing partially crystalline drugs, or solid solutions, containing completely amorphous drugs, are feasible [30]. In the case of multi-compartment 3D printed tablets, combination effects and the reciprocal influence of diffusion at the interfaces must also be considered [31, 32].

- **Tablet design**: What sets 3DP apart is the multitude of options for on-site and on-demand alteration of design parameters [22-26]. The drug release can be significantly influenced by the design of the following tablet properties, including the tablet scaling factor, volume, shape, body infill degree, and independent geometric transformations of tablet dimensions [22-26]. The release behavior of erosion-based matrixes crucially depends on the surface area to volume (SA/V) ratio and all of the mentioned factors directly impact this key parameter of drug release control [33-35].

Being able to tune drug releases to patient needs is highly beneficial as it allows for personalized treatment strategies and enables healthcare providers to optimize therapeutic outcomes while minimizing side effects [4-9].

1.2.3 Drug Co-Administration

When multiple tablets are administered to patients, it significantly impacts their adherence to the prescribed medication regimen [31, 32, 36]. Managing numerous pills leads to difficulties in keeping track of dosages and schedules, increasing the likelihood of intake irregularities or missed doses especially for individuals with cognitive, visual or physical impairments, or those managing multiple health conditions simultaneously [31, 32, 36]. These are typical complications that primarily but not exclusively affect geriatric patients and can be reduced through the concept of drug co-administration [37, 38]. Therefore, simplifying the medication regimen by reducing the number of tablets enhances overall treatment outcomes [31, 32, 36].

This study also focused on developing a bi-compartmental tablet [39]. In this process, two active ingredients were printed consecutively on top of each other, thus creating a single dosage form suitable for co-administration and combination therapy. The approach is also applicable to combination products of more than two drugs. The aim for the industry is to offer a product where multiple APIs can not only be combined for delivery but also in freely customizable dosages.

1.2.4 Elevated Patient Compliance by Tablet Design

The freedom of tablet design through 3DP knows almost no limitation. Healthcare providers can encourage patient adherence by optimizing the visual appearance and design of a dosage form for individual cases [40-44]. Visually appealing medications are more likely to be perceived positively by patients, reducing reluctance to intake [40-42]. This approach can particularly benefit pediatric patients who are especially sensitive to medication's appearance [40, 41, 43, 44]. For example, dying 3D printed tablets or individual tablet compartments by addition of pigments or colorants to the feeding formulation was already evaluated in research with promising results [41-43]. Furthermore, there are no limits to creativity in tablet design to motivate patients for medication intake. Particularly, shapes such as hearts, rings, gummi bears, and positively connotated brand logos have shown success in pediatric applications [40, 41, 44, 45].

1.2.5 Bioavailability Enhancement via Amorphous Solid Dispersions

In 3DP, the active ingredient, along with excipients, is introduced into a polymer matrix by previous hot-melt extrusion (HME). Regardless of the feeding strategy, 3D printers utilize the concept of, producing viscous polymer melts that exit the nozzle [46, 47]. With this manufacturing method, a drug can be present in the form of an amorphous solid dispersion (ASD) [48, 49]. The technical background is that the drug-polymer mixture in the extruder is heated to a temperature above the melting points of both the drug and the polymer [48, 49]. Through the extrusion screws and while being pushed through the nozzle, the molten mixture is subjected to homogenization and thorough mixing [48, 49]. The rapid cooling then locks the drug in an amorphous state within the polymer matrix and recrystallization is sought to be prevented [48, 49]. This is achieved through intermolecular forces such as ionic interactions, van der Waals forces or hydrogen bonding between functional groups of the polymer chains and the drug [48, 49]. Choosing the right polymer is crucial to create effective ASDs [48]. An effective polymer must comply with several key properties as it should stabilize the amorphous API in its solid form and sustain a supersaturated state [48]. Additionally, phase separation of the amorphous API and the polymer must not occur, which is why sufficiently strong intermolecular interactions between the drug and the polymer chains must exist [48]. In addition, there must be a topological structure capable of incorporating an appropriate amount of drug within the matrix [48]. In this work, three different polymers specifically developed for pharmaceutical extrusion applications were used [22, 50]. These include the polymers Kollidon VA64 (KVA64), Eudragit E PO (EPO), and Eudragit RL PO (ERL), which differ in their chemical structure, molecular weights, and hydrophilicity depending on their target application [51, 52]. Figure 2 shows the chemical structures of the respective polymers and allows conclusions to be drawn about the spatial topology based on the copolymer composition ratios [51, 52]. In all three polymers, both hydrogen bonds and van der Waals forces are possible [51, 52]. KVA64 is a pyrrolidone and vinyl acetate copolymer, while the two Eudragit copolymers compose of different methacrylates (see Figure 2) [51, 52]. Fundamentally, all three polymers are capable of forming ASDs when formulated accordingly.

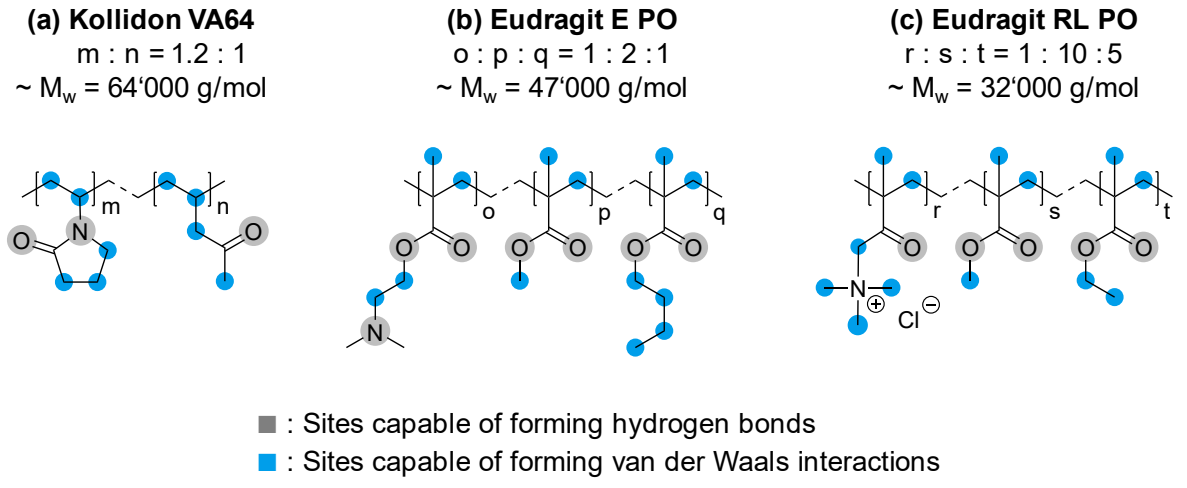

Figure 2. Chemical structures of copolymers: (**a**) KVA64 [52]; (**b**) EPO [51]; (**c**) ERL [51].

Solid dispersions improve the solubility and dissolution rate of poorly water-soluble drugs by dispersing them in a solid matrix [53]. Pre-solubilization often leads to better drug absorption in the body, resulting in increased bioavailability [53]. The application of solid dispersions is especially appealing for Biopharmaceutics Classification System (BCS) class II and IV drugs with low solubility [53]. Thus, pharmaceutical 3DP can facilitate administering drugs that were previously considered hard to formulate.

1.3 Challenges of Pharmaceutical 3D Printing

Besides the many advantages pharmaceutical 3DP offers, several challenges arise. These challenges have been categorized into the following main thematic groups:

- **Regulatory situation and GMP requirements:** Clear regulatory guidelines for the approval of 3D printed dosage forms are currently not available and still evolving [54, 55]. Regulatory agencies like the “Food and Drug Administration” (FDA) seek to develop frameworks for the evaluation of 3D printed pharmaceuticals, but these are not yet established, creating uncertainty for manufacturers and researchers [54, 55]. In Germany, the production and administration of 3D printed pharmaceuticals, like other conventional compounded formulations, is regulated under the legal framework of “formulation compounding” (“Rezepturherstellung”) [20, 56, 57]. This provision allows pharmacists to produce tailored medications, rather than relying solely on commercially available drugs. Under this framework, the pharmacist bears full liability for the compounded medication [20]. The pharmacist must self-verify the accuracy of the dosage form, the quality of the raw materials, and the precision of the 3DP process [20]. Compounded pharmaceuticals do not require authorization as long as they comply with the German Medicines Act (“Arzneimittelgesetz”; AMG) regulations [20]. The operation of pharmaceutical 3DP in a GMP environment, outside of pharmacies, presents the next challenge as there is a lack of available GMP compliant 3DP hardware and software setups [56, 58]. Especially important is the topic of cleaning validation between different pharmaceutical products [56, 58]. Until robust cleaning protocols are established and thoroughly validated, pharmaceutical manufacturers are required to use 3DP exclusively for single products (dedicated equipment) if possible at all. The question of how a safe use of intermediates can work remains unanswered mostly.

- **Challenging formulation development:** For the printing of solid dosage forms, there are numerous polymers, plasticizers, and other excipients available that have already been successfully used in the field of research and development [27]. However, finding a suitable formulation for a specific API is not trivial. Formulation development for pharmaceutical 3DP is a highly complex task that must unite many different requirements. This includes uniting rheological behavior, thermal drug stability, relevant drug loadings, and dissolution properties [27, 50, 59-61]. In terms of rheology, the formulation must exhibit optimal viscosity for smooth extrusion through the printer nozzle while maintaining the print shape post-extrusion [27, 50, 59, 60]. This requires a delicate balance of polymer and excipient concentrations [27, 50, 59, 60]. Researchers in the past struggled a lot to balance brittleness of the formulation and viscous behavior especially with filament strand fed printers [61, 62]. If

strands were too brittle conveying gears would break the filament strands and feeding came to abrupt halts [61, 62]. On the other hand, too mechanically soft filament strands were grounded down by the conveying gears and filament feeding was also impeded [61, 62]. Achieving relevant drug loadings further adds complexity, as the formulation must incorporate a high enough API concentration to ensure therapeutic efficacy at certain print object volumes without compromising printability or stability. Typically, researchers in the past have been able to show that high API concentrations lead to extreme shear thinning in the polymer matrix [23, 50, 59, 60]. Extrusion is hindered or very difficult due to this generally undesirable effect. Finally, ensuring proper dissolution properties is critical as the drug must release at the intended rate and location of action [27]. This factor not only limits the selection of available polymers but also the points mentioned above. Balancing these three aspects demands a nuanced understanding of material science, pharmaceutical technology, and 3DP technology and makes developing a suitable formulation resource intensive.

- **Lack of In-Process Control (IPC):** As of now, only a very limited number of pharmaceutical 3D printers have incorporated IPC tools, which are essential for real-time monitoring and evaluation of the printing process [63]. The lack of IPC tools means that issues such as deviations in material flow, layer adhesion, and print accuracy can go undetected [63]. This potentially compromises the quality of the printed dosage forms and puts therapy at risk. Technological possibilities for IPCs include advanced visual sensors that can monitor layer deposition and estimate printed volumes. Systems have already been developed Near-Infrared (NIR) spectroscopy to estimate the volume of individual tablets [64]. However, this technology is limited because, without multiple sensors, the rear non-visible part of the tablet must be roughly estimated [64]. Tablets with complex porosities or infills are also not easily evaluated this way [64]. Additionally, such IPC can significantly slow down the printing process, as real-time data processing poses a time-intensive task. Other researchers have tracked several relevant parameters influencing extrusion rheology using an in-built rheology sensor [59]. However, this tool is also limited because the parameter extrusion rheology cannot directly provide any information about potential print defects [59]. Most pharmaceutical 3D printers on the market do not even offer the ability to evaluate parameters like extrusion temperature, extrusion back pressure, and torque. Utilizing a real-time precision balance is also complicated, as the print object is built on a constantly moving print plate [65]. Incorporating these technologies into 3D printers can significantly enhance the reliability and precision of the printing process and is definitely needed in the future. To be precise, several separate IPCs will be required to assure patient safety that include gravimetric tracking of the printed dose and geometry assessment in combination. Additionally, the print operator will need capable software that can detect potential issues and ideally allows for automated correction.

- **Dose and release personalization:** It is important to understand that changing the dose or print volume of a dosage may also come with the risk of a change in the drug release properties, as demonstrated in this work [22, 39, 50]. Currently, two main approaches to dose individualization have been used in research and development. One is the so-called "layer addition" approach, and

the other is the "volume scaling" approach [22, 39, 50]. In the former, the dose is tailored by adding or removing individual tablet layers in the print file while the base geometry stays consistent [22, 66]. However, this also changes the SA/V ratio, which is a key parameter for controlling drug release with tablet designs where no specific porosity adjustments have been made to prevent this exact issue. This particularly affects erosion- and diffusion-controlled tablets without porosities, where the tablet can only come into contact with the dissolution medium at the outer surface of the tablet. In sustained release dosage forms, this can prevent the targeted drug release from being maintained, and in immediate release formulations, too low SA/V values can lead to too slow or incomplete drug release [39]. When personalizing a dose using the "volume scaling" approach, the SA/V parameter is also changed, leading to similar issues. Applying this, the overall volume of the tablet is geometrically scaled [22, 50, 67, 68]. A fine balance must be found between relevant dose increments and the printlet design to offer truly personalized therapy.

- **Aesthetics and patient perception:** In terms of appearance, 3D printed oral dosage forms differ significantly from traditional tablets. Studies show that preferences regarding patient-designed medicine and their appearance vary among respondents [69, 70]. This proves that patients only embrace the novelty of pharmaceutical 3DP if appealing shapes and colors are offered. Reaching acceptance in a broad spectrum of patients, further restricts the freedom in tablet design. This, in turn, limits the options for controlling the drug release of the tablets. The preferences of patients, such as tablet colors and textures, must be considered in the formulation development [69]. Those who responded to the appearances negatively in the study did not trust the technology [69]. A certain portion of patients is simply not open to novelties in the traditionally conservative sector of pharmaceutics.

1.4 Model Drugs

In this study, following the 3DP of an API for fundamental method development, three model drugs necessitating tailorization were primarily employed. Each subsection focuses on a specific model drug, detailing its mechanistic behavior, challenges in formulation, and potential benefits of being administered in a personalized way.

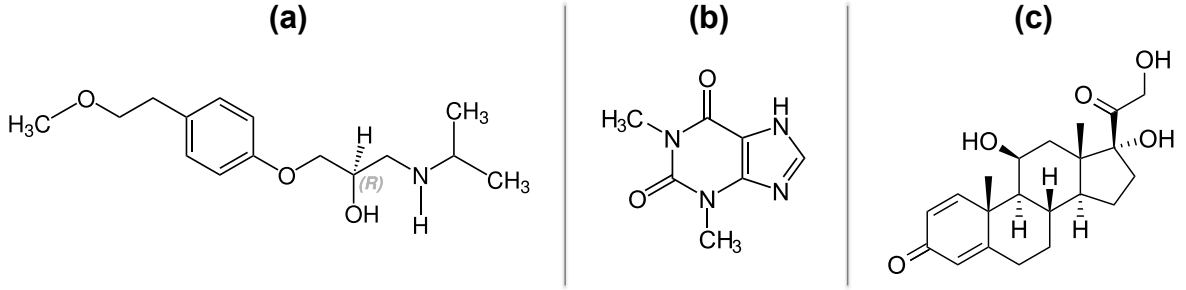

Figure 3. Chemical structure of the main model drugs: (**a**) Metoprolol; (**b**) Theophylline; (**c**) Prednisolone.

1.4.1 Metoprolol

For the initial assessment of the novel 3D printer setup in this work metoprolol was used as a model drug (see Figure 3a) [50]. The selective beta-blocker, reduces heart rate and myocardial contractility, making it effective for treating hypertension [71]. Metoprolol blocks beta-1 adrenergic receptors in the heart, thereby preventing the binding of adrenaline [71]. The receptors play an important role in the sinus node and the muscles of the heart [71]. The contraction force and relaxation of the heart is improved, while the irritability threshold is lowered [71]. In managing hypertension, a step-by-step controlled care approach is used to reach desired blood pressure levels [72, 73]. In practice, in addition to beta-blockers, a variety of other pharmaceuticals are also considered for the treatment of hypertension. These include, among others, diuretics, angiotensin-converting enzyme (ACE) inhibitors, angiotensin II receptor blockers (ARBs), alpha-blockers, vasodilators, and calcium channel blockers, each associated with different indications or advantages [72-74]. Often, combinations of multiple compounds are used in practice, with beta-blockers frequently being combined with alpha-blockers or diuretics [74]. Physicians typically start with a lowered dose and gradually increase it, monitoring the patient's response and potential adverse effects [72, 73]. Hypertension combination therapy is often used when monotherapy does not achieve the desired blood pressure control throughout the treatment process [72-74]. Pharmaceutical on-demand printing becomes valuable here, as the 3DP technology enables the creation of tailored dosage forms that match the patient's therapeutic progression not only for metoprolol but also in combining it with other hypertension drugs.

1.4.2 Theophylline

The drug TPH, a methylxanthine (see Figure 3b), is employed in treating respiratory conditions like asthma, chronic obstructive pulmonary disease (COPD), and recently, the coronavirus disease (Covid-19) [75-82]. Typically administered orally in sustained release fashion, it is fully absorbed systemically and facilitates bronchodilation and anti-inflammatory actions [75]. The therapeutic range is narrow, with effective serum concentrations between 5 to 20 µg/ml [75, 78]. Serum levels exceeding this range lead to adverse effects including hypokalemia, hyperglycemia, tremors, and arrhythmias [75]. Interindividual differences in metabolism due to factors such as age, weight, diet, and health conditions significantly affect clearance, particularly noted in pediatric patients and smokers [75, 78]. These reasons underscore the necessity for personalized and precise drug delivery, particularly through pharmaceutical 3DP, offering advantages for patients.

TPH is a representative NTW drug, substantially contributing to its diminishing role in pharmaceuticals in recent years [78]. Modern therapies for pulmonary diseases mainly involve inhaled β_2-adrenergic agonists, with TPH used as adjunct therapy. It is also administered orally to patients unable to inhale aerosols due to restricted lung function. The systemic administration route ensures reproducible drug absorption regardless of respiratory conditions [82]. Moreover, TPH has made a comeback in treating Covid-19 exacerbations and COPD, with researchers particularly promoting a low-dose approach to minimize side effects while maintaining therapeutic efficacy [79-81]. Notably, a synergistic effect exists between TPH and corticosteroids, where TPH reduces corticosteroid resistance by restoring histone deacetylase (HDAC) activity

improving anti-inflammatory outcomes [79, 81]. This work addresses the development of a 3D printed co-administration dosage form containing TPH and a corticosteroid, aiming to realize personalized dosing strategies [39].

1.4.3 Prednisolone

The corticosteroid PSL exerts potent anti-inflammatory effects, rendering it crucial in treatment of a multitude of conditions (see Figure 3c) [83-85]. Its pharmacology involves suppression of inflammatory mediators and modulation of gene transcription [83, 85]. Treating pulmonary conditions, PSL is typically administered through the oral route and immediate drug release is sought for [83-85]. Patients suffering from severe exacerbations may initially receive high doses of PSL to achieve rapid therapeutic levels [83, 84]. Once stabilized, transitioning to doses that maintain therapeutic drug levels is the norm [83, 84]. Towards the end of the therapy, the PSL dose is gradually tapered off [83, 84]. This process is essential with systemic corticosteroids to gradually restore adrenal gland function and to prevent a recurrence of the underlying condition [83, 85]. In pulmonary diseases, oral PSL is often prescribed as part of a stepwise treatment regimen to reduce airway inflammation and improve lung function [83, 84]. The dose regimen is carefully adjusted based on disease severity, response to treatment, and consideration of potential adverse effects [83, 84, 86]. Regular monitoring of pulmonary function and clinical symptoms guides adjustments in dosage or treatment duration to optimize therapeutic outcomes while minimizing side effects [83, 84, 86]. All these factors underline the need for on-demand personalization through technologies like pharmaceutical 3DP.

1.5 Technological Background of Pharmaceutical 3D Printing

Generally, the term "3DP" refers to the creation of three-dimensional objects from a digitally generated model [6-8, 13, 22-24, 27-29, 31-33, 35, 40, 42-47, 50, 58, 83, 87]. There are various technical principles involved in its implementation. Typically, these technologies are divided into three main groups: powder solidification, liquid solidification, and extrusion-based systems [6, 58, 87]. However, it is important to note that not every technical principle mentioned above is suitable for the production of pharmaceutical dosage forms, and each technology comes with specific advantages and disadvantages [58, 87]. Currently, research and development in the field primarily focuses on extrusion-based systems, which can be further divided into solid and semisolid extrusion [6, 58, 87].

1.5.1 Market Review: State-Of-The-Art Technologies

In practice, pharmaceutical 3DP is extensively researched and is already being used to produce personalized medicine in certain cases. It is no longer a technology of the future. The company *FabRx Ltd.* markets two 3D printers designed for pharmaceutical applications. The *M3DIMAKER 1*, equipped with a single Fused Deposition Modeling (FDM) printhead, allows the implementation of simple research tasks, formulation development and small-scale production of personalized medications (see Figure 4a). In contrast, the *M3DIMAKER 2*, featuring multiple printheads, can produce polypills using three separate printhead slots. These printers are equipped with interchangeable printhead systems and support FDM, semi-solid extrusion (SSE), and Direct Powder Extrusion (DPE) technologies. The company *Triastek Inc.* offers a special 3DP

technology, which is a modification of the classic FDM printing process (see Figure 4b). Here, objects are also built layer by layer through 3D nozzle movement, but the feeding method is significantly different. The Melt Extrusion Deposition (MED) technology, as *Triastek* calls it, prints the drug-polymer melt directly from a twin-screw hot-melt extruder (see Figure 4b). The feeding element, in turn, is supplied with individual powdered formulation components. Several single-screw extruders feed the drug, polymers, and other excipients into the main melt extruder, and the feeding rate can be adjusted in-process (see Figure 4b). The company *Digital Health Systems GmbH* developed the *FlexDose*™ 3D printer that also utilizes a modified FDM technology approach called granules fed single-screw extrusion (see Figure 4c). Since this printer has been used exclusively for this thesis, it is given a particularly detailed chapter in the following section.

One of the most prominent powder solidification 3DP examples is the product *Spritam*® by *Aprecia Pharmaceuticals LLC*. *Spritam*® is a 3D printed cylindrical dosage form applied for treating epilepsy, notably having received approval from the FDA [88]. The technology behind this product can be described as large-scale binder jetting, where a powder formulation mixture is precisely sprayed with binder fluid (see Figure 4d) [88]. After the dosage forms cured, excess powder is separated from the product [88]. As this is a continuous large-scale system the tablets will be pre-packaged in blisters at the production site [88]. The unique manufacturing process allows for the creation of a tablet with extremely high porosity, maintaining rapid disintegration properties and thus facilitating faster drug absorption compared to conventional products [88].

From the group of liquid solidification 3DP the technology of stereolithography (SLA) has been studied for pharmaceutical applications in particular [26, 89-91]. In SLA, a laser targets a drug-containing photosensitive polymer resin, causing localized polymerization and solidification at a chosen layer depth (see Figure 4e) [26, 89-91]. Epoxides, urethanes, ethers, or esters are primarily used for this application [26, 89-91]. The reservoir holding the resin then lowers, enabling the laser to create the next layer, thus constructing the desired shape layer by layer (see Figure 4e) [26, 89-91]. The product adheres to the laser plate and can be collected once the process is completed and the laser plate moves to an elevated position outside the resin reservoir (see Figure 4e) [26, 89-91]. SLA offers the advantage of exceptionally high print resolutions and speeds but leaves behind potentially toxic non-solidified monomer resin on the tablet, which requires additional cleaning steps [26, 89-91]. Currently, the application of pharmaceutical SLA is solely limited to research, as only a small number of polymers meet pharmaceutical standards in regard to the “Generally Recognized As Safe” list by the FDA [89].

Various types of 3D printers are already being utilized in clinical pharmacies and trial studies by legal status as compounded pharmaceuticals. The SSE based system developed by *CurifyLabs OY* is one such real-life application (Figure 4f) [92, 93]. The uniqueness of this technology lies in heating a drug-loaded polymer ink in the print head, which is then dispensed as a semi-solid into a blister (see Figure 4f) [92, 93]. A piston pushes the pharmaceutical formulation to the nozzle outlet. This technology is called SSE. The hemispheric cavities of blister slots create the rounded shape of the dosage forms (see Figure 4f) [92, 93]. Once cooled, the dosage forms solidify and can be ingested [92, 93].

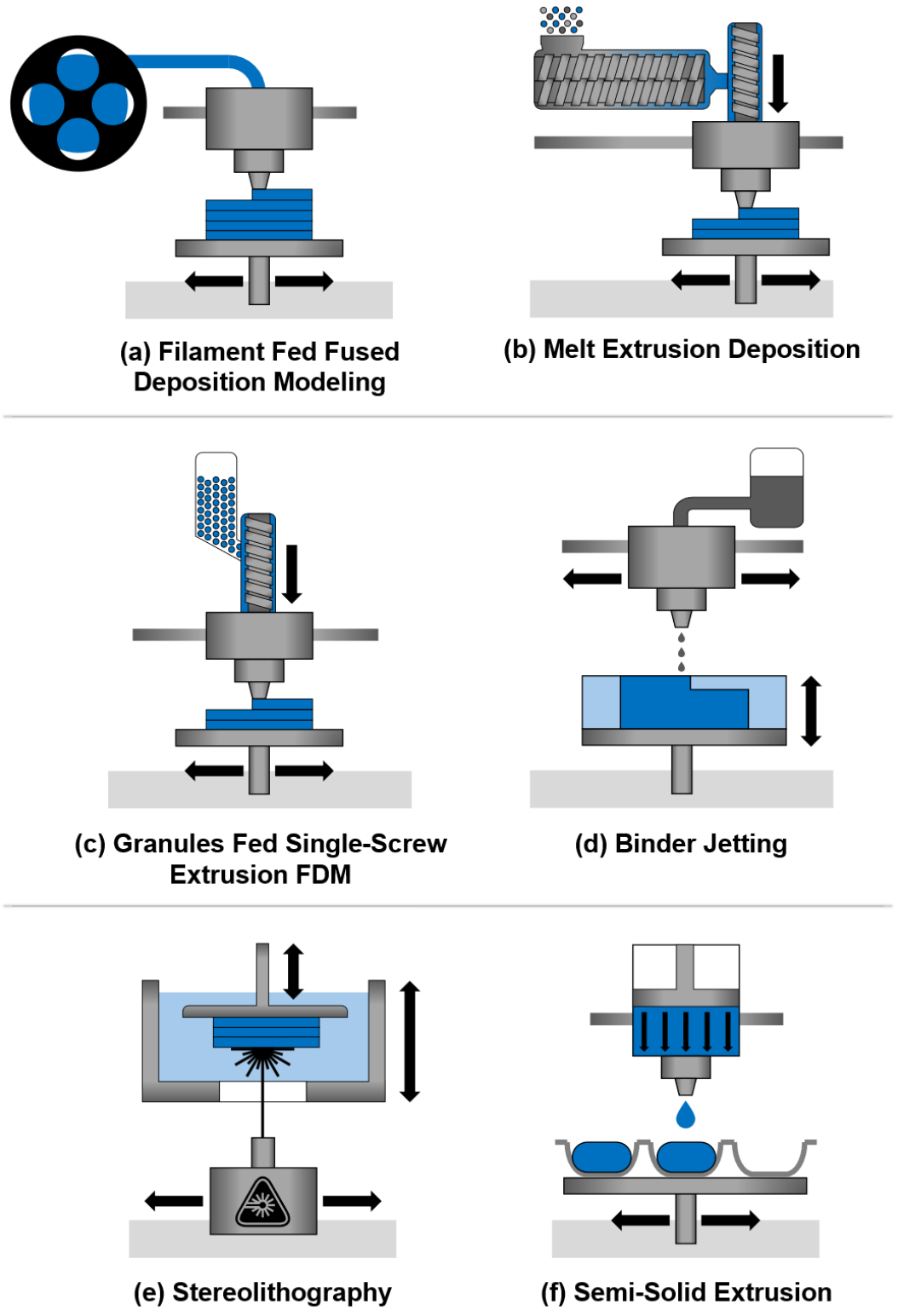

Figure 4. Currently commercially available pharmaceutical 3DP technologies on the market including: (**a**) *FabRx*'s filament fed FDM printer; (**b**) *Triastek*'s melt extrusion deposition printer; (**c**) *Digital Health System*'s granules fed single-screw extrusion FDM printer; (**d**) *Aprecia*'s binder jetting printer; (**e**) Stereolithography printer; (**f**) *CurifyLab*'s semi-solid extrusion printer.

1.5.2 The Flexdose™ 3D Printer

1.5.2.1 Hardware Setup

The 3D printer used in this study is called *Flexdose*™, supplied by *DiHeSys Digital Health Systems GmbH* (see Figure 5a) [94]. This printer is CE-certified, compliant with GMP requirements, and equipped with containment options for high potency drugs [94]. Its technical specifications include up to twelve print slots on the print bed, with multiple separately controllable print heads [94-97]. Accordingly, these heads can be loaded with different formulations and combined as desired during printing [94-97]. The operating principle is a modified form of FDM, where a drug-containing polymer melt is extruded from a nozzle (see Figure 4e and Figure 5b,c) [95-98]. By moving the print head in the Z-direction and the print bed in the XY-direction, tablets can be produced layer by layer [95, 96, 98]. The unique feature of this printer lies in its feeding principle and extrusion method [98]. In simplified terms, it employs a vertical single-screw extruder that is fed by drug-containing granules (see Figure 5c) [98]. These spherically shaped feeding granules come in glass containers, also called cartridges, which are sealed, of pharmaceutical grade and tinted. The cartridges are mounted upright directly onto the print heads via a mechanical attachment system, and the feeding flow occurs automatically through gravity [96]. The inlet to the extrusion zone is connected through a steep channel (see Figure 5c) [98]. Initially, the granules reach a conveying zone and are transported towards the hot end [98]. After passing through a sharp temperature gradient ensured by cooling ribs, they are melted and extruded (see Figure 5b,c) [98]. The granule feeding therefore is not pulsatile, the screw remains consistently loaded, what is ensuring a constant material output. All components in the printer, which are in direct contact with the drug, are made of either pharmaceutical compliant glass or stainless steel [98]. They can be detached in a push-fit system fashion, replaced or cleaned after a print run to prevent cross-contamination [96].

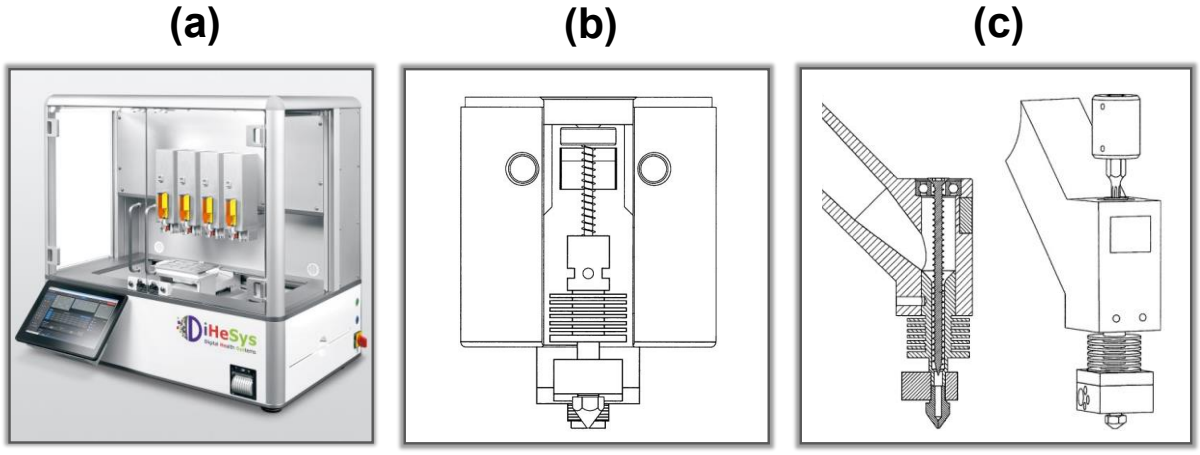

Figure 5. Hardware setup of the *FlexDose*™ 3D printer consisting of the: (**a**) front view of the printer [94], patented technical drawing of the (**b**) printhead and (**c**) exchangeable extrusion channel [98].

1.5.2.2 Operation and Software Setup

The *Flexdose*™ is equipped with proprietary software that can be operated by an integrated interface [94-97]. Each 3DP process begins with modeling an object in the form of a computer aided design (CAD) if no suitable object is available in the database [94-97]. However, the output file cannot be directly executed by the 3D printer. It must first be converted into G-code, which consists of printer commands and is the most common programming language used to drive manufacturing devices [94-97]. This transformation process is known as slicing. Subsequently, important printing settings can be adjusted within the software, such as object infill, start and regular printing and extrusion speed, layer height, and number of layers. For the sake of comparability, these parameters were kept consistent throughout the entire study for this application. The software is based on conditional G-codes, which can be further modified within the software if necessary. After inputting a base layer G-code, the desired number of tablets and layers can be selected without manually having to change the code. The printing process of tablets occurs consecutively for tablets containing only one active ingredient [94-97]. This means that the printing of a single tablet is completed entirely before the first layer of the subsequent tablet is executed [94-97]. For multi-component tablets, such as bi-tablets, one print head produces a set of all first tablet compartments before the second head follows [94-97]. Before a print run is initiated, the extrusion channels of the print heads are filled and flushed at specified print temperatures automatically, and their height is zeroized using contacting probes to ensure polymer adhesion to the printbed and comparable results [94-97]. Additionally, the print heads automatically wipe their nozzles in a designated waste area to prevent later stringing or other attachments to the nozzle tip [94-97].

1.5.3 From Granules to 3D Printed Products

1.5.3.1 Production Process Flow

Related to this work and the granule-fed 3D printer used, the production of 3D printed pharmaceuticals involves a comprehensive multi-step process, starting with the preparation of powdery physical mixtures as Figure 6 shows [22, 39, 50]. The mixtures include various formulation components, the API, carrier polymers, plasticizers, flow agents, and other excipients, which are homogenized in a closed container through tumble mixing [22, 39, 50]. Geometric mixing in three steps ensures drug distribution uniformity within the powder blends [22, 39, 50]. The physical mixtures are then transferred to table-top HME using a twin-screw setup with three temperature zones [22, 39, 50]. Although the screws lack kneading elements and consist solely of conveying elements, the combined effect of elevated temperature and shear exposure during HME, along with the pre-homogenization of the powder blend, results in the production of homogeneous extrudate strands [22, 39, 50]. These extrudates are subsequently downsized into fragment shaped granules using a rasp sieve apparatus [22, 39, 50]. Fine and powdery particles are separated from the granule batch through manual stack sieving. The resultant granules are then transferred into sealed cartridge-like containers, which are mounted on the 3DP heads, allowing for continuous granule feed during the actual printing process [22, 39, 50]. Using the printer software, print jobs can be entered, executed and physical tablets are received [22, 39, 50].

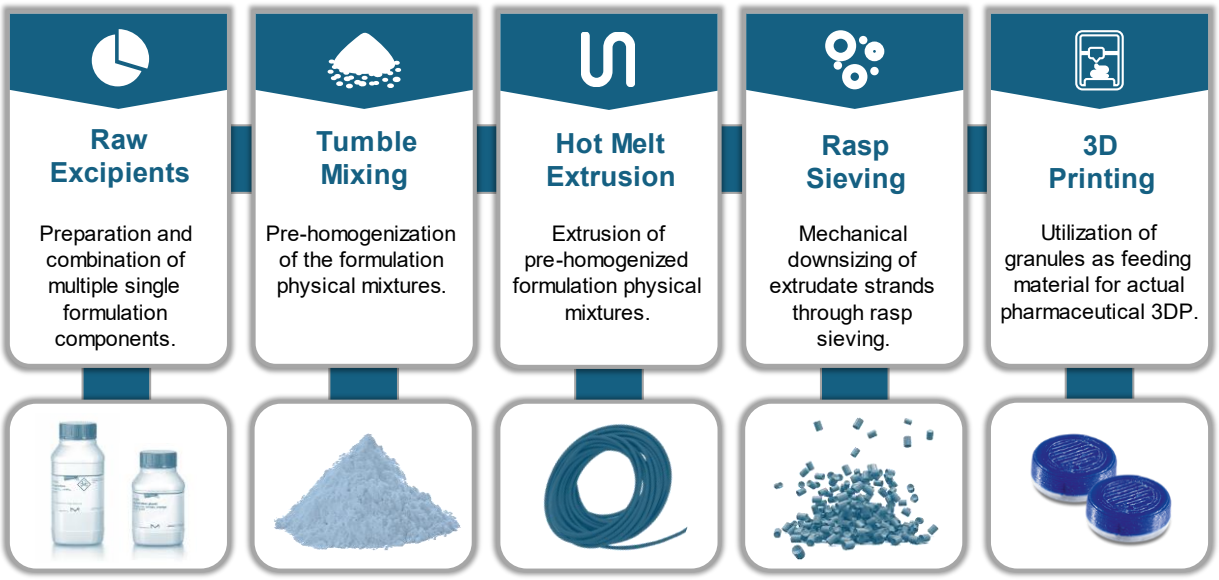

Figure 6. Process flow to produce 3D printed pharmaceuticals starting from single formulation components to final product.

1.5.3.1.1 Preparation of Homogeneous Physical Mixtures

Tumble mixing, a common technique for blending powder mixtures in pharmaceutical formulations, involves placing the powders into a rotating drum or barrel. The barrel continuously tumbles and mixes the ingredients through gravity and mechanical motion. It rotates around its central axis, allowing the powders to flow and mix through a combination of cascading motions [99, 100]. When using tumble mixing, it is crucial to consider factors such as the rotation speed, mixing time, and the filling volume of the powders [99, 100].

There are a few points that one must consider to achieve homogenous mixing. Overfilling the drum can impede effective mixing, while insufficient rotation speed may lead to inadequate blending [99, 100]. Overfilled drums cause the powders to be less able to move freely and blend effectively. Additionally, overfilling increases the risk of material compaction and creation of dead zones within the drum where the substances are not subjected to adequate mixing forces [99, 100]. Additionally, the particle sizes of the single formulation components influence the mixing efficiency. Components with significantly different particle sizes are susceptible to the effect of granular convection and segregate during mixing [99, 100]. This leads to the largest particles rising to the top, while smaller particles migrate towards the mixtures bottom area [99, 100]. To achieve optimal results, it is essential to monitor these parameters closely.

There are pharmaceutical additives that help enhancing the flowability of powder blends. Among these additives, highly dispersing silica, often referred to as colloidal silica or fumed silica, is particularly effective [27, 99]. These particles are extremely fine, with a high surface area. When added to a powder blend, highly dispersing silica acts as a flow agent by reducing inter-particle friction and cohesion. By keeping the other powder particles spatially apart, silica reduces inter-particle forces such as van der Waals forces, thereby mitigating agglomeration [99, 101]. Additionally, the

porous structure of the flow agent helps to disperse moisture within the batch, what reduces particle agglomeration [99].

1.5.3.1.2 Twin-Screw Hot-Melt Extrusion

Twin-screw HME operates by feeding a powder blend of a drug and polymer, often alongside other excipients, into an extruder where two intermeshing screws co-rotate to convey, mix, and melt the materials [102, 103]. Also counter-rotating screw setups, with screws rotating in opposite directions, are available. Screw co-rotation is particularly suitable for processes requiring intensive mixing and homogenization and high material throughput [102, 103]. Counter-rotating screws are ideal for shear-sensitive compounds due to its lower mechanical stress, and this setup allows for especially effective degassing of volatile gas-phase components [102, 103]. In HME, there are primarily two feeding approaches: constant feeding and pulsatile feeding [102]. Constant feeding involves delivering a continuous, steady stream of material into the extruder at a uniform rate [102]. This method ensures consistent processing conditions and uniform product quality, making it ideal for formulations requiring precise control over the extrusion parameters [102]. It is achieved using gravimetric or volumetric feeders that accurately measure and supply the material [102]. On the other hand, pulsatile feeding introduces the material in controlled bursts or pulses, which can be beneficial for mixing components with significantly different properties or for creating specific product characteristics, such as layered structures or controlled-release profiles [102]. Pulsatile feeding can also help manage heat-sensitive ingredients by reducing the time they spend at high temperatures [102]. Both feeding methods can be adjusted and optimized based on the specific requirements of the formulation and the desired properties of the final extrudate [102].

As the formulation passes through the extrusion channel, controlled heating and mechanical shear forces melt the polymer and disperse or even dissolve the drug within the matrix. Kneading elements can be introduced to the screw configuration to further emphasize drug homogenization [102]. If applicable, substances in gas form can exit via vents along the barrel to avoid the generation of elevated pressures [102]. The extrudate is then forced through a die, typically yielding continuous strands. This extrudate cools down, solidifies and can then be further processed [102]. HME is particularly beneficial for pharmaceutical production due to the process being solvent-free, mitigating risks associated with residual solvents [102]. Also, as a continuous process, HME is more efficient and scalable compared to small-batch methods. However, its operation at high temperatures is only suitable for thermally stable drugs and polymers.

In this study, a *ZE 9* device from *Three Tec GmbH* was utilized. The setup comprised co-rotating screw elements with screw diameters of 9 mm, four temperature zones in total, and a die diameter of 2 mm. The screws were simple intertwined conveying screws without kneading elements. The feeding temperature zone was actively cooled to room temperature by the dynamic oil temperature control system, *Petite Fleur*, from *Peter Huber Kältemaschinenbau SE* to prevent clumping during feeding. Constant feeding was conducted in all cases.

1.5.3.1.3 Rasp Sieving

Rasp sieving is a technology used in the pharmaceutical industry to convert extrudates into granules [22, 39, 50, 104]. The process begins after the HME of a formulation, where the extrudate is broken down into shorter segments or strands [22, 39, 50, 104]. Subsequently, rasp sieving uses an abrasive surface that grinds and breaks down the extrudate into smaller sized particles [22, 39, 50, 104]. The sieve typically consists of a perforated metal mesh with a rasp mechanism that grinds against the extrudate as it is fed through [22, 39, 50, 104]. This mechanical action facilitates the size reduction by shear and abrasion. The sieving process also allows for the removal of any oversized particles or irregularly shaped fragments, ensuring that the final granules meet the desired size specifications. Advantages of the technology include its efficiency and simple implementation with big batch sizes. However, rasp sieving includes the generation of dust or fine particles, requiring effective dust control measures to maintain a clean working environment and ensure worker safety. Fine particles also are undesired in the final granules product for 3DP, as they interfere with a narrow particle size distribution [22, 39, 50]. On top of that, dusty granules holding APIs are not suitable for handling during pharmaceutical 3DP [105]. For this reason, fine particles are usually separated mechanically using a stack sieve [22, 39, 50]. The fineness of the stack sieve can be freely adjusted to the desired particle sizes. Furthermore, rasp sieving may not be suitable for all types of extrudates, particularly those with very high or low hardness, as the mechanical action could either be insufficient or overly harsh, affecting the granule quality [105]. The resulting frictional forces can also generate temperatures that exceed the glass transition temperatures or melting temperatures of individual formulation components. Then there is the risk of jamming the rasp sieve holes and the extrudate will be unnecessarily sheared and damaged. Lastly, the granulation process may be resource-intensive as a certain proportion is in form of dusty particles. Despite these challenges, rasp sieving remains a valuable tool when applied under appropriate conditions.

Alternatives to downsizing pharmaceutical extrudates by rasp sieving include various methods that offer different benefits depending on the specific requirements and application of the formulation [105]. The technology of “spheronization” transforms extrudates into spherical granules through a process that involves cutting the extrudates into smaller segments and then subjecting them to abrasive rotational forces [105, 106]. In the rotating chamber, friction and centrifugal forces round the particles into smooth spheres [106]. This method is particularly advantageous for producing granules with excellent flowability, but requires precise control of parameters like moisture content and rotation speed [106]. The equipment involved can be complex and costly [106]. The amount of abrasion and loss of valuable formulation components is particularly high with this method and was not used in this work due to its uneconomical nature [106]. The technology of “ball milling”, on the other hand, involves grinding extrudates in a rotating cylindrical container filled with steel balls [107]. The collisions between the balls and the extrudates cause fractioning through kinetic impact, producing mostly fine powders [107]. This method is not able to produce particles with a narrow particle size distribution that are non-powdery [107]. Ball milling also generates significant heat by friction, which may cause degradation of sensitive formulation ingredients [107]. For these reasons, this method was not suitable for application in this work.

In this thesis, the obtained extrudate strands were downsized to granules through rasp sieve milling with a *U5 Underdriven Comil* from *Quadro Engineering Inc.* in all cases [22, 39, 50]. The downsizing was performed at 250 rpm, as this speed did not generate excessive friction temperatures that would exceed the formulation's glass transition temperatures and cause sticking [22, 39, 50]. Depending on the application, two different rasp sieve mesh inserts, G063 and G079, were used, with mesh hole sizes of 1.3 and 2.0 mm, respectively [22, 39, 50]. Granules less than 0.6 mm in size were subsequently separated manually using a stack sieve [22, 39, 50]. Fine particles are undesirable, as they expose the user to dust during later 3DP feeding and tend to feed poorly due to electrostatic charging.

1.5.3.2 Benefits of Granule Feeding

Pharmaceutical 3DP with granules as the intermediate and feed material is an uncommon method in the industry. Unlike the more widely used approaches that employ filament or powder feeding, granule-fed 3DP provides distinct benefits. According to the literature on filament-fed printheads, creating suitable filament materials is challenging [62, 108, 109]. The filament must meet exact mechanical requirements to be consistently fed by gear wheels, and only minimal deviations in filament diameter are tolerated [62, 108, 109]. In the production of these filaments, the composition of the formulation is strictly determined by pharmaceutical requirements [62, 108, 109]. The optimization for mechanical or viscosity-related properties is limited as composition changes directly influence drug release properties and other pharmaceutical parameters [62, 108, 109]. Finding a compromise between the mechanical stability of the filament and maintaining its feeding properties is challenging [62, 108, 109]. If the filament is too brittle, the feed gear wheels break the strand and feeding does not occur [59]. If the filament is not brittle enough, it results in “stripped” filament, where the polymer strand is ground away and feeding is also impeded [59].

In powder-feeding approaches, two main issues arise in pharmaceutical applications. First, multi-component powder blends tend to segregate, even when formulation adaptions are used to counteract this [110, 111]. Concentration fluctuations of the API content prevent the printing of uniform and reliable dosage forms [110, 111]. Another issue is that many pharmaceutical powder blends show comparably poor flowability and are prone to electrostatic charging [110].

All these challenges are not an issue with the granules-fed system, where segregation of individual components is impossible since the API is already incorporated into the polymer matrix of the granules. Additionally, there are clear requirement regimens regarding the melt viscosity of the granules, and the brittleness and mechanical strength of low importance. When feeding granules, high particle flowability is achieved due to their spherical shape. Furthermore, granules exhibit superior content uniformity, enhancing precision and reproducibility in the final dosage forms. The content uniformity within individual granule particles is high, as the API has already been pre-homogenized both while tumble mixing the powder blend and through shear application during HME. Their utilization as intermediates in 3DP pharmaceuticals in real-world applications is more realistic due to their handling and processing characteristics. Despite its potential, the granules feeding approach remains underexplored, necessitating further research to implement its capabilities into mainstream manufacturing of pharmaceuticals.

1.6 Analytical Background

In this work, formulation single components, physical mixtures, granules, and finished 3D printed tablets were extensively and comprehensively analytically evaluated. Each subsection focuses on a specific analytical tool and explains its underlying scientific principles, relevant applications in the field of pharmaceutical 3DP, advantages and disadvantages of setup modifications, technical features, and implementation in this thesis.

1.6.1 Thermogravimetric Analysis

TGA is a tool used to analyze a sample by exposing it to a stepwise temperature program while simultaneously tracking its mass with a thermobalance [112]. This technique evaluates combustion effects, desorption effects, absorption effects, and other solid-gas phase reactions [112]. The instrument typically includes an analytical balance within a temperature-controlled cell and a sample holder for small aluminum crucibles [112]. Samples, usually in the lower double-digit milligram range, are placed into these holders. The temperature program, including the heating rate and maximum temperature, can be freely adjusted [112]. Data output is typically presented as a thermogram plot showing the change in the sample's total mass over time or the corresponding sample temperature [112].

In this case, single formulation components, formulation physical mixtures, and granules intermediates were examined for the onset degradation temperatures at which thermal combustion of the sample occurs. Combustion of organic materials into gases leads to sample mass loss in the thermogram and samples are typically considered thermally stable up to 1.0% proportional mass loss. The scientific background of polymer combustion into gases involves oxidative reactions of the sample material [112]. Initially, when an organic substance is exposed to heat, it undergoes polymer chain or substance break down into smaller fragments through processes such as depolymerization, chain scission, and random bond cleavages [112]. These processes generate volatile organic compounds and free radicals. In the presence of oxygen, these volatile compounds further react in oxidative combustion reactions, leading to the formation of various gases, primarily carbon dioxide and water vapor, along with other potential byproducts like carbon monoxide, methane and other hydrocarbon gases [112]. The specific gases produced depend on the polymer's chemical structure and the combustion conditions, such as absolute temperatures, heating steps and oxygen availability. In pharmaceutical 3DP, the formulation is exposed to elevated process temperatures in two stages: the table-top HME process for granule production and the actual 3DP process [22, 39, 50]. It is crucial to maintain process temperatures well below the degradation temperatures to ensure the production of a safe pharmaceutical product that meets strict pharmaceutical standards.

TGA also measures moisture content, which can affect product properties and influence processing parameters [22, 39, 50]. In the thermogram, a desorption plateau is typically reached beyond the boiling point of water and the mass loss difference equals the samples' water content [22, 39, 50]. High water contents in formulations for pharmaceutical 3DP can have several unwanted effects. Firstly, increased water levels can lead to component demixing, promote degradation reactions, and affect the

material's morphology. Secondly, elevated water content can cause technical issues during 3DP, since the process typically occurs at temperatures above 100 °C and evaporating water creates hollow areas and irregularities in the extrusion strand. This leads to defects in the printed tablets.

1.6.1 Differential Scanning Calorimetry

DSC is an analytical tool that measures the difference in the heat required to increase the temperature of a sample compared to a reference as a function of temperature [113, 114]. Both the sample and reference are placed in aluminum crucibles and given into a sample chamber on a thermoelectric disk, which is surrounded by a furnace as Figure 7a shows [113, 114]. Measurements can be automated using an autosampler for multiple samples. Due to the heat capacity (C_p) of the sample, a temperature difference between the sample and reference crucible occurs, which is detected by thermocouples (see Figure 7a) [113, 114]. The resulting heat flow is calculated using the thermal equivalent of Ohm's law, where Q represents the heat flow, ΔT is the temperature difference between the sample and reference crucibles, and R_T is the thermal resistance of the thermoelectric disk (see Equation 1) [113, 114]. For a heat flux DSC device, as used in this study, the following assumptions are made: steady-state heat flow rates, no cross-interactions between the sample and reference, consideration only of the heat capacities of the sample and reference (C_S, C_R), and no heat exchange with the surroundings [113, 114]. Typically, the DSC temperature program involves a linear increase of temperature over time [113, 114]. The reference material should have a well-defined heat capacity over the temperature range scanned and must remain stable without material changes during the temperature scan [113, 114].

$$Q = \frac{\Delta T}{R_T} \qquad \text{Equation 1}$$

DSC results are usually presented as heat flow plotted against temperature as illustrated in Figure 7b. This tool is extensively used to investigate polymer-based formulations and determine their thermal properties, including the glass transition temperature (T_g), crystallization temperature (T_c), and melting point (T_m) [113, 114]. While T_g, T_c, and T_m are often known for single formulation components, their behavior in physical mixtures or granules typically deviates. Parameter T_g is the temperature at which the translational motion of polymer chain segments becomes active, with motion being frozen below the T_g and only vibration occurring [113, 114]. T_g is identified by the point of highest steepness before reaching a new plateau in the endothermic direction (see Figure 7b) [113, 114]. T_m is the temperature at which a crystalline solid sample transitions to an isotropic liquid. For semi-crystalline polymers, such as those used in this study, the endothermic peaks are often very broad [113, 114]. The T_m is determined by the intersection point of the tangents at the baseline and the ascending course of the melting peak (see Figure 7b) [113, 114]. Understanding these thermal transitions is crucial for developing appropriate formulations for 3DP.

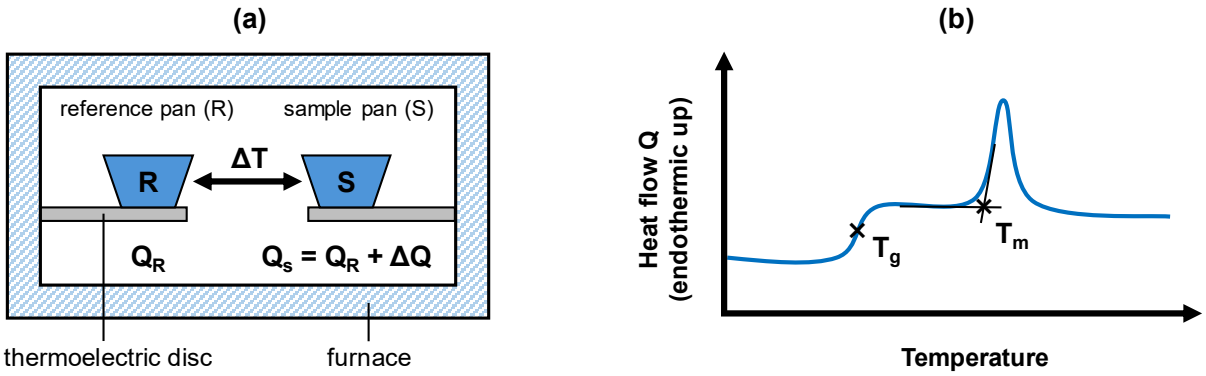

Figure 7. Two-part illustration regarding: (**a**) internal structure of a heat-flux DSC's furnace; (**b**) paradigm DSC result of a viscoelastic pharmaceutical formulation including glass transition and melting temperature.

1.6.2 Small Amplitude Oscillatory Shear Rheology

Small Amplitude Oscillatory Shear (SAOS) rheology is used to study the viscoelastic properties of polymer blends, especially pharmaceutical formulations in the form of extruded granules [22, 39, 50]. This method applies a small, sinusoidal shear strain to the material to measure its response without changing its structure [115-117]. This allows to determine two key properties: the storage modulus G' and the loss modulus G'' [115-117]. Typically, rotational rheometers are used for this purpose. They work by placing the sample between a stationary plate and a oscillating plate, though other setups are possible as shown in Figure 8a. The shear strain or stress is measured from the force detected by a sensor on the top plate, and the shear rate is proportional to the oscillation speed of the top plate [115-117].

Viscosity measurements are based on specific principles. In SAOS rheology, either shear stress or shear strain is controlled, while the other parameter is measured [115-117]. When controlling shear strain, the applied periodic sinusoidal strain helps determine the shear stress σ, which depends on the maximum strain amplitude γ_0, the angular frequency ω, and the time t of the experiment (see Equation 2) [115-117].

$$\sigma = \gamma_0 \cdot (G' \cdot \sin(\omega t) + G'' \cdot \cos(\omega t)) \qquad \text{Equation 2}$$

The complex viscosity η* is calculated using three parameters: angular frequency σ, storage modulus G', and loss modulus G'' [115-117]. The relationship is given by Equation 3.

$$\eta^* = \frac{\sqrt{(G')^2 + (G'')^2}}{\omega} \qquad \text{Equation 3}$$

The complex viscosity η* can also be used to determine the classical dynamic viscosity of a sample [115-117]. According to the Cox-Merz rule (see Equation 4), the complex viscosity η* measured during oscillatory shear tests at a specific angular frequency ω

is approximately equal to the dynamic viscosity η measured in steady shear flow at the corresponding shear rate γ [115-117].This rule helps relate the viscosity behavior observed under oscillatory conditions to that under steady shear conditions, making it easier to analyze complex polymer systems [115-117]. However, it is important to note that this rule is an approximation and might not be accurate for all materials but is for shear-thinning polymer melts [115-117].

$$\eta^*(\omega) = \eta(\gamma) \qquad \text{Equation 4}$$

It is crucial to perform SAOS measurements within the material's linear viscoelastic region (LVR), where stress and strain are proportional, and the sample's structure remains intact [115-117]. Outside this region, the measurements become non-reliable for correlating with rheological properties [115-117]. The LVR is determined through amplitude sweep tests, where shear stress or strain is gradually increased until the structure starts to break down, signified by decrease of the storage modulus G' as shown in Figure 8b [115-117]. After establishing the appropriate strain and stress amplitude from these tests, an oscillatory frequency sweep is conducted to measure the complex viscosity η* of the sample [115-117]. The results typically include plots of η*, G', and G'' against the angular frequency ω [115-117].

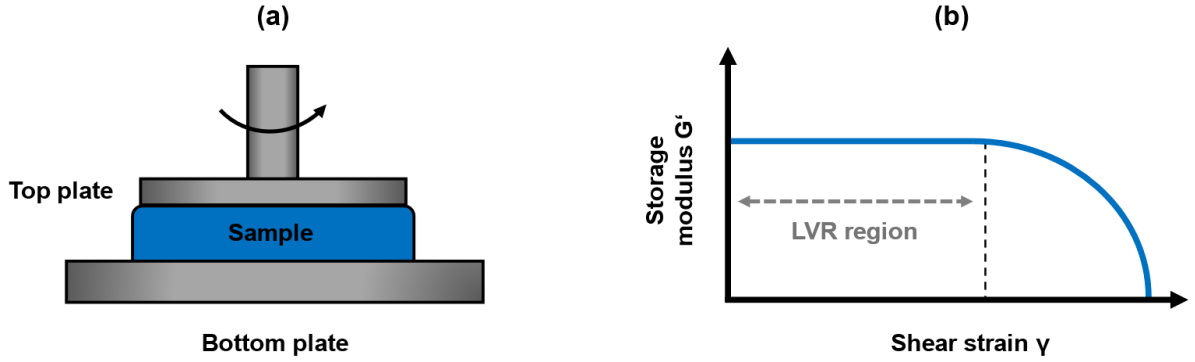

Figure 8. Two-part illustration of: (**a**) the geometry of a parallel plate rheometer; (**b**) the evaluation of exemplary amplitude sweep measurement results.

In pharmaceutical 3DP, viscoelastic polymer-based formulations, such as solid dispersions or solutions containing drugs and excipients, are used. Small molecule drugs act as plasticizers, altering the melt rheology by weakening the forces between polymer chains and disrupting the polymer's crystallinity [115-117]. The drug molecules move in between polymer chains and reduce intermolecular forces by weakening van der Waals forces between polymer chains [115-117]. Also, these formulations often show "shear thinning" behavior, where viscosity decreases with increasing shear rate. Unlike newtonian fluids, which have a constant viscosity, pharmaceutical formulations are generally non-newtonian [115-117]. Under shear stress, polymer chains align in the direction of flow, reducing resistance and overall viscosity [115-117].

Different processing methods in pharmaceutical technology, such as spraying, brushing, pumping, and hot melt extrusion (HME), can be compared by their shear rates to understand their effects on drug formulations [118]. Spraying, brushing, and

pumping usually involve low shear rates, while HME subjects materials to high shear rates by mixing them with screws at high temperatures and forcing them through a die [118]. The 3DP process is similar to HME, and the shear rate experienced by the formulation during printing can be estimated semi-empirically [27, 119, 120]. The apparent nozzle wall shear rate γ_{nw} helps define the relevant range of shear rates in 3DP and is depicted in Equation 5 [27, 119, 120]. The calculation includes the nozzle radius r_n and the volumetric flow rate $\dot{V}$.

$$\dot{\gamma}_{nw} = \frac{4 \cdot \dot{V}}{\pi \cdot r_n^3} \qquad \text{Equation 5}$$

In the field of 3DP, it is well known that a formulation must meet certain rheological requirements at apparent shear rates to be successfully printable [22, 23, 39, 50, 59, 60, 109]. The printability of a formulation depends on the three main SAOS parameters η*, G' and G'' [22, 23, 39, 50, 59, 60, 109]. These target regimes need to be individually determined for a specific 3DP setup. Generally, the complex viscosity must lie within an appropriate range to avoid undesirable technical effects [22, 23, 39, 50, 59, 60, 109]. If η* is too high for the given process parameters, extrusion cannot occur, and the extrusion channel may take physical damage [50]. The formulation will not emerge from the nozzle, causing clogs in the extrusion channel, leading to elevated torques and backpressure, which increases the risk of jamming [50]. Conversely, if η* is too low during the 3DP process, the polymer melt will begin to ooze from the nozzle, resulting in unusable print outcomes [50]. Additionally, in a single-screw extrusion 3DP setup, as used in this work, the phenomenon of "polymer melt backflow" occurs [50]. In this case, the polymer melt flows in the opposite direction of the intended flow as the flow resistance is lower in this direction [50]. Moreover, the ratio of the parameters G'' and G', known as the loss factor tan(δ), must also meet certain target regimes for successful 3DP [22, 23, 39, 50, 59, 60, 109]. The loss factor is shown in Equation 6.

$$\tan(\delta) = \frac{G''}{G'} \qquad \text{Equation 6}$$

This parameter provides insight into the balance between the elastic and viscous behavior of the polymer. The parameter must be high enough to ensure that individual printed layers adhere to each other [60]. However, it must also be low enough to prevent conveying energy from being converted into undesirable processes such as internal friction during the printing process. Suitable values need to be established for each 3DP geometry and process parameters individually.

1.6.3 Tests According to the European Pharmacopoeia

The Ph. Eur. outlines tests to evaluate the quality and uniformity of pharmaceutical preparations [121]. Two tests applied in this work are “2.9.5 Uniformity of mass of single-dose dosage forms” and “2.9.40 Uniformity of dosage units” [122, 123]. Test 2.9.5 generally distinguishes between tablets, capsules, granules, powders, suppositories, and pessaries, with 3D printed tablets falling under the category of tablets [123]. The test involves weighing twenty randomly selected dosage units from a batch and calculating the arithmetic mean of the mass [123]. Then, the individual masses are compared to the mean mass [123]. No more than two units are allowed to

deviate from the average by a specified percentage, which depends on the mean mass of the tablets [123]. For tablets, this percentage is 10% for weights under 80 mg, 7.5% for weights between 80 mg and 250 mg, and 5% for weights above 250 mg [123]. Additionally, no single unit may deviate by more than twice the corresponding percentage [123].

In test 2.9.40, various dosage forms, speaking of tablets, capsules, solids, and dosage forms not addressed by the other categories, are distinguished [122]. In this thesis, solely tablets were examined, with an additional distinction made for the subtype uncoated tablets [122]. The test involves two main approaches: the mass variation (MV) and content uniformity (CU) method [122]. MV is suitable for uncoated tablets where the dose and ratio of active substance make up more than 25% of the total mass or an absolute amount of at least 25 mg [122]. The CU method is used when the drug content is less than 25% or the absolute dose is below 25 mg [122]. In both the MV and CU methods, ten units are weighed, and their drug content is determined. The difference lies in the calculation of the acceptance values (AV), as in CU, it is calculated with the mean of individual contents, whereas in MV, it is calculated with the individual estimated contents [122]. In both cases, the AV must not exceed limit 1, specifically a value of 15 [122]. If the requirements for the first testing level are not met, twenty additional dosage forms need to be evaluated, and the total AV must not exceed 15 [122]. Additionally, no single dose may fail limit 2 by deviating from the reference value by more than 25% [122]. Equation 7 shows the calculation of the AV using the parameters $\bar{X}$, the arithmetic mean of individual contents, M, the label claim, k, the acceptability constant, which is 2.4 if ten samples were used and 2.0 for thirty samples, and SD [122].

$$AV = |M - \bar{X}| + k \cdot SD \qquad \text{Equation 7}$$

1.6.4 In-Vitro Dissolution

In-vitro dissolution testing is an essential analytical tool used to evaluate the drug release profile of pharmaceutical dosage forms [124]. The device typically employed for this purpose simulates the physiological conditions of the gastrointestinal tract and adheres to strict regulations outlined in various international pharmacopoeias [124]. Established test conditions for each API can be found in respective monographs, which include specific measurement geometries, dissolution media and volumes, stirring speeds, and other parameters [124]. The device generally consists of dissolution vessels filled with a dissolution medium and a stirring apparatus that agitates the medium, promoting the release of the drug from the tablet into the medium [124, 125]. The determination of the drug content present in the medium can be conducted through "online" or "offline" analysis [124, 125]. The two measurement methods “online” and “offline” differ in how the measurement samples are processed. In "online" dissolution measurements, samples are automatically drawn from the vessels using a pumping system in a closed loop and pumped into the respective spectrometry cells. After drug quantification, the samples are returned to the vessel, ensuring that the total volume of the dissolution medium remains unchanged [124, 125]. If applicable, the drug content is typically quantified using UV-Vis spectrophotometry, which involves comparison with a previously established calibration curve for the dissolution medium [124, 125]. This method offers the advantage of quick and effortless measurements

but cannot individually quantify multiple UV-Vis active substances [124, 125]. If the dissolution medium contains multiple substances, such as multiple APIs, dyes, or certain polymers that cause UV-Vis interference, it is impossible to accurately determine individual quantities due to overlapping spectra. In this case and when handling substances with low or no absorbance response, light-induced chemical instability or matrixes that cause scattering, "offline" dissolution testing is recommended [124, 125]. Here, samples are usually taken from the vessels by an autosampler and stored in tinted vials. In a subsequent step, the samples from the vials are separated into individual signals using High Performance Liquid Chromatography (HPLC), the signals are identified, and then quantified by UV-Vis spectrophotometry or other analytical tools [124, 125].

In the evaluation of 3D printed tablets, in-vitro dissolution testing provides a powerful method to study the release characteristics the printed designs. The 3DP technology enables the production of tablets with complex geometries which can be used to tailor drug release profiles. By conducting dissolution tests and analyzing the results, one can optimize the design and composition of 3D printed tablets to achieve desired therapeutic outcomes. As this work showed, the drug release profile of a 3D printed tablet is primarily influenced by two key parameters, the tablet's SA/V ratio and the utilized pharmaceutical formulation [22].

In-vitro drug release curves need to be fitted with mathematical models to accurately describe the release kinetics and mechanisms of drug release [126]. These models help to understand the drug release behavior, predict and compare release profiles, and optimize the formulation [126]. Out of a multitude of fits, the two main models following “Korsmeyer-Peppas” (KP) and “Higuchi” were focused on in this work [22, 39]. The KP model is used to analyze drug release, where the release mechanism may be complex. It is based on the power-law equation like Equation 8 shows, where M_t/M_{max} is the fraction of drug released at timepoint t, k is the release rate constant, and n is the drug release exponent indicating the mechanism of release [126]. If n is less than 0.45, it indicates pure Fickian diffusion, while values between 0.5 and 1.0 suggest anomalous transport [126]. In this range other release processes, like erosion of the tablet, add to the underlying drug release mechanism [126].

$$\frac{M_t}{M_{max}} = k \cdot t^n \qquad \text{Equation 8}$$

The Higuchi model, on the other hand, describes drug release from a homogeneous matrix as a process based on Fickian diffusion [126]. The model is built on the premise that the initial drug concentration is much higher than the solubility of the drug and that drug diffusion occurs only one directional [127]. It is also assumed that the drug particles in the matrix are much smaller than the thickness of the matrix, and that the matrix itself does not dissolve or swell [127]. Additionally, the drug diffusivity is considered constant, and "perfect sink conditions" are assumed [127]. For a homogeneous matrix, the dissolution is described according to Higuchi as shown in Equation 9 [127].

$$Q = \sqrt{D \cdot (2\,C_0 - C_s) \cdot C_s \cdot t} \qquad \text{Equation 9}$$

Here, Q represents the amount of drug released at time by area unit [127]. Parameter D is the diffusivity of the drug, C_0 is the initial drug concentration, and C_s is the solubility of the drug in the polymer matrix [127]. In general, the model can be simplified by introducing the Higuchi release constant k_H as summarized in Equation 10 [127]:

$$Q = k_H \cdot \sqrt{t} \qquad \text{Equation 10}$$

Thus, Equation 10 delineates proportionality between the amount of drug released and the square root of time.

1.6.5 Quality by Design and Design of Experiments

The Quality by Design (QbD) approach is a systematic method that emphasizes the understanding and control of production processes to ensure product quality and achieve target product characteristics [128, 129]. It starts with defining a target product profile, which includes the desired characteristics and performance attributes of the final product (see Figure 9a) [128, 129]. In the specific application of this thesis, the goal in a sub-project was to achieve certain sustained drug releases from 3D printed tablets [22]. The release profiles can be mathematically modeled using appropriate model fits or the mean dissolution time (MDT) to make it scientifically assessable [22]. Next, critical quality attributes (CQAs) are identified, which are the physical and chemical properties of the 3D printed tablet that need to be controlled to meet the desired product quality (see Figure 9a). From a variety of influencing parameters, suitable ones are selected, ideally ones that are quantitatively determinable and adaptable [128, 129]. In this work, the focus was on the three physical design factors "tablet scale factor," "tablet volume," and "tablet body infill," as well as the formulation-related factor "drug content in feeding granules" [22]. To understand which design factors significantly influence the output value and to perceive the relationship between design factors and dissolution profiles, a suitable DOE is set up (see Figure 9a) [128, 129]. The selected parameters are represented at appropriate factor levels, the corresponding 3D printed tablets are produced, and the dissolution profiles are investigated (see Figure 9a) [128, 129]. The scientific understanding built from the statistical analysis of the DOE results then allows for the adjustment of the significant design parameters to achieve the desired target product profiles (see Figure 9a) [128, 129]. The QbD approach is a self-contained system, which can be repeated and optimized until a satisfying product is achieved [128, 129].

In the following paragraph, the specific applications, advantages, disadvantages and modifications of DOEs used in this work are discussed in detail. A full-factorial DOE is a comprehensive method used to investigate the effects of multiple factors on a response variable [130]. With this design, every possible combination of factor levels is tested, ensuring that not only main effects but also all interactions between factors can be considered and statistically evaluated [130]. However, full-factorial DOEs become impractical with high numbers of factors l or factor levels k as shown in Equation 11 [130]. The number of required experimental runs n_{runs} grows exponentially with the number of factor levels, leading to high time and economical effort [130]. The number of experimental repetitions is given by n [130].

$$n_{runs} = n \cdot l^{k} \qquad \text{Equation 11}$$

Fractional factorial DOE approaches address the limitations of full-factorial designs by testing only a subset of all possible combinations of factor levels [130]. This approach reduces the number of experiments needed, making it more feasible for studies with a high number of factors [130]. The trade-off is that the design focuses on the most critical main effects only [130]. In factorial DOEs, n_{runs} also depends on the number of generators p, which describes the size of the fraction (see Equation 12) [130].

$$n_{runs} = n \cdot l^{k-p} \qquad \text{Equation 12}$$

The Taguchi design is a specific type of fractional factorial designs that emphasizes robustness and efficiency in experimental studies [131, 132]. This method uses orthogonal arrays to systematically vary the factors and levels in a way that captures the main effects and selected interactions with a minimal number of experiments [131, 132]. Taguchi designs are particularly valued for their ability to identify the most influential factors in form of effect size studies and interactions in complex systems while being comparably low in effort [131, 132]. Additionally, the S/N ratio quantifies the robustness of the process under varying conditions, allowing to further optimize product quality and performance [131, 132]. This study focused on achieving specific target values for the dissolution profiles of 3D printed sustained release tablets [22]. Rather than optimizing or minimizing the system, a "nominal the best" strategy was utilized for the S/N evaluation (see Equation 13) [131, 132]. The S/N ratio measures the variability around a target value by taking the average response $\bar{Y}$ and the variance s^2 into account (see Equation 13) [131, 132].

$$S/N = 10 \cdot \log\left\{\frac{\bar{Y}^2}{s^2}\right\} \qquad \text{Equation 13}$$

1.6.6 Physiologically Based Pharmacokinetic Modeling

PBPK modeling is an advanced computational approach used to predict the absorption, distribution, metabolism, and excretion (ADME) of drugs in the human body [133]. These models are crucial in understanding how different patient groups could respond to certain pharmaceutical dosage forms [133]. In drug development, PBPK models help forecast outcomes, optimize dosing, and minimize the need for extensive animal or human testing [133]. This study used PBPK modeling to simulate the drug blood concentration profiles of various patient populations over time, linked to specific sustained release in-vitro profiles [22, 39]. In this work, exclusively the PBPK tool *PK-sim*® within *OSP Suite version 11*, provided by *Open Systems Pharmacology Inc.* was employed for the simulation of TPH blood serum concentration profiles [22, 39]. *PK-sim*® uses organ specific differential transport equations to mimic drug movement and distribution within the body (see Figure 9b) [134]. An incorporated database provides essential parameters, such as the absorption rate constant and other chemical properties of a drug [134]. *PK-sim*® integrates the processes of drug ADME into a single, detailed model (see Figure 9b) [134]. Although complex, this approach offers a highly realistic depiction [134]. The software models oral drug absorption using

a "plug-flow" concept, treating the small intestine as a continuous compartment, with functions describing the drug's entry into the gut and its transit similar to a tubular plug reactor [134]. For 3D printed tablets of this work, the drug release into solution was described according to user-defined release functions [22, 39].

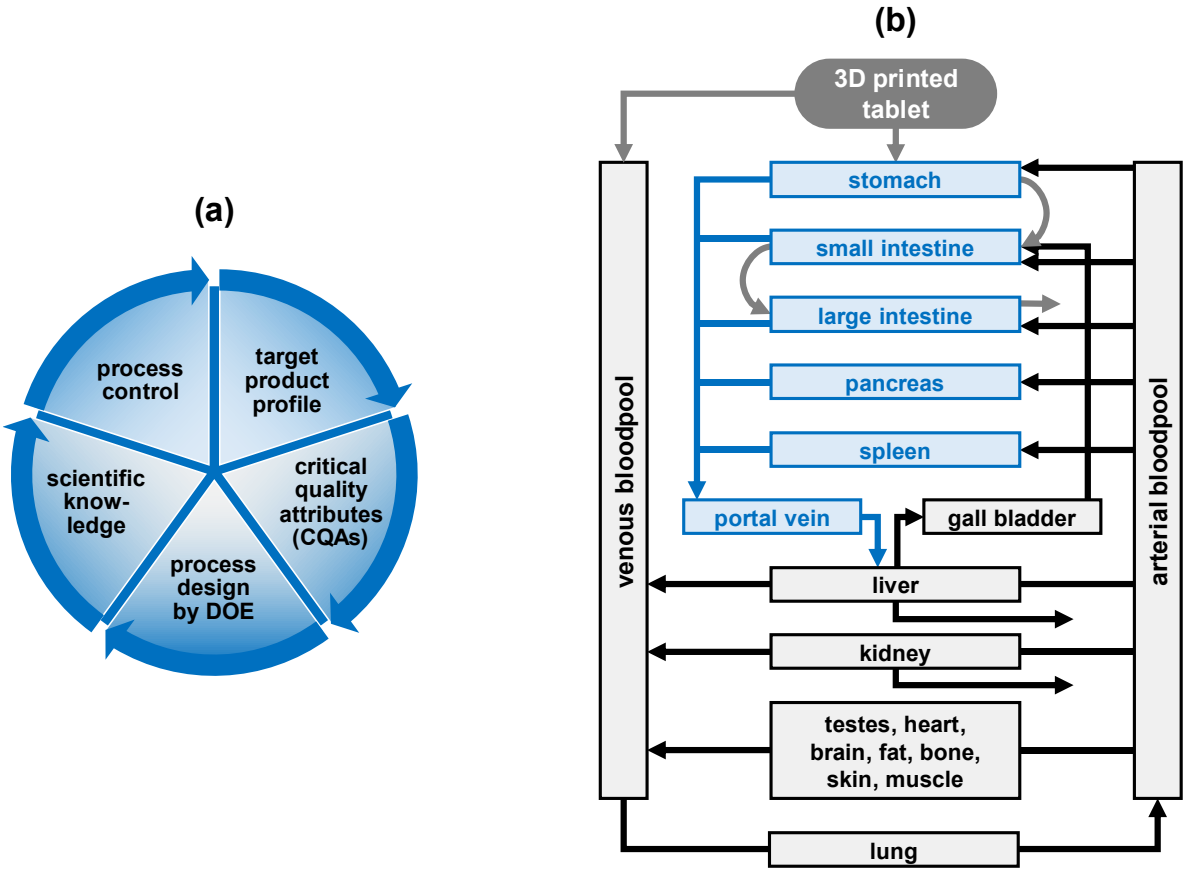

Figure 9. Two-part illustration regarding: (**a**) Quality by design approach cycle for the development of pharmaceuticals; (**b**) *PK-sim*® PBPK modeling of the human body according to organs with the oral absorption components (blue), the systemic distribution components (black) and dosage form travel (grey).

1.7 References

1. Anderson, S., *Making medicines: a brief history of pharmacy and pharmaceuticals*. 2005: Pharmaceutical Press.

2. Govender, R., et al., *Therapy for the individual: Towards patient integration into the manufacturing and provision of pharmaceuticals.* European Journal of Pharmaceutics and Biopharmaceutics, 2020. **149**: p. 58-76.

3. Dachtler, M., G. Huber, and T. Pries, *2D & 3D-Print-Technologien in der pharmazeutischen Industrie.* Digitale Transformation von Dienstleistungen im Gesundheitswesen VII: Impulse für die Pharmaindustrie, 2020: p. 53-66.

4. Dachtler, M., K. Eggenreich, and T. Pflieger. *Digital health-digital 2D/3D printing of personalized medication*. in *Proceedings of the 4rd International Symposium on Pharmaceutical Engineering Research (SPhERe), Online*. 2021.

5. Huber, G., M. Dachtler, and D. Edinger, *Digitalisierung in der Pharmaindustrie.* Digitale Transformation von Dienstleistungen im Gesundheitswesen II: Impulse für das Management, 2017: p. 241-255.

6. Serrano, D.R., et al., *3D printing technologies in personalized medicine, nanomedicines, and biopharmaceuticals.* Pharmaceutics, 2023. **15**(2): p. 313.

7. Vaz, V.M. and L. Kumar, *3D printing as a promising tool in personalized medicine.* Aaps Pharmscitech, 2021. **22**: p. 1-20.

8. Beer, N., et al., *Scenarios for 3D printing of personalized medicines-A case study.* Exploratory Research in Clinical and Social Pharmacy, 2021. **4**: p. 100073.

9. Abrahams, E., G.S. Ginsburg, and M. Silver, *The personalized medicine coalition: goals and strategies.* American Journal of Pharmacogenomics, 2005. **5**: p. 345-355.

10. Bush, W.S., et al., *Bridging the gaps in personalized medicine value assessment: a review of the need for outcome metrics across stakeholders and scientific disciplines.* Public health genomics, 2019. **22**(1-2): p. 16-24.

11. Vicente, A.M., W. Ballensiefen, and J.-I. Jönsson, *How personalised medicine will transform healthcare by 2030: the ICPerMed vision.* Journal of Translational Medicine, 2020. **18**: p. 1-4.

12. Mangoni, A.A., *Comprehensive geriatric assessment and personalized medicine.* Comprehensive geriatric assessment, 2018: p. 69-77.

13. Preis, M. and H. Öblom, *3D-printed drugs for children—are we ready yet?* AAPS PharmSciTech, 2017. **18**: p. 303-308.

14. Verrue, C., et al., *Tablet-splitting: a common yet not so innocent practice.* Journal of advanced nursing, 2011. **67**(1): p. 26-32.

15. Elliott, I., et al., *The practice and clinical implications of tablet splitting in international health.* Tropical Medicine & International Health, 2014. **19**(7): p. 754-760.

16. Gill, D., M. Spain, and B.J. Edlund, *Crushing or splitting medications: unrecognized hazards.* Journal of gerontological nursing, 2012. **38**(1): p. 8-12.

17. Habet, S., *Narrow therapeutic index drugs: clinical pharmacology perspective.* Journal of Pharmacy and Pharmacology, 2021. **73**(10): p. 1285-1291.

18. Blix, H.S., et al., *Drugs with narrow therapeutic index as indicators in the risk management of hospitalised patients.* Pharmacy practice, 2010. **8**(1): p. 50.

19. Marriott, J.F., *Pharmaceutical compounding and dispensing*. 2010: Pharmaceutical Press.

20. Shokri, J., et al., *The effect of surfactants on the skin penetration of diazepam.* International Journal of Pharmaceutics, 2001. **228**(1-2): p. 99-107.

21. Klang, V., et al., *Effect of γ-cyclodextrin on the skin permeation of a steroidal drug from nanoemulsions: Impact of experimental setup.* International Journal of Pharmaceutics, 2012. **423**: p. 535-542.

22. Pflieger, T., et al., *Influence of design parameters on sustained drug release properties of 3D-printed theophylline tablets.* International Journal of Pharmaceutics, 2024: p. 124207.

23. Elbadawi, M., et al., *3D printing tablets: Predicting printability and drug dissolution from rheological data.* International Journal of Pharmaceutics, 2020. **590**: p. 119868.

24. Windolf, H., R. Chamberlain, and J. Quodbach, *Predicting drug release from 3D printed oral medicines based on the surface area to volume ratio of tablet geometry.* Pharmaceutics, 2021. **13**(9): p. 1453.

25. Sharma, V., et al., *Investigations of process parameters during dissolution studies of drug loaded 3D printed tablets.* Proceedings of the Institution of Mechanical Engineers, Part H: Journal of Engineering in Medicine, 2021. **235**(5): p. 523-529.

26. Martinez, P.R., et al., *Influence of geometry on the drug release profiles of stereolithographic (SLA) 3D-printed tablets.* AAPS PharmSciTech, 2018. **19**: p. 3355-3361.

27. Azad, M.A., et al., *Polymers for extrusion-based 3D printing of pharmaceuticals: A holistic materials–process perspective.* Pharmaceutics, 2020. **12**(2): p. 124.

28. Lamichhane, S., et al., *Complex formulations, simple techniques: Can 3D printing technology be the Midas touch in pharmaceutical industry?* Asian journal of pharmaceutical sciences, 2019. **14**(5): p. 465-479.

29. Tian, P., et al., *Applications of excipients in the field of 3D printed pharmaceuticals.* Drug Development and Industrial Pharmacy, 2019. **45**(6): p. 905-913.

30. Deshkar, S., et al., *Hot melt extrusion and its application in 3D printing of pharmaceuticals.* Current Drug Delivery, 2021. **18**(4): p. 387-407.

31. Khaled, S.A., et al., *3D printing of five-in-one dose combination polypill with defined immediate and sustained release profiles.* Journal of controlled release, 2015. **217**: p. 308-314.

32. Khaled, S.A., et al., *3D printing of tablets containing multiple drugs with defined release profiles.* International journal of pharmaceutics, 2015. **494**(2): p. 643-650.

33. Obeid, S., et al., *Predicting drug release from diazepam FDM printed tablets using deep learning approach: Influence of process parameters and tablet surface/volume ratio.* International Journal of Pharmaceutics, 2021. **601**: p. 120507.

34. Sadia, M., et al., *Channelled tablets: An innovative approach to accelerating drug release from 3D printed tablets.* Journal of controlled release, 2018. **269**: p. 355-363.

35. Goyanes, A., et al., *Effect of geometry on drug release from 3D printed tablets.* International journal of pharmaceutics, 2015. **494**(2): p. 657-663.

36. Pourkavoos, N., *Unique risks, benefits, and challenges of developing drug-drug combination products in a pharmaceutical industrial setting.* Combination Products in Therapy, 2012. **2**: p. 1-31.

37. Hilmer, S.N., A.J. McLachlan, and D.G. Le Couteur, *Clinical pharmacology in the geriatric patient.* Fundamental & clinical pharmacology, 2007. **21**(3): p. 217-230.

38. Hughes, C.M., *Medication non-adherence in the elderly: how big is the problem?* Drugs & aging, 2004. **21**: p. 793-811.

39. Pflieger, T., et al., *An Investigation of the Drug Release Kinetics of 3D-Printed Two Compartment Theophylline and Prednisolone Tablets.* SSRN, 2024.

40. Scoutaris, N., S.A. Ross, and D. Douroumis, *3D printed "Starmix" drug loaded dosage forms for paediatric applications.* Pharmaceutical research, 2018. **35**: p. 1-11.

41. Goh, O., et al., *Preferences of healthcare professionals on 3D-printed tablets: a pilot study.* Pharmaceutics, 2022. **14**(7): p. 1521.

42. Goyanes, A., et al., *Patient acceptability of 3D printed medicines.* International journal of pharmaceutics, 2017. **530**(1-2): p. 71-78.

43. Goyanes, A., et al., *Automated therapy preparation of isoleucine formulations using 3D printing for the treatment of MSUD: First single-centre, prospective, crossover study in patients.* International Journal of Pharmaceutics, 2019. **567**: p. 118497.

44. Herrada-Manchón, H., et al., *3D printed gummies: Personalized drug dosage in a safe and appealing way.* International Journal of Pharmaceutics, 2020. **587**: p. 119687.

45. Goyanes, A., et al., *3D printing of medicines: engineering novel oral devices with unique design and drug release characteristics.* Molecular pharmaceutics, 2015. **12**(11): p. 4077-4084.

46. Wang, S., et al., *A review of 3D printing technology in pharmaceutics: technology and applications, now and future.* Pharmaceutics, 2023. **15**(2): p. 416.

47. Chen, G., et al., *Pharmaceutical applications of 3D printing.* Additive Manufacturing, 2020. **34**: p. 101209.

48. Zhang, J., et al., *Advances in the development of amorphous solid dispersions: The role of polymeric carriers.* Asian Journal of Pharmaceutical Sciences, 2023: p. 100834.

49. He, Y. and C. Ho, *Amorphous solid dispersions: utilization and challenges in drug discovery and development.* Journal of pharmaceutical sciences, 2015. **104**(10): p. 3237-3258.

50. Pflieger, T., et al., *Novel Approach to Pharmaceutical 3D-Printing Omitting the Need for Filament—Investigation of Materials, Process, and Product Characteristics.* Pharmaceutics, 2022. **14**(11): p. 2488.

51. Patra, C.N., et al., *Pharmaceutical significance of Eudragit: A review.* Future Journal of Pharmaceutical Sciences, 2017. **3**(1): p. 33-45.

52. BASF, *Technical Data Sheet "Kollidon VA64".* 2022.

53. Repka, M.A., et al., *Melt extrusion with poorly soluble drugs–An integrated review.* International journal of pharmaceutics, 2018. **535**(1-2): p. 68-85.

54. Krishnan, A.V., S.A. Lakshman, and A. Bhargav, *3D Printing and Regulatory Considerations*, in *3D & 4D Printing Methods for Pharmaceutical Manufacturing and Personalised Drug Delivery: Opportunities and Challenges*. 2023, Springer. p. 45-68.

55. Mirza, M. and Z. Iqbal, *3D printing in pharmaceuticals: Regulatory perspective.* Current Pharmaceutical Design, 2018. **24**(42): p. 5081-5083.

56. Cui, M., et al., *Opportunities and challenges of three-dimensional printing technology in pharmaceutical formulation development.* Acta Pharmaceutica Sinica B, 2021. **11**(8): p. 2488-2504.

57. van den Heuvel, K.A., et al., *3D-powder-bed-printed pharmaceutical drug product tablets for use in clinical studies.* Pharmaceutics, 2022. **14**(11): p. 2320.

58. Jamróz, W., et al., *3D printing in pharmaceutical and medical applications–recent achievements and challenges.* Pharmaceutical research, 2018. **35**: p. 1-22.

59. Lima, A.L., et al., *Oscillatory shear rheology as an in-process control tool for 3D printing medicines production by fused deposition modeling.* Journal of Manufacturing Processes, 2022. **76**: p. 850-862.

60. Thumsorn, S., et al., *Rheological behavior and dynamic mechanical properties for interpretation of layer adhesion in FDM 3D printing.* Polymers, 2022. **14**(13): p. 2721.

61. Muehlenfeld, C., et al., *Polymers for Pharmaceutical 3D Printing: Printability and Critical Insight into Material Properties*, in *3D Printing: Emerging Technologies and Functionality of Polymeric Excipients in Drug Product Development*. 2023, Springer. p. 97-137.

62. Nasereddin, J.M., et al., *Development of a simple mechanical screening method for predicting the feedability of a pharmaceutical FDM 3D printing filament.* Pharmaceutical research, 2018. **35**: p. 1-13.

63. Rahman, Z., et al., *Additive manufacturing with 3D printing: progress from bench to bedside.* The AAPS journal, 2018. **20**: p. 1-14.

64. Trenfield, S.J., et al., *Releasing fast and slow: Non-destructive prediction of density and drug release from SLS 3D printed tablets using NIR spectroscopy.* International Journal of Pharmaceutics: X, 2023. **5**: p. 100148.

65. Bendicho-Lavilla, C., et al., *Ensuring the quality of 3D printed medicines: Integrating a balance into a pharmaceutical printer for in-line uniformity of mass testing.* Journal of Drug Delivery Science and Technology, 2024. **92**: p. 105337.

66. El Aita, I., et al., *3D-Printing with precise layer-wise dose adjustments for paediatric use via pressure-assisted microsyringe printing.* European Journal of Pharmaceutics and Biopharmaceutics, 2020. **157**: p. 59-65.

67. Pietrzak, K., A. Isreb, and M.A. Alhnan, *A flexible-dose dispenser for immediate and extended release 3D printed tablets.* European journal of pharmaceutics and biopharmaceutics, 2015. **96**: p. 380-387.

68. Cui, M., et al., *Exploration and preparation of a dose-flexible regulation system for levetiracetam tablets via novel semi-solid extrusion three-dimensional printing.* Journal of Pharmaceutical Sciences, 2019. **108**(2): p. 977-986.

69. Fastø, M.M., et al., *Perceptions, preferences and acceptability of patient designed 3D printed medicine by polypharmacy patients: a pilot study.* International Journal of Clinical Pharmacy, 2019. **41**(5): p. 1290-1298.

70. Januskaite, P., et al., *I spy with my little eye: a paediatric visual preferences survey of 3D printed tablets.* Pharmaceutics, 2020. **12**(11): p. 1100.

71. Regårdh, C.-G. and G. Johnsson, *Clinical pharmacokinetics of metoprolol.* Clinical pharmacokinetics, 1980. **5**(6): p. 557-569.

72. Glynn, L.G., et al., *Interventions used to improve control of blood pressure in patients with hypertension.* Cochrane database of systematic reviews, 2010(3).

73. Carey, R.M., P.K. Whelton, and A.A.H.G.W. Committee*, *Prevention, detection, evaluation, and management of high blood pressure in adults: synopsis of the 2017 American College of Cardiology/American Heart Association Hypertension Guideline.* Annals of internal medicine, 2018. **168**(5): p. 351-358.

74. Gradman, A.H., et al., *Combination therapy in hypertension.* Journal of the American Society of Hypertension, 2010. **4**(2): p. 90-98.

75. Barnes, P.J., *Theophylline.* American journal of respiratory and critical care medicine, 2013. **188**(8): p. 901-906.

76. Wall, G.C., et al., *Pentoxifylline or theophylline use in hospitalized COVID-19 patients requiring oxygen support.* The clinical respiratory journal, 2021. **15**(7): p. 843-846.

77. Dahiya, A., et al., *Role of Etophylline and Theophylline Prolonged Release Tablet in COVID-19 Associated Sinus Node Dysfunction.* The Journal of the Association of Physicians of India, 2022. **70**(1): p. 11-12.

78. Montaño, L.M., et al., *Theophylline: Old drug in a new light, application in COVID-19 through computational studies.* International Journal of Molecular Sciences, 2022. **23**(8): p. 4167.

79. Devereux, G., et al., *Low-dose oral theophylline combined with inhaled corticosteroids for people with chronic obstructive pulmonary disease and high risk of exacerbations: a RCT.* Health technology assessment (Winchester, England), 2019. **23**(37): p. 1.

80. Siddharthan, T., et al., *Effectiveness of low-dose theophylline for the management of biomass-associated COPD (LODOT-BCOPD): study protocol for a randomized controlled trial.* Trials, 2021. **22**: p. 1-9.

81. Cosio, B.G., et al., *Low-dose theophylline enhances the anti-inflammatory effects of steroids during exacerbations of COPD.* Thorax, 2009. **64**(5): p. 424-429.

82. Barnes, P.J., *Therapy of chronic obstructive pulmonary disease.* Pharmacology & therapeutics, 2003. **97**(1): p. 87-94.

83. Williams, D.M., *Clinical pharmacology of corticosteroids.* Respiratory care, 2018. **63**(6): p. 655-670.

84. Singh, J., et al., *Corticosteroid therapy for patients with acute exacerbations of chronic obstructive pulmonary disease: a systematic review.* Archives of internal medicine, 2002. **162**(22): p. 2527-2536.

85. Pickup, M., *Clinical pharmacokinetics of prednisone and prednisolone.* Clinical pharmacokinetics, 1979. **4**: p. 111-128.

86. Poetker, D.M. and D.D. Reh, *A comprehensive review of the adverse effects of systemic corticosteroids.* Otolaryngologic Clinics of North America, 2010. **43**(4): p. 753-768.

87. Samiei, N., *Recent trends on applications of 3D printing technology on the design and manufacture of pharmaceutical oral formulation: a mini review.* Beni-Suef University Journal of Basic and Applied Sciences, 2020. **9**: p. 1-12.

88. Larrucea, E., et al., *Combined effect of oleic acid and propylene glycol on the percutaneous penetration of tenoxicam and its retention in the skin.* European Journal of Pharmaceutics and Biopharmaceutics, 2001. **52**(2): p. 113-119.

89. Wang, J., et al., *Stereolithographic (SLA) 3D printing of oral modified-release dosage forms.* International journal of pharmaceutics, 2016. **503**(1-2): p. 207-212.

90. Deshmane, S., et al., *Stereolithography 3D printing technology in pharmaceuticals: a review.* Drug Development and Industrial Pharmacy, 2021. **47**(9): p. 1362-1372.

91. Mohammed, A.A., et al., *3D Printing in medicine: Technology overview and drug delivery applications.* Annals of 3D Printed Medicine, 2021. **4**: p. 100037.

92. Rautamo, M., et al., *3PC-031 Usability of semi-solid extrusion 3D printing in hospital pharmacy settings to produce personalised oral medications for paediatric patients*. 2024, British Medical Journal Publishing Group.

93. Santoyo, S., et al., *Penetration enhancer effects on the in vitro percutaneous absorption of piroxicam through rat skin.* International Journal of Pharmaceutics, 1995. **117**(2): p. 219-224.

94. Cevc, G. and G. Blume, *Hydrocortisone and dexamethasone in very deformable drug carriers have increased biological potency, prolonged effect, and reduced therapeutic dosage.* Biochimica et Biophysica Acta (BBA) - Biomembranes, 2004. **1663**(1–2): p. 61-73.

95. *Patent EP4264617A1: Method for producing patient-optimised dosage forms*. 2021, Dihesys Digital Health Systems GmbH.

96. *Patent WO2021198308A1: Apparatus and method for 3d-printing medicament mixtures to form pharmaceutical administration forms using a rotatable or movable material supply device*. 2021, Dihesys Digital Health Systems GmbH.

97. *Patent WO2023094565A1: Printing apparatus and additive manufacturing method comprising automatic position calibration*. 2021, Dihesys Digital Health Systems GmbH.

98. *Patent DE202022002120U1: Printing device for additive manufacturing processes with screw device for material feeding*. 2022, Dihesys Digital Health Systems GmbH.

99. Fahr, A., *Voigt's pharmaceutical technology*. 2018: John Wiley & Sons.

100. Florian-Algarin, M. and R. Méndez, *Blend uniformity and powder phenomena inside the continuous tumble mixer using DEM simulations.* AIChE Journal, 2015. **61**(3): p. 792-801.

101. Jonat, S., *The mechanism of hydrophilic and hydrophobic colloidal silicon dioxide types as glidants*. 2005, Universität Tübingen.

102. Ghebre-Sellassie, I., et al., *Pharmaceutical extrusion technology*. 2003: CRC Press.

103. Laske, S., et al., *Continuous Melt Extrusion and Direct Pelletization.* Continuous Manufacturing of Pharmaceuticals, 2017: p. 337-368.

104. *Quadro Engineering Inc. "Quadro Comil Data Sheet"*. 2024.

105. Hickey, A.J. and S. Giovagnoli, *Pharmaceutical powder and particles*. 2018: Springer.

106. Muley, S., T. Nandgude, and S. Poddar, *Extrusion–spheronization a promising pelletization technique: In-depth review.* Asian journal of pharmaceutical sciences, 2016. **11**(6): p. 684-699.

107. Loh, Z.H., A.K. Samanta, and P.W.S. Heng, *Overview of milling techniques for improving the solubility of poorly water-soluble drugs.* Asian journal of pharmaceutical sciences, 2015. **10**(4): p. 255-274.

108. Quodbach, J., et al., *Quality of FDM 3D printed medicines for pediatrics: considerations for formulation development, filament extrusion, printing process and printer design.* Therapeutic Innovation & Regulatory Science, 2021: p. 1-19.

109. Gottschalk, N., et al., *Brittle polymers in Fused Deposition Modeling: An improved feeding approach to enable the printing of highly drug loaded filament.* International Journal of Pharmaceutics, 2021. **597**: p. 120216.

110. Jakubowska, E. and N. Ciepluch, *Blend segregation in tablets manufacturing and its effect on drug content uniformity—a review.* Pharmaceutics, 2021. **13**(11): p. 1909.

111. Norman, J., et al., *A new chapter in pharmaceutical manufacturing: 3D-printed drug products.* Advanced drug delivery reviews, 2017. **108**: p. 39-50.

112. Prime, R.B., et al., *Thermogravimetric analysis (TGA).* Thermal analysis of polymers: Fundamentals and applications, 2009: p. 241-317.

113. Gill, P., T.T. Moghadam, and B. Ranjbar, *Differential scanning calorimetry techniques: applications in biology and nanoscience.* Journal of biomolecular techniques: JBT, 2010. **21**(4): p. 167.

114. Höhne, G.W.H., W. Hemminger, and H.-J. Flammersheim, *Differential scanning calorimetry*. Vol. 2. 2003: Springer.

115. Larson, R.G., *The structure and rheology of complex fluids*. Vol. 150. 1999: Oxford university press New York.

116. Shaw, M.T. and W.J. MacKnight, *Introduction to polymer viscoelasticity*. 2018: John Wiley & Sons.

117. Rudolph, N. and T.A. Osswald, *Polymer rheology: fundamentals and applications*. 2014: Carl Hanser Verlag GmbH Co KG.

118. Carnicer, V., et al., *Microfluidic rheology: A new approach to measure viscosity of ceramic suspensions at extremely high shear rates.* Open Ceramics, 2021. **5**: p. 100052.

119. Boetker, J., et al., *Modifying release characteristics from 3D printed drug-eluting products.* European Journal of Pharmaceutical Sciences, 2016. **90**: p. 47-52.

120. Jackson, S. and T. Dickens, *Rheological and structural characterization of 3D-printable polymer electrolyte inks.* Polymer Testing, 2021. **104**: p. 107377.

121. *European Pharmacopoeia (Ph. Eur.)*. Vol. 11. 2023: European Directorate for the Quality of Medicines & Healthcare.

122. *"Uniformity of dosage units" in European Pharmacopoeia (Ph. Eur.)*. 2023, European Directorate for the Quality of Medicines & Healthcare.

123. *"Uniformity of mass of single dose dosage forms" in European Pharmacopoeia (Ph. Eur.)*. 2023, European Directorate for the Quality of Medicines & Healthcare.

124. Long, M. and Y. Chen, *Dissolution testing of solid products*, in *Developing solid oral dosage forms*. 2009, Elsevier. p. 319-340.

125. Dressman, J.B. and J. Krämer, *Pharmaceutical dissolution testing*. 2005, Taylor & Francis Boca Raton, FL:.

126. Elmas, A., et al., *Mathematical modelling of drug release.* Research on Engineering Structures and Materials, 2020. **6**(4).

127. Bruschi, M.L., *Strategies to modify the drug release from pharmaceutical systems*. 2015: Woodhead Publishing.

128. Yu, L.X., *Pharmaceutical quality by design: product and process development, understanding, and control.* Pharmaceutical research, 2008. **25**: p. 781-791.

129. Yu, L.X., et al., *Understanding pharmaceutical quality by design.* The AAPS journal, 2014. **16**: p. 771-783.

130. Antony, J., *Design of experiments for engineers and scientists*. 2023: Elsevier.

131. Roy, R.K., *A primer on the Taguchi method*. 2010: Society of manufacturing engineers.

132. Klein, B., *Versuchsplanung–Design of Experiments: Einführung in die Taguchi und Shainin-Methodik*. 2021: Walter de Gruyter GmbH & Co KG.

133. Peters, S.A., *Physiologically based pharmacokinetic (PBPK) modeling and simulations: principles, methods, and applications in the pharmaceutical industry*. 2021: John Wiley & Sons.

134. Willmann, S., et al., *PK-Sim®: a physiologically based pharmacokinetic 'whole-body'model.* Biosilico, 2003. **1**(4): p. 121-124.

2. Objectives

The overall objective of this thesis was to examine pharmaceutical 3DP as a comprehensive concept and further develop this novel technology into a real-life application, so that patients and the healthcare sector can benefit from it in the future. For this purpose, a novel printing technology called “granules-fed single screw extrusion FDM”, was used, which has not yet been studied or described in detail. While extensive characterization work has been done for filament-fed FDM printers in the pharmaceutical field, this has not been the case for a granules-fed system. Therefore, it was necessary to scout and understand the key parameters that influence successful printability of a pharmaceutical granule formulation. In the first part of this work, the goal was to develop a system that could predict the printability and suitability of pharmaceutical granules for the corresponding application and printer geometry based on its melt rheology. To achieve this, a set of different polymers with a model drug was tested for printability at various temperatures and thus rheological properties. Target regimes were established concerning the complex viscosity and the ratio of the storage modulus to the loss modulus, ensuring a successful 3DP process without unwanted extrusion defects. Once a basic technological understanding was developed, the second study aimed to investigate the parameters controlling the drug release kinetics of a 3D printed sustained release dosage form. The drug TPH was employed, which, as an NTW drug in the field of pulmonary diseases, is suitable for individualized delivery via 3DP. The objective was to examine the influence of the four main parameters “drug content of formulation”, “tablet scale factor”, “tablet body infill”, and “tablet volume” on drug release retardation using a fractional factorial experimental design and statistical analysis. The effect sizes and statistical significances of these parameters are essential for understanding which design parameters are truly decisive in controlling drug release. These four parameters were chosen because they can be practically modified on-demand to achieve different drug release rates and are therefore most relevant. In the course of the work for a third study, this research was further expanded to develop a bi-tablet containing two distinctive drugs, TPH and PSL. The goal was not only to find a suitable design that allows the combination of the two APIs but also to develop a dosage form that permits drug personalization through layer adaptation without significantly affecting the proportional drug release. The combination of a sustained release compartment and an immediate release compartment in a single 3D printed bi-tablet is novel and, according to the latest scientific findings, can be particularly effective in helping to manage exacerbations of pulmonary diseases.

3. Novel Approach to Pharmaceutical 3D-Printing Omitting the Need for Filament — Investigation of Materials, Process, and Product Characteristics

Thomas Pflieger[1], Rakesh Venkatesh[1], Markus Dachtler[1,2], Karin Eggenreich[2], Stefan Laufer[3], Dominique Lunter[4,*]

[1] DiHeSys Digital Health Systems GmbH, 73529 Schwäbisch Gmünd, Germany

[2] Gen-Plus GmbH & Co. KG, 81477 Munich, Germany

[3] Pharmaceutical Chemistry, Eberhard Karls University, 72074 Tübingen, Germany

[4] Pharmaceutical Technology, Eberhard Karls University, 72074 Tübingen, Germany

* Corresponding author

Pharmaceutics

Year 2022, Volume 14, Issue 11, Pages 2488-2504
DOI: https://doi.org/10.3390/pharmaceutics14112488

pharmaceutics

MDPI

Article

Novel Approach to Pharmaceutical 3D-Printing Omitting the Need for Filament—Investigation of Materials, Process, and Product Characteristics

Thomas Pflieger [1], Rakesh Venkatesh [1], Markus Dachtler [1,2], Karin Eggenreich [2], Stefan Laufer [3] and Dominique Lunter [4,*]

[1] Digital Health Systems GmbH (DiHeSys), 73529 Schwaebisch Gmuend, Germany
[2] Gen-Plus GmbH & Co., KG, 81477 Munich, Germany
[3] Pharmaceutical Chemistry, Eberhard Karls University, 72074 Tuebingen, Germany
[4] Pharmaceutical Technology, Eberhard Karls University, 72074 Tuebingen, Germany
* Correspondence: dominique.lunter@uni-tuebingen.de; Tel.: +49-7071-2974558

Abstract: The utilized 3D printhead employs an innovative hot-melt extrusion (HME) design approach being fed by drug-loaded polymer granules and making filament strands obsolete. Oscillatory rheology is a key tool for understanding the behavior of a polymer melt in extrusion processes. In this study, small amplitude shear oscillatory (SAOS) rheology was applied to investigate formulations of model antihypertensive drug Metoprolol Succinate (MSN) in two carrier polymers for pharmaceutical three-dimensional printing (3DP). For a standardized printing process, the feeding polymers viscosity results were correlated to their printability and a better understanding of the 3DP extrudability of a pharmaceutical formulation was developed. It was found that the printing temperature is of fundamental importance, although it is limited by process parameters and the decomposition of the active pharmaceutical ingredients (API). Material characterization including differential scanning calorimetry (DSC) and thermogravimetric analyses (TGA) of the formulations were performed to evaluate component miscibility and ensure thermal durability. To assure the development of a printing process eligible for approval, all print runs were investigated for uniformity of mass and uniformity of dosage in accordance with the European Pharmacopoeia (Ph. Eur.).

Keywords: pharmaceutical three-dimensional printing (3DP); hot-melt extrusion (HME); printability; oscillatory rheology; novel printhead design

Citation: Pflieger, T.; Venkatesh, R.; Dachtler, M.; Eggenreich, K.; Laufer, S.; Lunter, D. Novel Approach to Pharmaceutical 3D-Printing Omitting the Need for Filament—Investigation of Materials, Process, and Product Characteristics. *Pharmaceutics* **2022**, *14*, 2488. https://doi.org/10.3390/pharmaceutics14112488

Academic Editor: Ingunn Tho

Received: 5 October 2022
Accepted: 11 November 2022
Published: 17 November 2022

1. Introduction

Recent advances in additive manufacturing including 3D printing have undoubtedly had a major global influence on technology across different fields [1]. Numerous drug delivery systems and devices in the medical and pharmaceutical sector are already being successfully printed in a research environment. In regard to the pharmaceutical industry, additive manufacturing offers the option of extensive medication customization [1–4]. Integrating additive processes has several advantages over the current, well-established but outdated and rigid "one size fits all" approach that provides limited flexibility in dosage tailoring [1,3]. Aside from the two major advantages of avoiding medication errors and enabling a flexible treatment to the patient, printing tailored oral dosage forms is financially attractive for both costly medications as well as small scale on-demand production [3–5]. The development of dosage forms, production of sample batches, and modification of samples can be done with little effort compared to generic powder-pressed tablets or filled capsules which require heavy pharmaceutical machinery [4,5]. Alongside the mentioned advantages of pharmaceutical 3DP, the technology enables prompt assessment of feasibility and applicability of highly complex dosage forms and devices. Recent research efforts reveal that innovations such as personalized fluoride-eluting mouthguards, individualized

nasal piston devices, compartment-, combi-, core-, shell-, alternating-, bi-, or poly-pills are solely possible thanks to advances in pharmaceutical 3DP technology [6–10].

Currently, the majority of drug formulations have a predetermined dosage of one or more active pharmaceutical ingredients (API) [4,11]. This does not adapt to the physiological constitution of the patient. Dosing drugs accurately depends on genetic, metabolic, and gender-specific properties as well as disease state [3,12]. Highly potent drugs in particular have a narrow therapeutic window, which varies from patient to patient. This calls for an individual treatment through personalized healthcare. Non-tailored drugs fail to meet the requirements for treating patients immaculately and there is the possibility of dosing inaccuracy [13].

Hypertension (HTN) is a medical condition in which blood pressure is persistently elevated. Long-term high blood pressure levels lead to an increased risk for cardiovascular and renal complications [14]. Therapy for stage one hypertension incorporates β1-receptor blockers such as the model drug Metoprolol Succinate (MSN) [14,15]. In practice, the administration of hypertension reducers is implemented by a stepwise controlled care approach to reach target levels of blood pressure improvement [16]. During the course of the treatment, various medications with different doses are administered [14,16]. This is where pharmaceutical on-demand printing comes in handy. 3DP technology offers the possibility to customize dosage forms in coordination with the therapeutic progression [1].

The 3D printhead used in this work utilizes a special functional principle. The Flexdose^{TM} printer (FDP) developed by DiHeSys: Digital Health Systems GmbH (DiHeSys) is an extrusion-based printer, whereby the feeding is achieved by granules. The granules comprise pharmaceutical polymer formulations that hold particular active ingredients and are prepared by table-top HME starting from powder formulations. This FDM printhead gradually builds up three-dimensional oral dosage forms by dispensing polymer melt through an extruder nozzle in horizontal layers. FDM emerged to the most used 3D printing technique in pharmaceutical research and development due to its economic acquisition cost and reasonably low equipment and setup requirements [17–19]. This technology offers extensive design freedom, the ability to realize complex structures, and rapid prototyping [17,18]. The printing success is based on a sophisticated interplay between model design, hardware, process parameters, and polymer formulation [17,19].

To overcome the filament strand limitation for pharmaceutical fused deposition modeling (FDM), alternative extrusion methods such as powder and pellet direct extrusion have come into focus just recently [20–22]. As the literature for filament-fed printheads exhibits, the fabrication of suitable filament materials is difficult [18,23,24]. The strand must fulfill precise mechanical requirements to be able to be fed regularly by gear wheels and the printer only allows small deviations in the filament diameter [18,25]. These problems do not arise with the granules system. To ensure continuous extrusion, the complex melt viscosity of the viscoelastic polymer granules must be examined and adapted to the specific properties of the extrusion channel design [26].

The aim of this study was to investigate crucial process parameters for DiHeSys' novel granules-fed pharmaceutical Flexdose^{TM} printer emphasizing melt rheology of printable MSN polymer systems and characterization of product printlets. Regarding the final drug delivery systems, an immediate release (IR) of the model drug is aimed for. Therefore, the pharma-grade IR polymers KVA64 and EPO were utilized. These include a co-povidone polymer with an erodible instant release matrix and a methacrylate co-polymer that is soluble in acidic media, respectively. The polymers' solubility attributes suit the in vitro dissolution method applied in this work.

2. Materials and Methods

2.1. Materials

The model substance used was the hypertension drug Metoprolol Succinate (MSN) with purity >98% supplied by Hangzhou Longshine Bio-Tech Co., Ltd., Hangzhou, China. The polymers Kollidon® VA64 (KVA64) and Eudragit® E PO (EPO) were kindly donated by

BASF Pharma SE, Ludwigshafen, Germany and Evonik AG, Essen, Germany, respectively. The pharma grade plasticizer Lipoxol® 6000 (PEG) was obtained from Sasol Chemicals AG, Johannesburg, South Africa. All chemicals used were of analytical grade and used as received.

2.2. Methods

2.2.1. Formulation of Blends

The formulations consist of a single carrier and diluent polymer KVA64 or EPO, model drug MSN and plasticizer PEG optionally. The formulation compositions can be found in Table 1. The blends represent the final formulations that were used for additive manufacturing. The batch size for each of the four formulations was 50 g. Blend components were pre-weighed and three-step geometrically mixed at 49 rpm for 15 min in a Turbula® T2F tumble mixer from WAB Group AG, Muttenz, Switzerland.

Table 1. Compositions and designations of the formulations consisting of Metoprolol Succinate (MSN), Kollidon VA64 (KVA64), Eudragit E PO (EPO), or Lipoxol® 6000 (PEG).

Formulation	MSN (% *w/w*)	KVA64 (% *w/w*)	EPO (% *w/w*)	PEG (% *w/w*)
KVA64/PEG	-	70	-	30
KVA64/PEG/MSN	25	65	-	5
EPO	-	-	100	-
EPO/MSN	25	-	75	-

2.2.2. Production of Granules

The prepared physical mixtures underwent twin-screw hot melt extrusion with lab scale extruder ZE HM9 from Three Tec GmbH, Seon, Switzerland. The module comprises co-rotating elements with a die diameter of 2 mm. Table 2 shows extrusion temperatures, torques, and screw speeds set and obtained for HME of each blend. The extrusion channel consists of three equivalent temperature zones. The extrusion screws are solely conveying screws and have no kneading elements. Since the filament diameter of the output is irrelevant for the production of granules, it has not been monitored. The extrudates were kept in sealed plastic bags to avoid moisture sorption. The extrudate strands were downsized to granules through rasp sieve milling with a U5 Comil® from Quadro Engineering Corp., Waterloo, Canada, at 250 rpm. Granules with maximum diameter of 2 mm were obtained. Granules less than 0.6 mm in size were separated using a stack sieve.

Table 2. Twin-screw tabletop HME parameters for the production of selected polymer blends.

	KVA64/PEG	KVA64/PEG/MSN	EPO	EPO/MSN
Extrusion T. (°C)	100	100	140	140
Torque (N·m)	2.0	2.2	2.4	2.1
Screw speed (rpm)	100	100	100	100
3DP T. (°C)	140	140	180	140

2.2.3. Printlet Design and 3D Printing Process

Tablets were fabricated by 3DP using the pharmaceutical 3D extruder printer from DiHeSys GmbH, Schwaebisch Gmuend, Germany. Figure 1 shows the biplane tablet printed in this work. The stereolithography template (r = 6.00 mm; h = 6.00 mm; V = 0.679 cm^3) was sliced into g-code (.gcode) with Ultimaker® Cura 4.10.0 by Ultimaker B.V., Utrecht, Netherlands. For printlet mass scalability and mass uniformity studies, the mentioned stereolithography template was additionally scaled to a volume of 75% (r = 5.45 mm; h = 5.45 mm; V = 0.509 cm^3) and 50% (r = 4.76 mm; h = 4.76 mm; V = 0.339 cm^3). Tablets were printed using standardized settings as follows: fine resolution slicing; extrusion factor

1.131 mm^3/s; speed factor 25 mm/s; wall thickness by three circumnavigations; 100% body infill; no base brim, supports, or rafts; build plate temperature of 50 °C. The nozzle temperature was set according to the respective formulation as stated in Table 2.

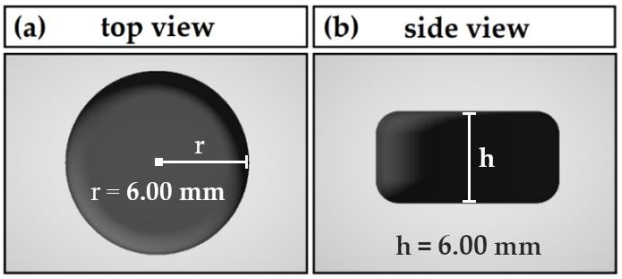

Figure 1. Dimensions and appearance of biplane tablet printlet: (**a**) top view; (**b**) side view.

2.2.4. Printability Runs

A print run is considered successful under the requirement of continuous polymer melt extrusion without major print defects, clogging, polymer melt backflow, or generation of printer casing damaging backpressure for at least 24 min (3 × 8 min). This is the time required to print three standard 100% body infilled biplane tablets at standard extrusion and moving speed. The printlet shows no free spaces, air hollows, irregularities, warping, sharp edges, under- or over-extrusion, offsets, stringing, or other undesirable effects.

2.2.5. Differential Scanning Calorimetry (DSC)

The DSC studies were carried out on a DSC 1 from Mettler Toledo, Columbus, OH, USA, using 100 µL aluminum crucibles with 8–15 mg of sample in duplicates. Working conditions covered a range of 25 °C to a maximum of 175 °C with a heating rate of 10 °C/min, under nitrogen atmosphere with a flow rate of 30 mL/min. The tests were performed on physical mixtures and granules to follow the API physical state conversions along different processing steps.

2.2.6. Thermogravimetric Analysis (TGA)

The proportional weight loss was determined by a STA 409 PC/PG Luxx® from Netzsch GmbH, Selb, Germany, in nitrogen atmosphere (flowrate 20 mL/min) from 30 °C to 230 °C with a heating rate of 10 °C/min. Duplicate tests were performed on unprocessed substances, blended physical mixtures, and granules in order to choose processing temperatures that would not result in harmful degradation effects. All samples were measured no later than one day after production.

2.2.7. Rheology: Small Amplitude Oscillatory Shear (SAOS)

The SAOS tests were performed with a Physica MCR301 Rheometer from Anton Paar GmbH, Graz, Austria, in oscillation mode with parallel plate configuration. Rheological measurements exclusively involved extruded blends. Samples were placed on a pre-heated Peltier plate, melted, and compressed to a 1.0 mm gap by a 25 mm diameter disposable stainless steel plate. The measurements were performed within the linear viscoelastic region (LVR), established by strain sweeps executed at the minimal processing temperature. Strain sweeps were conducted from 0.01% to 10.0% strain at 10 rad/s angular frequency. Consequently, frequency sweeps were performed within the LVR range at decreasing angular frequencies from 500 to 1 rad/s as to determine material viscoelastic behavior in relation to time and frequency. The rheological evaluations were carried out in duplicates.

2.2.8. Uniformity of Mass of Single-Dose Dosage Forms

For the development of an applicable process, a high degree of printlet mass uniformity is crucial. In accordance with the European Pharmacopoeia 2.9.5 "Uniformity of mass of single-dose dosage forms", ten single oral dosage forms (ODFs) were printed with

formulations KVA64/PEG/MSN and EPO/MSN [27]. For ODFs with a mass of more than 250 mg, it is required that not more than one of the individual masses deviate from the average by more than 5% and none deviates by more than 10%. For each preparation, 20 tablets were weighed individually and the arithmetic mean masses and standard deviations were calculated following the mentioned monograph.

2.2.9. Evaluation of Content Uniformity

The uniformity of dosage units was evaluated according to the European Pharmacopoeia 2.9.40 "Uniformity of dosage units" [28]. Regarding the monograph, the acceptance value (AV) was calculated for each batch. The AV is required to not exceed a value of 15 (limit 1; L1). If the requirements for the first testing level (n = 10) are not met, 20 additional dosage forms need to be evaluated and the total AV is not allowed to exceed 15. In addition, no single dose may deviate from the reference value by more than 25% (limit 2; L2). For the sampling of 3DP tablets, 10 separate specimens were used and measured using the analytical method described below.

The preparations were crushed using a mortar and pestle. The samples were mixed with acetonitrile, agitated for 12 h and filtered through a 0.45 µm filter from Millipore Ltd., Dublin, Ireland. The individual contents of model drug were determined by UV-HPLC Agilent 1200 series from Agilent Technologies Inc., Santa Clara, CA, USA. The eluent was screened at a wavelength of 223 nm. The method showed linearity between 1 and 280 mg/L with R^2 = 0.99996 under the same conditions. The limit of detection (LOD) and the limit of quantitation (LOQ) for MSN were estimated to be 0.06 mg/L and 0.10 mg/L, respectively.

2.2.10. In Vitro Dissolution

Determination of the in vitro drug release was performed using USP type II dissolution apparatus Sotax AT7 from Sotax AG, Basel, Switzerland, in 900 mL of 0.1 M hydrochloric acid at 37 °C with a paddle speed of 100 rpm. Sampling was executed every 5 min for the first 20 min, every 15 min of the following 2 h, and continuing with every hour up to 4 h. Dissolution studies were performed in triplicate and the average proportional cumulative drug release was plotted as a function of time. The MSN concentration in the dissolution medium was measured using a HP 8453 UV-Vis Spectrophotometer from Agilent Technologies Inc., Santa Clara, CA, USA, at a wavelength of 223 nm in a 1 cm cell versus a blank solution consisting of 0.1 M hydrochloric acid. The applied calibration range was between 1 and 280 mg/L. The LOD and LOQ were found to be 0.17 mg/mL and 0.50 mg/L, respectively (R^2 = 0.99997).

3. Results

3.1. Thermogravimetric Analysis

During the production process of 3D printed dosage forms, the substances are exposed to elevated temperatures in two separate processes. These include tabletop extrusion to produce drug loaded granules and the actual 3D printing process. Shear forces, inner friction, and other temperature increasing deviations can occur during these process steps. Thus, all formulations are supposed to be processed below the decomposition temperatures of the pure API and at lowest possible processing temperatures in general. Since temperature degradation of the API and other excipients must be avoided during all process steps, TGA measurements were performed. Samples are considered to be thermally stable up to an accumulated gravimetric mass loss of 3%.

The degradation temperature of pure drug MSN was found to be 177 °C (Figure 2a). The sample did not show water evaporation, which leads to the assumption that the drug batch is dry. The placebo systems KVA64/PEG and EPO are thermally stable over the entire observed temperature range up to 230 °C (Figure 2b). The initial mass plateau drops are attributed to the loss of adsorbed water in both cases. While EPO lost 0.6 wt.%, KVA64/PEG lost 2.4 wt.% adsorbed water. This trend also continues with physical mixtures and extruded granules. The KVA64-based systems draw more moisture than the EPO-based blends.

Starting from the plateau, after complete moisture evaporation, KVA64/PEG/MSN and EPO/MSN blends show decomposition temperatures of 212 °C and 206 °C pre-extrusion, respectively (Figure 2c). While EPO/MSN granules show a comparatively low water content of 0.72 wt.%, KVA64/PEG/MSN granules' water content increased to 2.9 wt.%. The results indicate that the additional HME processing step influences the samples by making them more vulnerable to water absorption. Since the samples were transferred directly into sealed plastic bags after extrusion, the moisture sorption must have occurred during HME processing. Starting from the dry plateaus, KVA64/PEG/MSN and EPO/MSN granules are thermally stable up to 207 °C and accordingly 206 °C (Figure 2d).

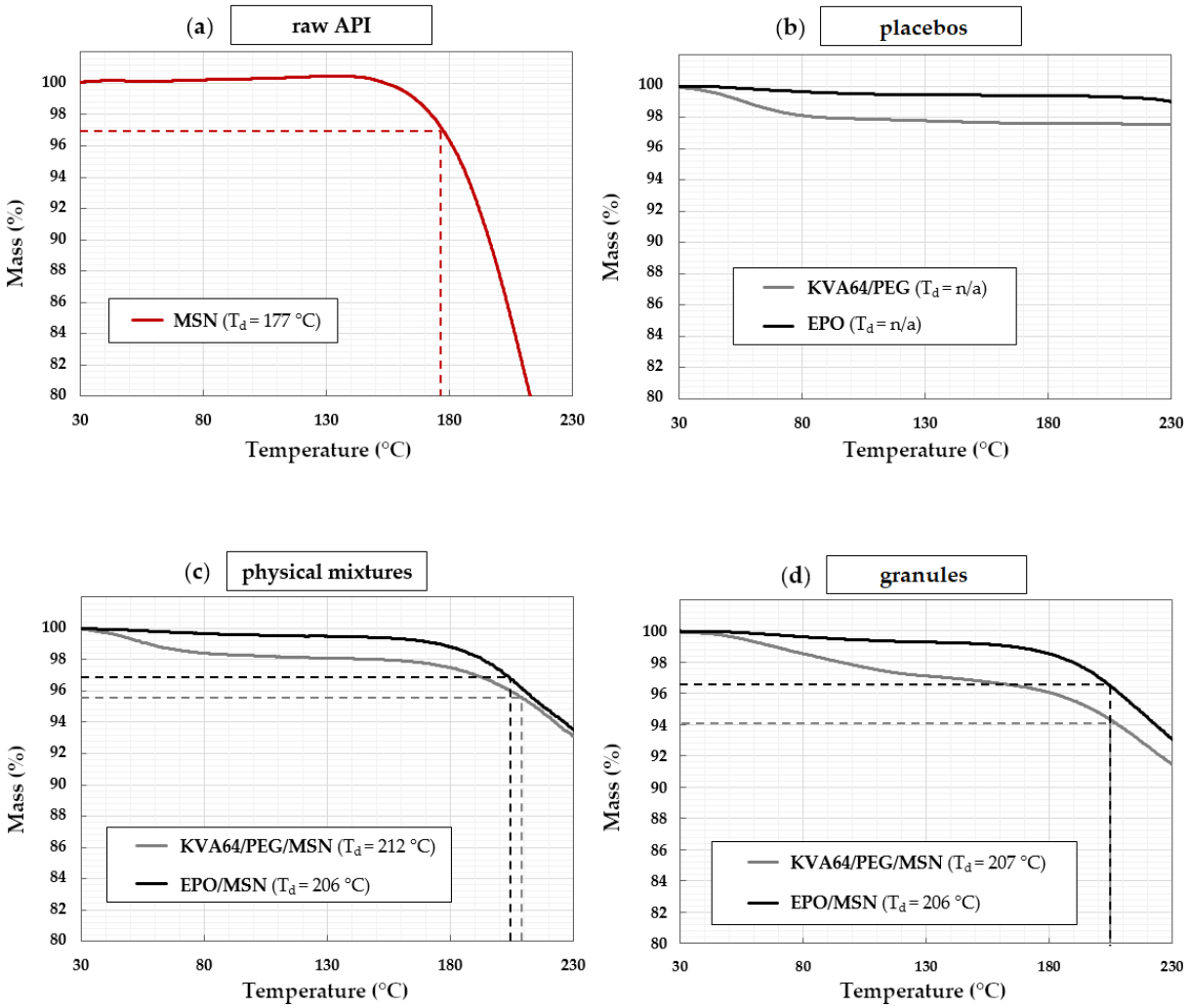

Figure 2. TGA results: (**a**) model drug MSN; (**b**) placebo polymers KVA64/PEG and EPO; (**c**) pre-HME physical mixtures KVA64/PEG/MSN and EPO/MSN; (**d**) post-HME granulated KVA64/PEG/MSN and EPO/MSN.

3.2. Differential Scanning Calorimetry

DSC data of formulations KVA64/PEG/MSN, EPO/MSN and according single blend components are shown in Figures 3 and 4. Raw model drug MSN's melting point was found to onset at 138 °C, as expected (Figure 3a) [29]. All formulations that contain MSN indeed display this melt peak to a certain extent (Figures 3d–f and 4c–e). This indicates that MSN is partially present in crystalline form in both polymer matrixes no matter if post- or pre-HME [30]. As no amorphous solid dispersion was aimed for, this result is acceptable. It should be mentioned that exothermic events only occur during the analysis

of EPO/MSN granules and 3D extrudates (Figure 4d,e). The KVA64-based formulation shows no exothermic events (Figure 3d–f).

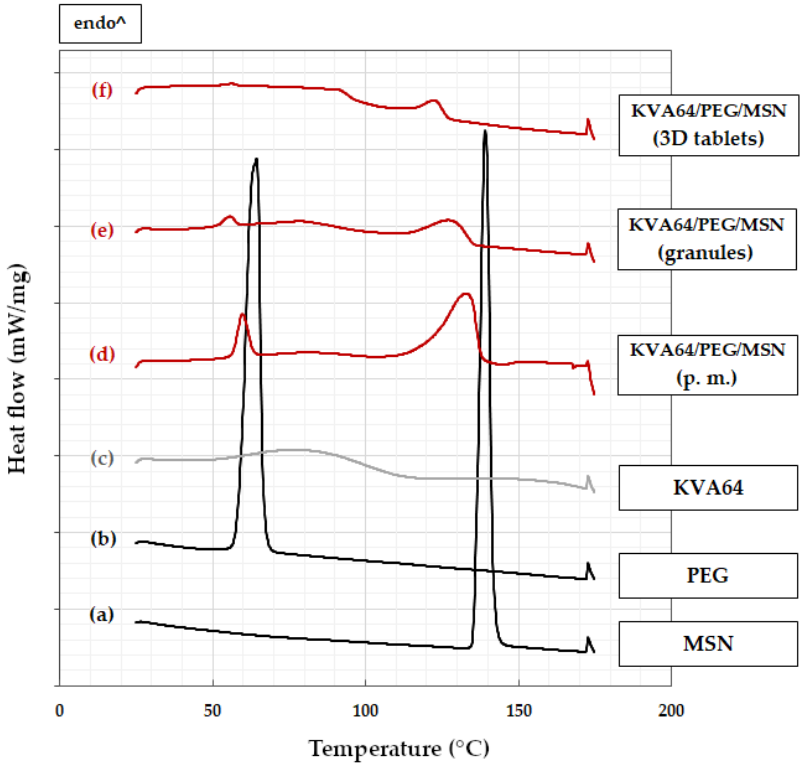

Figure 3. DSC measurements: (**a**) MSN; (**b**) PEG; (**c**) KVA64; (**d**) KVA64/PEG/MSN physical mixture (p. m.); (**e**) KVA64/PEG/MSN granules; (**f**) KVA64/PEG/MSN 3D-printed tablets.

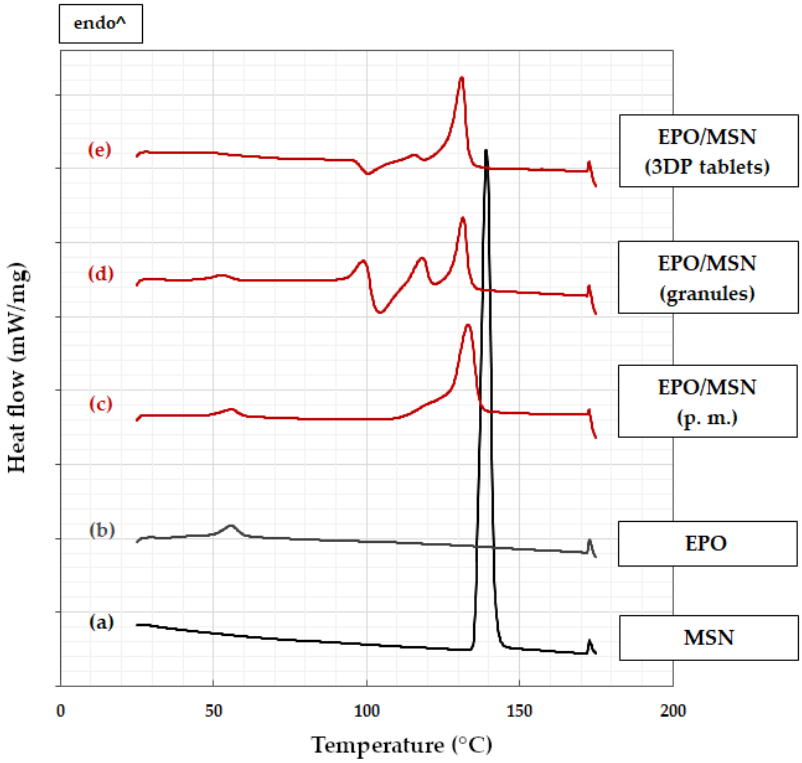

Figure 4. DSC measurements: (**a**) MSN; (**b**) EPO; (**c**) EPO/MSN physical mixture (p. m.); (**d**) EPO/MSN granules; (**e**) EPO/MSN 3D-printed tablets.

3.2.1. KVA64-Based Formulation

In KVA64PEG/MSN samples, model drug melting point depression occurs increasing with processing step progress (Figure 3d–f). From physical mixture to post-print tablet, the intensity of the MSN and PEG melting signals decrease. This indicates progressively enhanced solution of these two substances in the carrier polymer. Nevertheless, the model drugs saturation limit seems to be reached. Due to desorption of water, raw polymer KVA64 has a broad endothermic peak in the moderate temperature range below 100 °C (Figure 3c), which cannot be found to the same extent in processed samples.

3.2.2. EPO-Based Formulation

MSN has reached its solubility capacity in EPO, since the intensity of the model drug melting peak remains identical across all processing steps (Figure 4c–e). EPO/MSN granules' DSC data at 90–125 °C is particularly remarkable (Figure 4d). While the actual MSN melting peak persists, endothermic and exothermic events occur in this area in a narrow temperature range in direct succession. After processing the granules into tablets, this area changes into two clear single thermal events almost identical to the thermal events in the physical mixture (Figure 4e). By reason of low water content in pure EPO, no water desorption can be detected, only a weak endothermic signal of unknown origin (Figure 4b).

3.3. Small Amplitude Oscillatory Shear Rheology

3.3.1. Technical Challenges Regarding Melt Viscosity

There are two main viscosity-related issues causing damage to the extrusion channel or ceasing material output which can be understood with rheology measurements. For continuous extrusion, the already mentioned qualitative effects "clogging" and "polymer melt backflow" must be avoided by controlling the polymer melt rheology. The term clogging describes highly viscous polymer melt building up a clog alongside the extrusion channel that blocks polymer conveying [26,31]. It leads to elevated torques, backpressure, and risk of jamming [26,31]. Polymer melt backflow is an undesirable effect in HME where low-viscous polymer melt is migrating in direction of the channel top instead of the nozzle [32]. Chiruvelle et al. showed that the aforementioned flow phenomenon is strongly linked to the viscosity of the polymer via the energy equation [33]. The viscosity of non-Newtonian fluids is a function of temperature and shear rate [32,33]. Polymer melt backflow restrains polymer conveying, extrusion, and therefore material output.

3.3.2. Establishing Target Rheological Properties with Placebos

To establish a first estimation of target rheological parameters, printability runs were performed with the placebo formulations at different temperatures. The aim was to identify a relation between rheological properties of a polymer system and its printability. A formulation was considered printable if it exhibited continuous extrusion of the polymer melt without substantial print errors, clogging, polymer melt backflow, or formation of casing damaging backpressure for 3DP of at least three tablets. The printability was correlated to the rheological properties of the melts.

Shear rate dependent complex viscosity results were gathered for placebo formulations KVA64/PEG and EPO. Four measurements each at different temperatures of 120 °C, 140 °C, 160 °C, and 180 °C were recorded (Figure 5). KVA64/PEG and EPO both show flat viscosity curves at each measuring temperature, which indicates high shear rate independence at all temperatures. With increasing temperature, the complex viscosity levels decrease as expected. At 180 °C, KVA64/PEG's shear rates above 80 s^{-1} could not be monitored due to the polymer melt being highly liquid. The sample did not remain in between the rheometer's parallel plate setup.

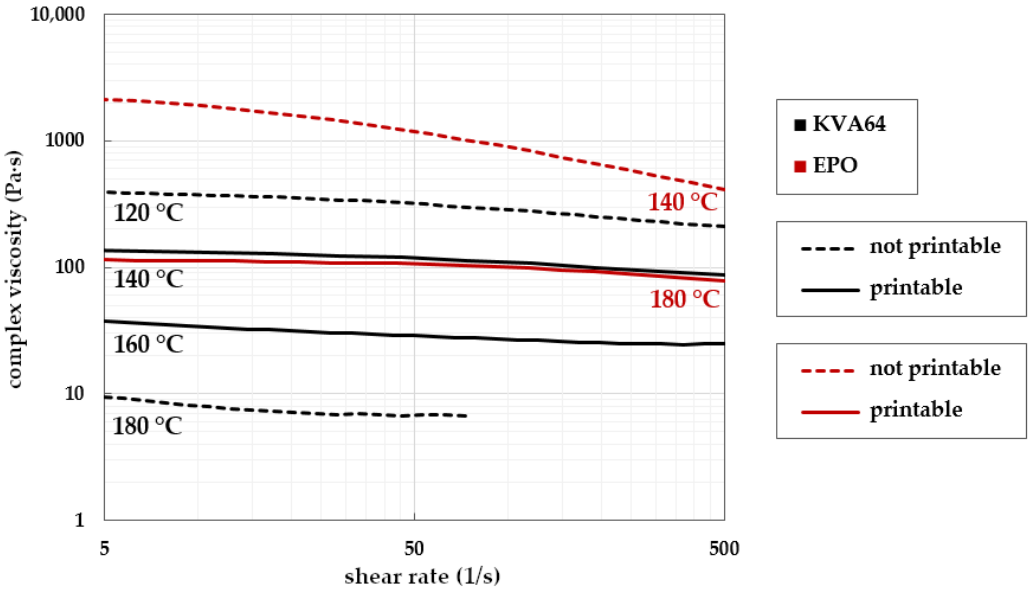

Figure 5. Complex viscosities of placebo formulations KVA64/PEG (black lines) and EPO (red lines) in relation to shear rate monitored at different temperatures; temperatures for successful print runs are symbolized by continuous lines, unsuitable temperature runs in dotted lines.

Printability tests showed that for KVA64/PEG, there was no extrusion possible at 120 °C nozzle temperature due to clogging. The extrusion channel jammed because of a highly viscous and hardened polymer clog. The effect occurred instantly and at no point was polymer melt obtained from the printing nozzle. The same effect occurred with EPO's print run at 140 °C nozzle temperature.

At 180 °C nozzle temperature, no extrusion of KVA64/PEG was possible either. In this case, the polymer melt showed inapplicability regarding low viscosity. From a technical point of view, the driving force of pushing a polymer melt through the nozzle is the generation of pressure in flow direction caused by the conveying of polymer. At 180 °C, generation of backpressure occurred, and polymer melt flowed into the direction of the channel top instead of being pushed to and out of the nozzle.

With nozzle temperatures of 140 °C and 160 °C for KVA64/PEG and 180 °C for EPO, flawless printability was observed. All necessary parameters and requirements for continuous extrusion were met. Therefore, the three viscosity curves serve as reference points for the viscosity of future polymer formulations and as soft limits. A viscosity between 20 and 100 Pa·s seems to be suitable for 3DP. The study shows that the printing temperature, in strong correlation to the viscosity of a material, is a crucial parameter for 3DP application. This was verified with drug–polymer mixtures.

3.3.3. Transfer to Drug Loaded Formulations

Rheology results of blend KVA64/PEG/MSN were compared with the target regime of the placebo KVA64 (Figure 6). It is noticeable that the complex viscosity window of KVA64/PEG/MSN is tight compared to that of the placebo. Small changes in temperature resulted in relatively strongly deviating viscosity results.

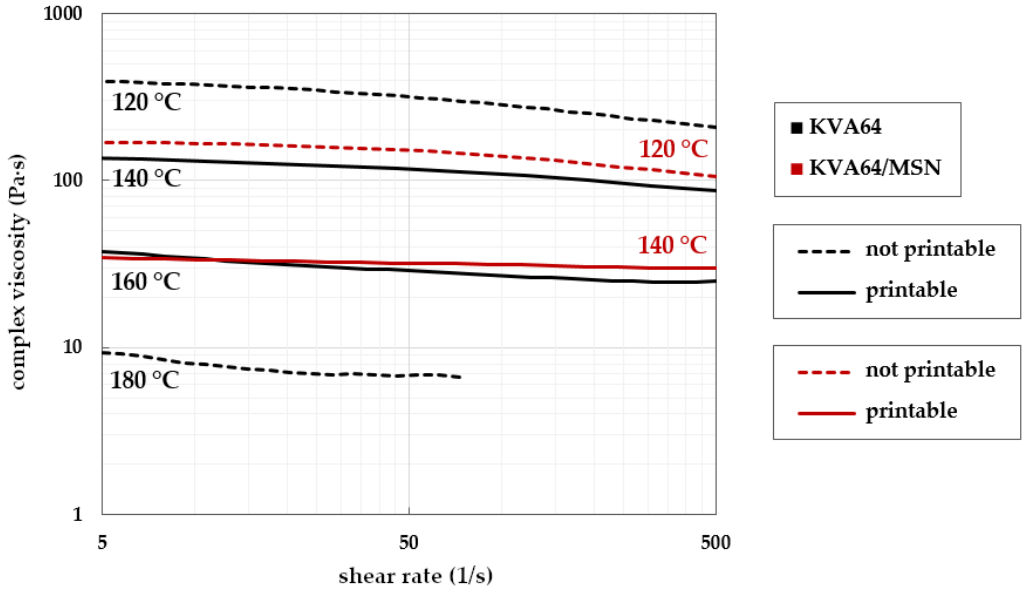

Figure 6. Complex viscosities of placebo formulation KVA64/PEG (black lines) and KVA64/PEG/MSN (red lines) in relation to shear rate monitored at different temperatures; temperatures for successful print runs are symbolized by continuous lines, unsuitable print runs in dotted lines.

At 160 °C, taking a measurement with KVA64/PEG/MSN was not possible due to it reaching an almost water-like low viscosity. The measurements taken at 120 °C and 140 °C show flat gradients and therefore high shear rate independency similar to placebo KVA64/PEG (Figure 6).

The printability test runs showed that for KVA64/PEG/MSN at 120 °C, extrusion was possible in principle, but it was discontinuous and fragile (Figure 6). At increased temperature of 140 °C, a smooth print was achieved. At 160 °C, KVA64/PEG/MSN's low-viscous polymer melt migrated backwards, no extrusion was realized, and the printhead including the extrusion channel was physically damaged because of hardened polymer at the tip of the channel.

When investigating EPO/MSN mixtures, it can be seen that MSN has a strong plasticizing effect (Figure 7). Compared to placebo EPO, lower viscosities are observed at the same temperatures and even small increases in temperature have a strong influence on the viscosity. In the case of the drug-loaded system EPO/MSN, there are comparatively large differences in viscosity, especially between the measurement temperatures of 120 °C and 140 °C.

In Figure 7, almost congruent viscosity curves were obtained for the samples EPO at 140 °C and EPO/MSN at 120 °C. Successful printability could not be achieved at either temperature. In both cases, the printhead's extrusion channel clogged. There was no successful 3DP for placebo EPO even at 160 °C, since stringent torque prevented extrusion. At elevated shear rates, a rheological investigation of EPO/MSN at 160 °C was not feasible due to the sample leaking the rheometer's measuring gap. The polymer melt showed severe low-viscous behavior. Smooth prints were achieved with samples of EPO at 180 °C and EPO/MSN at 140 °C fitting previously gained results for printability.

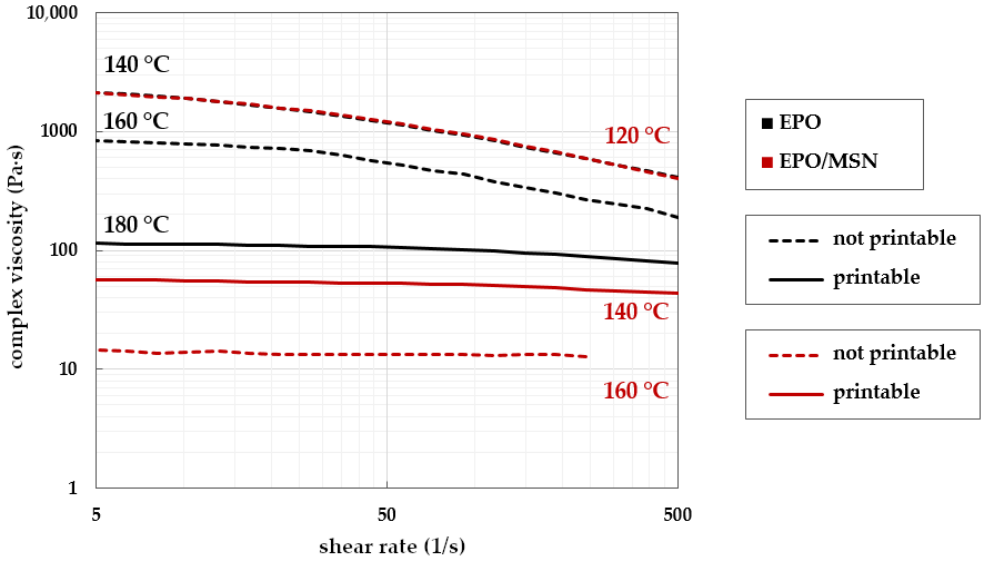

Figure 7. Complex viscosities of placebo formulation EPO (black lines) and EPO/MSN (red lines) in relation to shear rate monitored at different temperatures; temperatures for successful print runs are symbolized by continuous lines, unsuitable print runs in dotted lines.

3.4. Uniformity of Mass

There are several fundamental approaches to deliver tailored drug doses through 3D printing [34]. Dosage flexibility is realized by altering the number of printed layers, printing multiple objects, adjustment of feed drug loading, or modification of tablet volume [34–38]. In this study, printlets of three different volume scale factors were examined to assess the approach's eligibility for customized drug administration.

The results of the mass variation evaluation are presented in Table 3. For both formulations, the same print file and print settings were used. Theoretically expected printlet masses calculated for the assumption of perfect full printlet infill with proportional true densities of the blends' single components are stated for comparison as well. Both formulations display different densities due to their differing composition. For full printlet infill, the true densities of the blends' yield ρ(KVA64/MSN) = 1.192 g/cm^3 and ρ(EPO/MSN) = 0.906 g/cm^3. Consequently, a higher mass is to be expected for KVA64/PEG/MSN tablets than for EPO/MSN tablets when printing an identical 3D object.

Table 3. Comparison of average printlet mass, standard deviation, and mass uniformity limits for formulations KVA64/PEG/MSN and EPO/MSN.

Formulation	Printlet Scale Factor [1]	Mean Mass [mg]	±SD	First Ph. Eur. Limit [2]	Second Ph. Eur. Limit [3]
KVA64/PEG/MSN	50%	482	1.75%	10/10	10/10
	75%	691	3.73%	9/10	10/10
	100%	854	4.34%	9/10	10/10
EPO/MSN	50%	371	2.92%	9/10	10/10
	75%	550	1.65%	10/10	10/10
	100%	691	2.62%	10/10	10/10

[1] identical printlet regarding geometry ratio with scale factor relating solely to the objects volume. [2] allowing a maximum of 5% deviation from average mass [27]. [3] allowing a maximum of 10% deviation from average mass [27].

Table 3 shows the results of the mass uniformity test. A certain amount of printlets exceeded the first specification limit but the secondary pharmacopeial specification limit was not surpassed in any of the print runs. Thus, all printing processes met the requirements

of the Ph. Eur. monograph for single oral dosage forms [27]. The obtained data show that a process eligible for approval is feasible for both polymer systems.

Regarding standard deviations in Table 3, formulation KVA64/PEG/MSN displays a trend worth mentioning. With increasing printlet volume, the standard deviation within the print runs rises. Consequently, the printing process becomes less precise as the printlet volume increases. This trend cannot be transferred to EPO/MSN. The highest mass uniformity is obtained with a volume scaled to 75% in this case. The printing process of EPO/MSN is superior to that of KVA64/PEG/MSN in terms of printlet mass reproducibility, especially for tablet volumes scaled to 50% and 100%.

3.5. Printlet Volume–Mass Correlation

For an ideally scalable printing process, there is a linear correlation between the tablet mass and the volume of the tablet print file. In this case, by adjustment of the printlets volume, altered masses and thus amounts of pharmaceutical ingredient can be realized in an individualized and reproducible manner. Figure 8 illustrates the relation of printlet masses to volume scale factor. Complete scalability linearity is not achieved with either formulation (Figure 8). With blend KVA64/PEG/MSN, the obtained printlet mass offsets at 100% volume compared to the other points. With this formulation, the process comes closer to the target tablet mass especially with large printlets. Further optimization of the nozzle throughput can be addressed in multiple ways by adjusting print parameters such as the printing temperature, print speed, screw speed, or layer height [26,39,40]. On top of that, introducing a correction factor is an option.

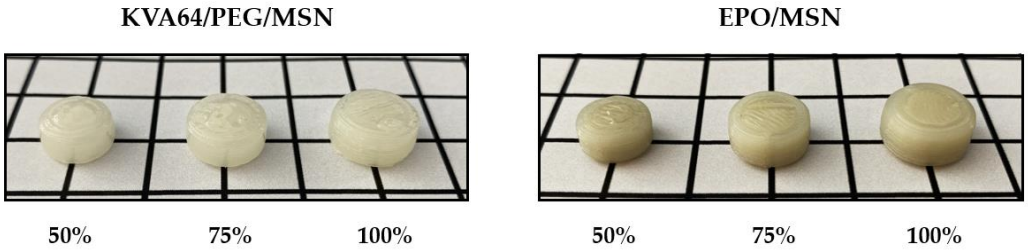

Figure 8. Sample 3DP tablets obtained from formulations KVA64/PEG/MSN and EPO/MSN. The volume scaling factors 100%, 75%, and 50% refer to the standard printlet file mentioned.

A key finding from Figure 9 is that with both formulations, higher printlet masses were obtained for all volumes examined than theoretically calculated. The calculation of theoretical printing masses was carried out under the assumption of full object infill by utilization of the blend components' proportional true densities. This indicates slight over-extrusion, which is a typical 3D printing phenomenon where more polymer melt is dispensed than needed to create the object. Dimensional inaccuracies, layer drooping, oozing, or blobbing can accompany over-extrusion even though these effects have not been observed in the current study and appropriate tablets were obtained [41–43]. Moderate and particularly constant over-extrusion is a purely technical challenge that can be solved by optimizing printing parameters, such as extrusion speed, nozzle moving speed, or the object's layer height [41–43]. As long as over-extrusion takes place in a constant manner, the introduction of a volume–mass correction factor can be considered once more.

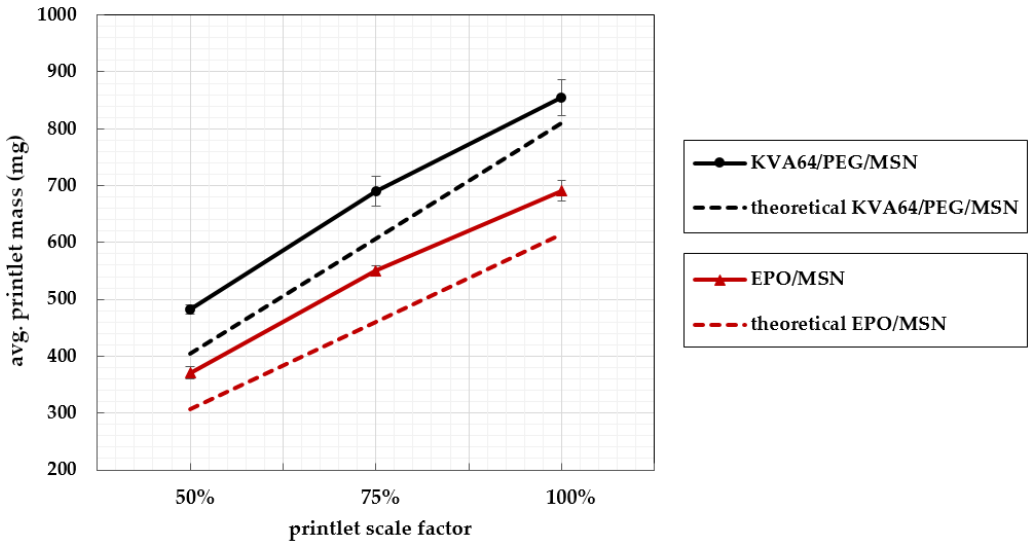

Figure 9. KVA64/PEG/MSN and EPO/MSN's mean printlet masses with standard deviations versus the printlet volume scale factors 100%, 75%, and 50%.

3.6. Uniformity of Dosage Units

Investigation of the uniformity of dosage units is crucial in order to guarantee consistency of API content within the batches of 3DP tablets. The results of the mean API contents and acceptance values (AV) are summarized in Table 4. According to Ph. Eur. Monograph 2.9.40 "uniformity of dosage units", the AV is required to be below 15 [28]. If the AV is greater than 15, 20 additional dosage units need to be tested. In this case the requirements are met if the final AV of 30 dosage units is less than or equal to 15 and no individual dosage unit content deviates from the reference values by more than 25% [28].

Table 4. Drug content uniformity of MSN in KVA64/PEG/MSN and EPO/MSN granules and tablets.

	KVA64/PEG/MSN		EPO/MSN	
	Granules	**3DP Tablets**	**Granules**	**3DP Tablets**
Mean API content (%) [1]	96.9 ± 1.5	96.1 ± 1.7	99.7 ± 1.8	98.3 ± 1.3
Acceptance value	5.2	6.5	4.2	3.3

[1] corresponding to the expected drug content; (n = 10).

Within each batch, no single dose deviates by more than 15% from the respective mean value. All samples met the pharmacopeial specifications regarding the AV and the capability of the multi-step operation to fabricate tablets within acceptable in-batch drug content variations was therefore proven.

3.7. In Vitro Dissolution of Solid Oral Dosage Forms

Figure 10 shows the dissolution profiles of the printed MSN tablets. Independently of the polymer used, a complete drug release was achieved within 60 min. The release rates of both formulations are highly similar. The USP considers a single oral dosage IR if an accumulated drug release of more than 80% is achieved within 30 min [44,45]. The recommendation of the Ph. Eur. specifies a drug release equal to or more than 80% in less than 45 min for a conventional IR tablet [46]. The drug release profiles of both formulations meet the specifications of the European Pharmacopoeia. The obtained dissolution results of both formulations do slightly miss the requirements of the USP for immediate release dosage forms, despite the model drug MSN being freely water soluble [44,47]. A major reason accounting for impeded drug release is the compactness and high density of the printed tablets due to full body infill. The polymer melts leave no air inclusions inside the tablet due to their low viscosity. Arafat et al. showed that the dissolution behavior is

strongly dependent on the printlet infill. In their studies, decreasing the infill density by introducing cavities into the print file led to increased dissolution rates [48]. By changing the print geometry, the release can also be accelerated. Goyanes' et al. previously published research has stated that high surface area to volume ratios result in quicker drug release [49]. These aspects could be used to further tailor the release kinetics of the present printlets.

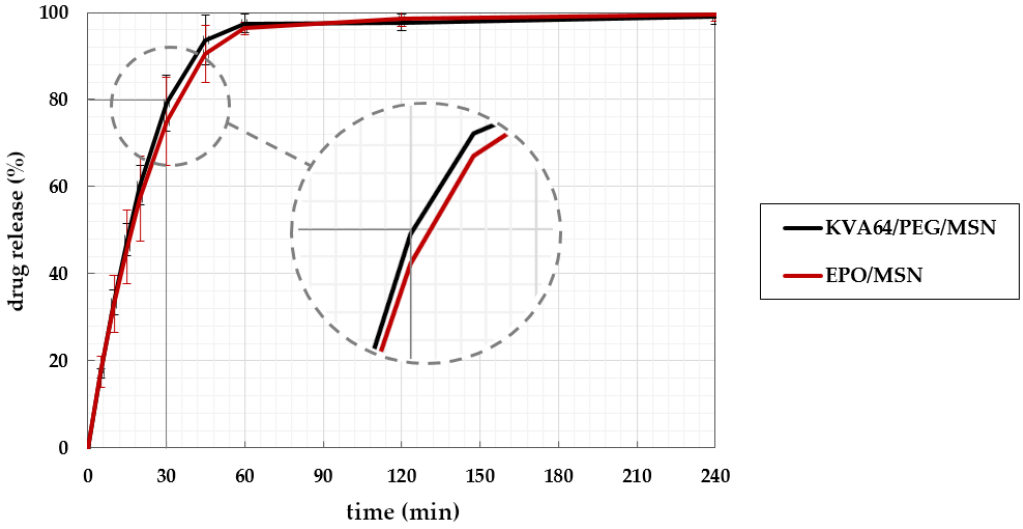

Figure 10. In vitro drug release of the model drug in KVA64/PEG/MSN (black) and EPO/MSN (red) 3DP printlets. The USP criterion for IR is highlighted along the x- and y-axis [44].

4. Conclusions

In this work, polymer systems were developed applicable for a granules-fed 3D extruder printhead. Both printable placebo blends and drug-containing systems were produced using the carrier polymers KVA64 and EPO. The granules obtained were examined for thermal durability in order to prevent decomposition processes during 3DP. The selected 3DP temperature of 140 °C is considered to be safe in terms of thermal degradation for both formulations. In addition, partial drug miscibility of both blends' components was perceived. Correlation of viscosity profiles with the printability of the formulations shows that the printing temperature is a crucial parameter for successful extrusion and closely related to melt viscosity attributes. Improper printing temperatures lead to physical damaging or inoperability of the printing channel. All formulations display a limited processability window in regards of melt viscosity. The knowledge gained about the required melt viscosity can be incorporated into the development of future pharmaceutical 3DP formulations. With regard to mass uniformity, every print run of both blends fulfilled the European pharmacopeial requirements. While every single printlet fitted the broader second pharmacopeial specification limit, the majority also met the first uniformity criterion. The Assay of actual drug content in the 3DP tablets proves that neither KVA64/MSN/PEG nor EPO/MSN has undergone major API degradation in the course of multiple processing steps from mixture to final product. The Ph. Eur. monograph testing for uniformity of dosage units was met in all cases. Additionally, the drug release properties of both formulations show that immediate drug release is feasible. By further administering improvements such as print geometry optimization, infill adjustments, or addition of disintegrants, the technology holds potential for providing individualized therapy to hypertension patients. In terms of mass and content uniformity, this research work proves that a process eligible for approval by regulatory pharma authorities is possible.

Author Contributions: Conceptualization, M.D., D.L. and S.L.; methodology, D.L, S.L., K.E. and R.V.; validation, T.P.; investigation, T.P.; resources, M.D.; writing—original draft preparation, T.P.; writing—review and editing, D.L., S.L., M.D., K.E. and R.V.; visualization, T.P.; supervision, D.L., S.L., K.E. and R.V. All authors have read and agreed to the published version of the manuscript.

Funding: This research received APC funding support by the Open Access Publishing Fund of University of Tuebingen.

Institutional Review Board Statement: Not applicable.

Informed Consent Statement: Not applicable.

Conflicts of Interest: The authors declare no conflict of interest. The company had no role in the design of the study; in the collection, analyses, or interpretation of data; in the writing of the manuscript, and in the decision to publish the results.

References

1. Huber, G.; Dachtler, M.; Edinger, D. Digitalisierung in der Pharmaindustrie. In *Digitale Transformation von Dienstleistungen im Gesundheitswesen II*; Springer: Berlin/Heidelberg, Germany, 2017; pp. 241–255.
2. Pravin, S.; Sudhir, A. Integration of 3D printing with dosage forms: A new perspective for modern healthcare. *Biomed. Pharmacother.* **2018**, *107*, 146–154. [CrossRef] [PubMed]
3. Dachtler, M.; Eggenreich, K.; Pflieger, T. Digital Health-Digital 2D/3D Printing of Personalized Medication. In Proceedings of the 4rd International Symposium on Pharmaceutical Engineering Research (SPhERe), Online, 15–17 September 2021.
4. Dachtler, M.; Huber, G.; Pries, T. 2D & 3D-Print-Technologien in der Pharmazeutischen Industrie. In *Digitale Transformation von Dienstleistungen im Gesundheitswesen VII*; Springer: Berlin/Heidelberg, Germany, 2020; pp. 53–66.
5. Awad, A.; Trenfield, S.J.; Goyanes, A.; Gaisford, S.; Basit, A.W. Reshaping drug development using 3D printing. *Drug Discov. Today* **2018**, *23*, 1547–1555. [CrossRef] [PubMed]
6. Berger, V.; Luo, Z.; Leroux, J.-C. 3D printing of a controlled fluoride delivery device for the prevention and treatment of tooth decay. *J. Control. Release* **2022**, *348*, 870–880. [CrossRef] [PubMed]
7. Menegatou, I.-M.; Papakyriakopoulou, P.; Rekkas, D.M.; Dallas, P.; Valsami, G. Design of a Personalized Nasal Device (Matrix-Piston Nasal Device, MPD) for Drug Delivery: A 3D-Printing Application. *AAPS PharmSciTech* **2022**, *23*, 1–9. [CrossRef] [PubMed]
8. Zhang, B.; Teoh, X.Y.; Yan, J.; Gleadall, A.; Belton, P.; Bibb, R.; Qi, S. Development of combi-pills using the coupling of semi-solid syringe extrusion 3D printing with fused deposition modelling. *Int. J. Pharm.* **2022**, *625*, 122140. [CrossRef]
9. Zhang, P.; Xu, P.; Chung, S.; Bandari, S.; Repka, M.A. Fabrication of bilayer tablets using hot melt extrusion-based dual-nozzle fused deposition modeling 3D printing. *Int. J. Pharm.* **2022**, *624*, 121972. [CrossRef]
10. Melocchi, A.; Uboldi, M.; Briatico-Vangosa, F.; Moutaharrik, S.; Cerea, M.; Foppoli, A.; Maroni, A.; Palugan, L.; Zema, L.; Gazzaniga, A. The Chronotopic™ System for Pulsatile and Colonic Delivery of Active Molecules in the Era of Precision Medicine: Feasibility by 3D Printing via Fused Deposition Modeling (FDM). *Pharmaceutics* **2021**, *13*, 759. [CrossRef]
11. Rahman, Z.; Ali, S.F.B.; Ozkan, T.; Charoo, N.A.; Reddy, I.K.; Khan, M.A. Additive manufacturing with 3D printing: Progress from bench to bedside. *AAPS J.* **2018**, *20*, 1–14. [CrossRef]
12. Chen, G.; Xu, Y.; Kwok, P.C.L.; Kang, L. Pharmaceutical applications of 3D printing. *Addit. Manuf.* **2020**, *34*, 101209. [CrossRef]
13. Reiner, G.; Pierce, S.L.; Flynn, J. Wrong drug and wrong dose dispensing errors identified in pharmacist professional liability claims. *J. Am. Pharm. Assoc.* **2020**, *60*, e50–e56. [CrossRef]
14. Whelton, P.K.; Carey, R.M.; Aronow, W.S.; Casey, D.E.; Collins, K.J.; Dennison Himmelfarb, C.; DePalma, S.M.; Gidding, S.; Jamerson, K.A.; Jones, D.W. A guideline for the prevention, detection, evaluation, and management of high blood pressure in adults: A report of the American College of Cardiology/American Heart Association Task Force on Clinical Practice Guidelines. *J. Am. Coll. Cardiol.* **2018**, *71*, e127–e248. [CrossRef]
15. Staessen, J.A.; Wang, J.; Bianchi, G.; Birkenhäger, W.H. Essential hypertension. *Lancet* **2003**, *361*, 1629–1641. [CrossRef]
16. Fahey, T.; Schroeder, K.; Ebrahim, S.; Glynn, L. Interventions used to improve control of blood pressure in patients with hypertension. *Cochrane Database Syst. Rev.* **2006**, *4*, CD005182.
17. Govender, R.; Kissi, E.O.; Larsson, A.; Tho, I. Polymers in pharmaceutical additive manufacturing: A balancing act between printability and product performance. *Adv. Drug Deliv. Rev.* **2021**, *177*, 113923. [CrossRef]
18. Parulski, C.; Jennotte, O.; Lechanteur, A.; Evrard, B. Challenges of fused deposition modeling 3D printing in pharmaceutical applications: Where are we now? *Adv. Drug Deliv. Rev.* **2021**, *175*, 113810. [CrossRef]
19. Krueger, L.; Miles, J.A.; Popat, A. 3D printing hybrid materials using fused deposition modelling for solid oral dosage forms. *J. Control. Release* **2022**, *351*, 444–455. [CrossRef]
20. Liu, X.; Chi, B.; Jiao, Z.; Tan, J.; Liu, F.; Yang, W. A large-scale double-stage-screw 3D printer for fused deposition of plastic pellets. *J. Appl. Polym. Sci.* **2017**, *134*, 45147. [CrossRef]
21. Goyanes, A.; Allahham, N.; Trenfield, S.J.; Stoyanov, E.; Gaisford, S.; Basit, A.W. Direct powder extrusion 3D printing: Fabrication of drug products using a novel single-step process. *Int. J. Pharm.* **2019**, *567*, 118471. [CrossRef]
22. Fanous, M.; Gold, S.; Muller, S.; Hirsch, S.; Ogorka, J.; Imanidis, G. Simplification of fused deposition modeling 3D-printing paradigm: Feasibility of 1-step direct powder printing for immediate release dosage form production. *Int. J. Pharm.* **2020**, *578*, 119124. [CrossRef]

23. Okafor-Muo, O.L.; Hassanin, H.; Kayyali, R.; ElShaer, A. 3D printing of solid oral dosage forms: Numerous challenges with unique opportunities. *J. Pharm. Sci.* **2020**, *109*, 3535–3550. [CrossRef]
24. Palo, M.; Holländer, J.; Suominen, J.; Yliruusi, J.; Sandler, N. 3D printed drug delivery devices: Perspectives and technical challenges. *Expert Rev. Med. Devices* **2017**, *14*, 685–696. [CrossRef] [PubMed]
25. Cui, M.; Pan, H.; Su, Y.; Fang, D.; Qiao, S.; Ding, P.; Pan, W. Opportunities and challenges of three-dimensional printing technology in pharmaceutical formulation development. *Acta Pharm. Sin. B* **2021**, *11*, 2488–2504. [CrossRef] [PubMed]
26. Azad, M.A.; Olawuni, D.; Kimbell, G.; Badruddoza, A.Z.M.; Hossain, M.; Sultana, T. Polymers for extrusion-based 3D printing of pharmaceuticals: A holistic materials–process perspective. *Pharmaceutics* **2020**, *12*, 124. [CrossRef] [PubMed]
27. Uniformity of Mass of Single-Dose Preparations. In *European Pharmacopoeia*, 10th ed.; EDQM Council of Europe: Strasbourg, France, 2019; Volume 1, pp. 335–336.
28. Uniformity of Dosage Units. In *European Pharmacopoeia*, 10th ed.; EDQM Council of Europe: Strasbourg, France, 2019; Volume 1, pp. 357–359.
29. *Safety Data Sheet: Metoprolol Succinate*; Hangzhou-Longshine: Hangzhou, China, 2019.
30. Goyanes, A.; Fina, F.; Martorana, A.; Sedough, D.; Gaisford, S.; Basit, A.W. Development of modified release 3D printed tablets (printlets) with pharmaceutical excipients using additive manufacturing. *Int. J. Pharm.* **2017**, *527*, 21–30. [CrossRef] [PubMed]
31. Lewis, J.A.; Gratson, G.M. Direct writing in three dimensions. *Mater. Today* **2004**, *7*, 32–39. [CrossRef]
32. Jaluria, Y. Heat and Mass Transfer in the Extrusion of Non-Newtonian Materials. In *Advances in Heat Transfer*; Elsevier: Amsterdam, The Netherlands, 1996; Volume 28, pp. 145–230.
33. Chiruvella, R.V.; Jaluria, Y.; Sernas, V.; Esseghir, M. Extrusion of non-Newtonian fluids in a single-screw extruder with pressure back flow. *Polym. Eng. Sci.* **1996**, *36*, 358–367. [CrossRef]
34. Lafeber, I.; Ruijgrok, E.J.; Guchelaar, H.-J.; Schimmel, K.J. 3D Printing of Pediatric Medication: The End of Bad Tasting Oral Liquids?—A Scoping Review. *Pharmaceutics* **2022**, *14*, 416. [CrossRef]
35. El Aita, I.; Rahman, J.; Breitkreutz, J.; Quodbach, J. 3D-Printing with precise layer-wise dose adjustments for paediatric use via pressure-assisted microsyringe printing. *Eur. J. Pharm. Biopharm.* **2020**, *157*, 59–65. [CrossRef]
36. Saydam, M.; Takka, S. Improving the dissolution of a water-insoluble orphan drug through a fused deposition modelling 3-dimensional printing technology approach. *Eur. J. Pharm. Sci.* **2020**, *152*, 105426. [CrossRef]
37. Buanz, A.; Saunders, M.H.; Basit, A.W.; Gaisford, S. Preparation of personalized-dose salbutamol sulphate oral films with thermal ink-jet printing. *Pharm. Res.* **2011**, *28*, 2386–2392. [CrossRef]
38. Goyanes, A.; Madla, C.M.; Umerji, A.; Piñeiro, G.D.; Montero, J.M.G.; Diaz, M.J.L.; Barcia, M.G.; Taherali, F.; Sánchez-Pintos, P.; Couce, M.-L. Automated therapy preparation of isoleucine formulations using 3D printing for the treatment of MSUD: First single-centre, prospective, crossover study in patients. *Int. J. Pharm.* **2019**, *567*, 118497. [CrossRef]
39. Loflin, W.A.; English, J.D.; Borders, C.; Harris, L.M.; Moon, A.; Holland, J.N.; Kasper, F.K. Effect of print layer height on the assessment of 3D-printed models. *Am. J. Orthod. Dentofac. Orthop.* **2019**, *156*, 283–289. [CrossRef]
40. Ferretti, P.; Leon-Cardenas, C.; Santi, G.M.; Sali, M.; Ciotti, E.; Frizziero, L.; Donnici, G.; Liverani, A. Relationship between FDM 3D printing parameters study: Parameter optimization for lower defects. *Polymers* **2021**, *13*, 2190. [CrossRef]
41. Shaqour, B.; Abuabiah, M.; Abdel-Fattah, S.; Juaidi, A.; Abdallah, R.; Abuzaina, W.; Qarout, M.; Verleije, B.; Cos, P. Gaining a better understanding of the extrusion process in fused filament fabrication 3D printing: A review. *Int. J. Adv. Manuf. Technol.* **2021**, *114*, 1279–1291. [CrossRef]
42. Shaik, Y.P.; Schuster, J.; Shaik, A. A Scientific Review on Various Pellet Extruders Used In 3D Printing FDM Processes. *Open Access Libr. J.* **2021**, *8*, 1–19. [CrossRef]
43. Kumar, L.J.; Pandey, P.M.; Wimpenny, D.I. *3D Printing and Additive Manufacturing Technologies*; Springer: Berlin/Heidelberg, Germany, 2019; Volume 311.
44. *Dissolution Testing and Acceptance Criteria for Immediate-Release Solid Oral Dosage Form Drug Products Containing High Solubility Drug Substances-Guidance for Industry*; US Department of Health and Human Services-Food and Drug Administration: Silver Spring, MD, USA, 2018.
45. Anand, O.; Yu, L.X.; Conner, D.P.; Davit, B.M. Dissolution testing for generic drugs: An FDA perspective. *AAPS J.* **2011**, *13*, 328–335. [CrossRef]
46. Recommendation on Dissolution Testing. In *European Pharmacopoeia*, 10th ed.; EDQM Council of Europe: Strasbourg, France, 2019; Volume 1, pp. 727–729.
47. Budavari, S.; O'Neil, M.; Smith, A.; Heckelman, P.; Kinneary, J. *The Merk Index. An Encyclopedia of Chemicals, Drugs and Biologicals*, 13th ed.; Merck and Co. Inc.: Whitehouse Station, NJ, USA, 2001; Volume 1097, p. 1096.
48. Arafat, B.; Wojsz, M.; Isreb, A.; Forbes, R.T.; Isreb, M.; Ahmed, W.; Arafat, T.; Alhnan, M.A. Tablet fragmentation without a disintegrant: A novel design approach for accelerating disintegration and drug release from 3D printed cellulosic tablets. *Eur. J. Pharm. Sci.* **2018**, *118*, 191–199. [CrossRef]
49. Goyanes, A.; Martinez, P.R.; Buanz, A.; Basit, A.W.; Gaisford, S. Effect of geometry on drug release from 3D printed tablets. *Int. J. Pharm.* **2015**, *494*, 657–663. [CrossRef]

4. Influence of Design Parameters on Sustained Drug Release Properties of 3D-Printed Theophylline Tablets

Thomas Pflieger[1,4], Rakesh Venkatesh[1], Markus Dachtler[1], Karin Cooke[2], Stefan Laufer[3], Dominique Lunter[4,*]

[1] DiHeSys Digital Health Systems GmbH, 73529 Schwäbisch Gmünd, Germany

[2] Gen-Plus GmbH & Co. KG, 81477 Munich, Germany

[3] Pharmaceutical Chemistry, Eberhard Karls University, 72074 Tübingen, Germany

[4] Pharmaceutical Technology, Eberhard Karls University, 72074 Tübingen, Germany

* Corresponding author

International Journal of Pharmaceutics

Year 2024, Volume 658, Article 124207
DOI: https://doi.org/10.1016/j.ijpharm.2024.124207

International Journal of Pharmaceutics 658 (2024) 124207

Contents lists available at ScienceDirect

International Journal of Pharmaceutics

journal homepage: www.elsevier.com/locate/ijpharm

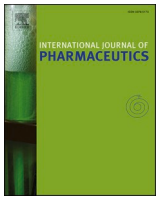

Influence of design parameters on sustained drug release properties of 3D-printed theophylline tablets

Thomas Pflieger [a,d], Rakesh Venkatesh [a], Markus Dachtler [a], Karin Cooke [b], Stefan Laufer [c], Dominique Lunter [d,*]

[a] DiHeSys Digital Health Systems GmbH, Marie-Curie-Strasse 19, 73529 Schwaebisch Gmuend, Germany
[b] Gen-Plus GmbH & Co. KG, Staffelseestrasse 6, 81477 Munich, Germany
[c] Chair of Pharmaceutical Chemistry, Eberhard Karls University, Auf der Morgenstelle 8, 72074 Tuebingen, Germany
[d] Chair of Pharmaceutical Technology, Eberhard Karls University, Auf der Morgenstelle 8, 72074 Tuebingen, Germany

ARTICLE INFO

Keywords:
Pharmaceutical three-dimensional printing (3DP)
Theophylline
Individualized treatment
Pulmonary diseases
Sustained drug release
Oral dosage forms (ODF)

ABSTRACT

The application of three-dimensional printing (3DP) in the pharmaceutical industry brings a broad spectrum of benefits to patients by addressing individual needs and improve treatment success. This study investigates the sustained release properties of 3DP tablets containing Theophylline (TPH), which is commonly used to treat respiratory diseases and recently having a comeback due to its potential in the treatment of conditions like Covid-19. Since TPH is a narrow therapeutic window (NTW) drug with serious side effects in the event of overdose, the release properties must be observed particularly closely. We employed a state-of-the-art single screw extrusion 3D printer, which is fed with granules containing the drug. By employing a Taguchi orthogonal array design of experiments (DOE), tablet design parameters and factor related process stability were sought to be evaluated fundamentally. Following this, examinations regarding tailored TPH dosages were undertaken and a relationship between the real printed dose of selected tablet designs and their sustained drug release was established. The release profiles were analyzed using different mathematical model fits and compared in terms of mean dissolution times (MDT). Finally, in-vivo/in-vitro correlation (IVIVC) and physiologically based pharmacokinetic (PBPK) modeling showed that a paradigm patient group could be covered with the dosage forms produced.

1. Introduction

Three-dimensional printing (3DP) has already found its way into the pharmaceutical industry and represents a promising technology for medication tailorization and combination (Chen et al., 2020; Dachtler et al., 2021; Dachtler et al., 2020; Huber et al., 2017). In contrast to conventional manufacturing methods such as powder compaction or encapsulation, 3DP products can be adapted to the individual needs of patients on-site and on-demand (Chandekar et al., 2019; Dachtler et al., 2020; Souto et al., 2019). For patient-centered therapy it is imperative to consider a wide range of variables and address factors such as gender, weight, age, disease progression, disease state, and numerous other parameters (Drumond, 2020; Trivedi et al., 2018; Wishart, 2016). When administering a precise dose of medications, a combination of separate dosage forms are used traditionally (Menditto et al., 2020). This leads to inconvenient or even challenging medication intake and puts treatment adherence at risk (Menditto et al., 2020; Robinson et al., 2008). Providing customized drug amounts in a single 3DP tablet offers a smart solution to overcome these issues.

The utilized Flexdose™ 3D printer applies additive manufacturing by direct granules extrusion to produce oral dosage forms (ODF) (Pflieger et al., 2022). This particular device is fed by polymer granules containing active pharmaceutical ingredients (API), which are conveyed along an extrusion channel and dispensed from the nozzle in form of a polymer melt (Pflieger et al., 2022; Seoane-Viaño et al., 2021). Through movement of the printhead and bed according to a set 3D computer aided design (CAD) model, the object is gradually built up in horizontal layers (Pflieger et al., 2022; Seoane-Viaño et al., 2021).

TPH, a bronchodilator, has been used for the treatment of respiratory diseases such as bronchial asthma and chronic obstructive pulmonary disease (COPD) for over a century, establishing its position in the pharmaceutical field (Barnes, 2003; Karow and Lang-Roth, 2020). Due to its narrow therapeutic window, it is crucial to be able to precisely control both the absolute dosage and the release kinetics (Ratiopharm,

* Corresponding author at: University of Tuebingen, Chair of Pharmaceutical Technology, Auf der Morgenstelle 8, 72076 Tuebingen, Germany.
E-mail address: dominique.lunter@uni-tuebingen.de (D. Lunter).

https://doi.org/10.1016/j.ijpharm.2024.124207
Received 13 December 2023; Received in revised form 3 May 2024; Accepted 4 May 2024
Available online 6 May 2024

2020). Currently, TPH is administered in accordance with the patient's body weight (BW), with initial recommendations starting from 11 to 13 mg/kg BW daily (Ratiopharm, 2020). In practice, the blood serum concentration is closely monitored throughout the course of the treatment and adjusted if necessary, which is where particularly pharmaceutical 3DP comes in handy (Barnes, 2003; Paloucek and Rodvold, 1988). In addition, it is noteworthy that currently available market products (MP) do not offer sufficient dose increments to cover a diverse spectrum of patients. Recent findings suggest that TPH helps treating various respiratory diseases and most interestingly Covid-19, in a progressive low-dose administration approach (Montaño et al., 2022; Pouya et al., 2020). As demonstrated by multiple studies, TPH has been shown to exhibit promising results in improving respiratory symptoms, particularly at low blood serum concentrations of 1–5 μg/mL (Barnes, 2003; Cosio et al., 2009; Devereux et al., 2019; Siddharthan et al., 2021). This innovative administration strategy shifts required absolute dosages and dose increment precision (Asmus et al., 1997). The typically available 100–125 mg increments of current TPH products do not facilitate the implementation of this new therapeutic strategy, necessitating a reevaluation by pharmaceutical 3DP (Asmus et al., 1997; Ratiopharm, 2020).

The first aim of our study was to resort to a Taguchi DOE, that serves as an initial evaluation of the impact of chosen design parameters and to establish an understanding of the stability of the printing process. To this end, tablets with varying drug concentrations in feeding granules (DC), printlet volumes (V), scale factors (SF), and tablet body infills (INF) were examined. In a second step, considerations regarding dose individualization are made, establishing a correlation between actual printed doses and the sustained drug release properties of selected tablet designs. Following this relationship and to complete the work, we have shown through IVIVC and PBPK modeling that a paradigm patient group could be covered according to the progressive low blood level approach.

2. Materials and methods

2.1. Materials

The anhydrous drug Theophylline (TPH), with purity >99 %, was supplied by Thermo Fisher Scientific Inc., Waltham, USA and the polymer Eudragit® RL (ERL) and flow agent Aerosil® R972 were provided by Evonik AG, Essen, Germany. The polyethylene glycol plasticizer Lipoxol® 6000 MED (PEG) was received from Sasol Chemicals LLC, Houston, USA. All chemicals used were of analytical grade and used as received. The German market product Theophyllin-retard ratiopharm® 250 mg used for comparison of drug release profiles was purchased from ratiopharm GmbH, Ulm, Germany, which is a hard capsule dosage form filled with sustained-release granules.

2.2. Methods

2.2.1. Design of experiments

A statistical experimental design known as the robust Taguchi orthogonal array system was employed to design the printed tablets. This involves a highly fractional selected subset of combinations of multiple factors at multiple levels. The design comprises of four three-level main factors and consequently nine experimental runs with three repetitions. Table 1 shows the four factors chosen and observed with according factor levels: drug content (DC), volume of printlet (V), scale factor of printlet (SF) and body infill (INF). The MDTs of according drug releases were considered as the system response.

The SF is based on the ratio between the radius $r_{cylinder}$ and height $h_{cylinder}$ of the respective cylinder as Eq. (1) depicts:

$$SF = \frac{r_{cylinder}}{h_{cylinder}} \quad (1)$$

The SF is closely linked to the surface area to volume ratio (SA/V), but is in itself independent of the actual volume of the cylinder and therefore chosen. A SF of 0.50 represents, independent of the absolute volume, a cylindrical body with the minimum possible SA/V.

Table 1
Statistical experimental design to evaluate four separate multi level factors that are considered to influence TPH drug release.

Experiment		DC (% *w/w*)	V (mm^3)	SF	INF (%)
TPH-10	E1	10	300	0.50	30
	E2	10	550	1.00	60
	E3	10	800	1.50	100
TPH-30	E4	30	300	1.00	100
	E5	30	550	1.50	30
	E6	30	800	0.50	60
TPH-50	E7	50	300	1.50	60
	E8	50	550	0.50	100
	E9	50	800	1.00	30

2.2.2. Formulation of blends

Regarding TPH, three different formulations with varying drug loadings were utilized for 3DP of the respective tablet design sets. When altering the drug content, the mass ratio of the other excipients was held constant to achieve comparable formulations (ERL:PEG 4:1). The formulation compositions can be found in Table 2. The blends represent the final formulations that were used for the production of granules. The blend components were pre-weighed and three-step geometrically mixed at 49 rpm for 15 min in a Turbula® T2F tumble mixer from WAB Group AG, Muttenz, Switzerland.

2.2.3. Production of granules

The prepared physical mixtures underwent twin-screw HME with a lab-scale extruder ZE HM9 from Three Tec GmbH, Seon, Switzerland. The hardware setup comprises co-rotating screw elements with a die diameter of 2 mm. The extrusion temperatures of formulations TPH-10, TPH-30 and TPH-50 can be found in Table 3. The extrusion channel consists of three equivalent temperature zones and the extrusion screws are solely conveying screws that have no kneading elements. Since the filament diameter of the extrudates is irrelevant for the production of granules due to subsequent milling, it has not been monitored. The extruded strands were downsized to granules through rasp sieve milling with a U5 Comil® from Quadro Engineering Corp., Waterloo, Canada, at 250 rpm. Granules with maximum diameter of 1.3 mm were obtained and particles less than 0.6 mm in size were separated using a stack sieve. The products were kept in sealed and tinted containers to avoid moisture sorption or potential alteration by light.

2.2.4. Printlet design and 3D printing process

Fig. 1 illustrates the biplane cylindrical tablet designs that were prepared individually adapting the cylinders height (h) and base area radius (r). The respective CAD tablet models were sliced into g-code (.gcode) with Ultimaker® Cura 4.10.0 by Ultimaker B.V., Utrecht, Netherlands. All CAD models were sliced without enclosed cylinder top and bottom lid surfaces, ensuring that factor INF is not affected by delay effects. This modification makes the factor INF a directly scalable

Table 2
Composition of formulations TPH-10, TPH-30, TPH-50 consisting of Theophylline (TPH), Eudragit RL (ERL), Lipoxol 6000 MED (PEG) and Aerosil R972 (R972).

Formulation	TPH (% *w/w*)	ERL (% *w/w*)	PEG (% *w/w*)	R972 (% *w/w*)
TPH-10	10.0	72.0	17.5	0.50
TPH-30	30.0	56.0	13.5	0.50
TPH-50	50.0	40.0	9.50	0.50

Table 3
HME production and 3DP parameters for selected polymer blends TPH-10, TPH-30 and TPH-50.

		TPH-10	TPH-30	TPH-50
HME	Extrusion T. (°C)	120	120	120
	Screw speed (rpm)	100	100	100
3DP	Nozzle T. (°C)	150	155	180
	Print bed T. (°C)	50	70	90

parameter for later evaluation and optimization purposes. Tablets were fabricated by direct granules extrusion applying the pharmaceutical 3D printer Flexdose™ supplied by DiHeSys Digital Health Systems GmbH, Schwaebisch Gmuend, Germany. 3D printing and g-code generation included standardized settings as follows: fine resolution slicing; extrusion factor 1.2 mm^3/s; nozzle speed factor 25 mm/s; set single layer height 240 µm; three wall circumnavigations; no base brim, supports or rafts; build plate bed and nozzle printing temperatures respective to 3.

2.2.5. Statistical test evaluation according to Taguchi

The generation and factor combinations of the statistical design set, evaluation of response means, effect sizes, signal-to-noise (S/N) ratios and relative standard deviations (SD), and graphical illustration of data was carried out with the software Minitab® version 21 by Minitab GmbH, Munich, Germany.

2.2.5.1. Taguchi experminental design and signal-to-noise (S/N) evaluation. Taguchi data analysis enables the prediction of optimum levels and performance based on the gathered information. As clear target drug release characteristics were set in form of MDTs instead of system maximization or minimization, a "nominal the best" (NTB) analysis approach was chosen (see Eq. (2)). The S/N ratio expresses the scatter around a target value by incorporating the mean of responses $\overline{Y}$ and variance s^2 (Klein, 2021; Roy, 2010).

$$S/N_i = 10 \bullet \log\left\{\frac{\overline{Y}^2}{s^2}\right\} \quad (2)$$

2.2.5.2. Analysis of variance (ANOVA). To assess the statistical significance of factors, one-way ANOVA was conducted. Important outcome parameters in this analysis include p-values, coefficient of determination (R^2), and residual plots of effects. P-values lower than the predetermined significance level of 0.10 indicate statistical significance among the means for a particular effect (Rizzuti and De Napoli, 2020; Roy, 2010). Conversely, non-significant effects were pooled. The suitability of model fits was evaluated using the coefficient of determination (Roy, 2010).

2.2.6. Differential scanning calorimetry (DSC)

DSC experiments were conducted utilizing a DSC 1 from Mettler Toledo, Columbus, USA. Sample preparation included 100 µL aluminum crucibles, and each crucible contained 10–20 mg of sample, with duplicates for each measurement. Working conditions covered a range of 30 °C to a maximum of 230 °C with a heating rate of 5 °C/min. The DSC measurements were performed under nitrogen atmosphere, with a flow rate of 30 mL/min. Physical state transformations and thermal events were observed in between processing steps, by analyzing physical mixtures and pre-print granules.

2.2.7. Thermogravimetric analysis (TGA)

The proportional weight loss was determined by a STA 409 PC/PG Luxx from Netzsch GmbH, Selb, Germany, in nitrogen atmosphere (flowrate 20 mL/min) from 50 °C to 230 °C with a heating rate of 5 °C/min. For the selection of suitable processing and 3DP temperatures without thermal degradation effects, duplicate tests on single components and excipients, physical mixtures, and granules were conducted. All samples were measured no later than one day after production.

2.2.8. Rheology: Small amplitude oscillatory shear (SAOS)

The SAOS tests were performed with a Physica MCR301 Rheometer from Anton Paar GmbH, Graz, Austria, in oscillation mode with parallel plate configuration. Rheological measurements exclusively involved extruded blends. Samples were placed on a pre-heated Peltier plate, molten and compressed to a 1.0 mm gap by a 25 mm diameter stainless-steel plate. The measurements were performed within the linear viscoelastic region (LVR), established by strain sweeps executed at the minimal processing temperature. Strain sweeps were conducted from 0.01 % to 10.0 % strain at 10 rad/s angular frequency. Consequently, frequency sweeps were performed at decreasing angular frequencies from 500 to 1 rad/s as to determine material viscoelastic behavior in relation to time and frequency. The rheological evaluations were carried out in duplicates.

2.2.9. In vitro dissolution

The dissolution parameters were chosen according to USP monograph "Theophylline Extended-Release Capsules: Test 9" (USP, 2020). The measurements were performed using the USP type I dissolution apparatus Sotax AT7 from Sotax AG, Basel, Switzerland, in 900 mL of pH 1.2 simulated gastric fluid for the first hour and simulated intestinal fluid without enzymes at pH 6.8 for the remaining seven hours. The rotation speed was set to 50 rpm at a constant measurement temperature of 37 ± 0.5 °C and studies were performed in triplicates ($n = 3$). Sampling was executed every 5 min for the first 20 min, every 15 min for the following 2 h and continuing with every hour up to 8 h. The average proportional drug releases were plotted as functions of time. The drug concentration in the dissolution medium was measured using a HP 8453 UV-Vis Spectrophotometer from Agilent Technologies Inc., Santa Clara, USA, at a wavelength of 271 nm in a 0.1 cm cell versus a blank solution consisting of pH 1.2 simulated gastric fluid or simulated intestinal fluid without enzymes at pH 6.8. The applied calibration range for the first hour was in between 2.8 and 111 mg/L ($R^2 = 0.9999$; LOD = 2.8 mg/L; LOQ = 8.3 mg/L), while 5.5–220 mg/L ($R^2 = 0.9999$; LOD = 5.5 mg/L; LOQ = 16.7 mg/L) after the pH change.

2.2.10. Determination of granules drug loading

To ensure homogenous drug content distribution within granules of each formulation batch, 21 samples were weighed in total, and

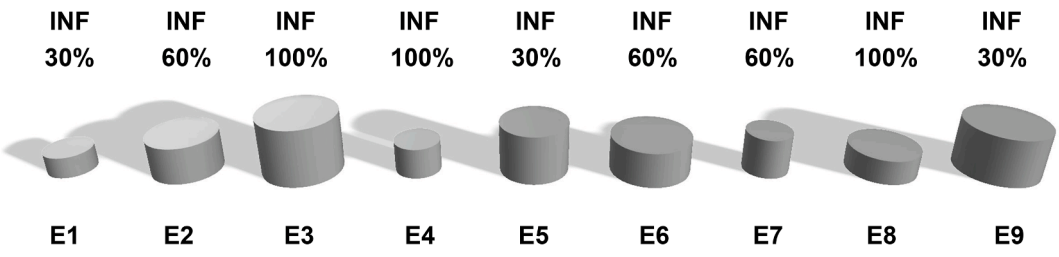

Fig. 1. Appearance of biplane cylindrical tablet printlets according to the selected multiple level and fator design: E1 to E9.

transferred to 250 mL volumetric flasks containing pH 6.8 phosphate buffer. The flasks were exposed to 24 h of magnetic stirring until complete drug dissolution and TPH concentrations were measured at 271 nm ($n = 7$; sample mass 100 mg each), utilizing 0.1 cm cells in a HP 8453 UV-Vis Spectrophotometer from Agilent Technologies Inc., Santa Clara, USA.

2.2.11. Mathematical fitting and comparison of dissolution curves

Various fit models were used for the mathematical assessment and description of the release curves. The Korsmeyer-Peppas (KP) model depicts the amount of active substance M_t released at a time t in relation to the maximum release amount M_{max} according to the power law principle (see Eq. (3)) (Korsmeyer et al., 1983). The release rate constant k, or geometry constant, is used to describe the shape of the investigated tablet. The diffusion exponent n allows conclusions to be drawn about the release mechanisms present. The model is able to picture pure Fick diffusion ($n \leq 0.45$) and case-II transport ($n \geq 0.89$) as well as anomalous transport ($0.45 < n < 0.85$) (Jahromi et al., 2020; Korsmeyer et al., 1983; Trucillo, 2022).

$$\frac{M_t}{M_{max}} = k \bullet t^n \tag{3}$$

Additionally, two alternative kinetic models, namely the Peppas Sahlin (PS) model and quadratic polynomials (QP), were employed. The PS model facilitates an examination of drug transport mechanisms influenced by both Fickian diffusion and case-II relaxations (see Eq. (4)).

$$\frac{M_t}{M_{max}} = k_1 \bullet t^n + k_2 \bullet t^{2n} \tag{4}$$

In contrast, the QP model solely permits a mathematical fitting of the release curves, irrespective of kinetic mechanisms (see Eq. (5)).

$$\frac{M_t}{M_{max}} = a \bullet t^2 + b \bullet t + c \tag{5}$$

The mean dissolution time (MDT) is a straightforward parameter for evaluating the release prolongation efficiacy of a pharmaceutical formulation (Tanigawara et al., 1982). Typically given in minutes, it quantifies the arithmetic mean dissolution time of the respective drug molecule within a medium (see Eq. (6)) (Tanigawara et al., 1982). The value t_i^* gives the time at the midpoint between t_i and t_{i-1} relating to ΔM_i, which gives the additional amount of API dissolved between timepoints t_i and t_{i-1}.

$$MDT = \frac{\sum_{i=1}^{n} t_i^* \bullet \Delta M_i}{\sum_{i=1}^{n} \Delta M_i} \tag{6}$$

2.2.12. In vitro/In vivo correlation and PBPK prediction

PBPK modeling was conducted utilizing the PK-sim® software within OSP Suite version 11, provided by Open Systems Pharmacology Inc., Boston, USA. The physico-chemical properties of the model drug TPH and information pertaining to the processes of absorption, distribution, metabolism, and excretion were derived from an extensive literature review and predominantly the PK-Sim® database. The corresponding average population models were generated based on PK-Sim® data sets. The market product, which was subsequently employed for I -vivo profile comparisons, was tested on the following average population according to its technical datasheet: group size of $n = 24$, individuals aged 20–25, male, of Caucasian ethnicity, non-smokers, and otherwise in good health, with body weights falling within a range deviating by a maximum of 20 % from their ideal body weight. For the simulation of blood profiles of the obtained 3DP tablets, the aforementioned patient group was adopted, albeit with varying real body weights. Dosage forms E4-163, E4-183, E4-219, E4-256, E4-291, and E4-322 mg were applied to patient populations weighing 50, 55, 68, 72, 75, and again 75 kg, respectively. TPH is a substance characterized by complete drug absorption. Furthermore, the previously reported systematic model-building approach was closely tied to with and retrospectively validated against published literature regarding IVIVC.

3. Results

3.1. Thermogravimetric analysis

During the 3DP production process of pharmaceutical ODFs, the galenic components undergo exposure to elevated temperatures at two stages. These include tabletop lab-scale HME, employed to manufacture API loaded granules, as well as the actual 3DP process. Hence, it is mandatory that all considered formulations are processed clearly below the decomposition temperatures of single formulation components, ideally at the lowest feasible processing temperatures (Ramos, 2022). TGA measurements ascertain the thermal stability and samples are considered to exhibit thermal stability until a cumulative gravimetric mass loss of 1 % is reached. If a sample contains water, the gravimetric mass loss refers to the plateau following moisture desorption.

The TGA measurements show that the active ingredient TPH starts to decompose at a temperature of 225 °C based on the aforementioned criteria and is completely anhydrous. On the other hand, polymer ERL retains a relatively high amount of adsorbed water, with a mass fraction of 1.10 wt%. The degradation temperature of ERL is the lowest among all single components, at 195 °C. In context of formulation development, ERL primarily constrains thermal resistance and influences water content. The plasticizer PEG remains stable throughout the entire temperature range and contains 0.25 wt% water (see Fig. A.1a). In order to identify appropriate parameters for tabletop HME, physical mixtures of the selected formulations were investigated. The degradation temperatures of formulations TPH-10, TPH-30, and TPH-50 are 202 °C, 205 °C, and 208 °C, respectively (see Fig. A.1b). At the HME process temperature of 120 °C during the production of granules, no thermal decay is to be expected. It is noteworthy that the proportion of ERL and PEG positively correlates with the water content of each formulation, increasing from TPH-50 to TPH-10. The formulations TPH-10, TPH-30, and TPH-50 show 2.23 %, 1.53 %, and 1.28 % respective water contents. The physical mixtures contain higher water amounts than the single components. During the mixing or weighing process, the formulations therefore adsorb additional water due to prolonged exposure to air. Granules were also examined to determine whether the selected 3D printing temperatures can be considered safe. All granules samples exhibit decomposition temperatures within a comparable range, specifically 215 °C for TPH-10, 212 °C for TPH-30, and 217 °C for TPH-50 (see Fig. A.1c). The 3D printing temperatures, which range between 150 °C and 180 °C, are clearly below these threshold values. TPH-50, the formulation with the lowest proportion of PEG and ERL, has desorbed water through the HME process in comparison to its physical mixture. This is not the case for TPH-10 and TPH-30, as they possess similar water contents in relation to their physical mixtures.

3.2. Differential scanning calorimetry

DSC results of formulations TPH-10, TPH-30 and TPH-50 were recorded in form of physical mixtures and granules plus respective single excipients. TPH's and ERL's melting point is outside the investigated temperature range of up to 230 °C (see Fig. A.2a-b). All samples were analyzed up to the previously determined degradation temperature of TPH, which was found to be 225 °C. A distinct melting peak with an onset at 67 °C was observed for plasticizer PEG (see Fig. A.2c). All formulations that contain PEG still display this melting peak to a certain extent (see Fig. A.2b–d). This shows that the plasticizer PEG is only partially dissolved in the formulation matrix even after shear force and temperature intensive HME (see Fig. A.2c).

3.3. Small amplitude oscillatory shear rheology

As demonstrated in previous research, melt rheology is a central parameter influencing the printability of a polymer melt (Pflieger et al., 2022). For the Flexdose™ 3D printer, a specific range of target viscosities has been established, enabling homogeneous extrusion under given printing parameters (Pflieger et al., 2022). While a polymer melt with excessively low viscosity leads to undesirable polymer melt backflow in the extrusion channel, an overly high viscosity results in physical damage of the extrusion channel due to jamming.

The rheological results depicted in Fig. 2 were recorded at the respective actual 3DP temperatures to comprehend polymer rheology within the practically relevant range. Initially, it is important to recognize that the chosen printing temperatures for the three formulations result in almost identical viscosity levels (see Fig. 2a), as established in own earlier studies (Pflieger et al., 2022). Furthermore, at these selected temperatures, there is a low shear rate dependency in the granules melts, which is inherently a desirable attribute. The curves of the three formulations closely align and remain within the previously determined range, spanning from 90 to 290 Pa·s (see Fig. 2a).

In the context of 3D printing, formulations undergo a certain shear stress similar to that encountered in traditional extrusion processes. The shear rate acting on the chosen formulations during the standardized printing process can be estimated semi-empirically. The complex viscosity is a highly shear rate-dependent parameter and calculating the apparent nozzle wall shear rate $\dot{\gamma}_{nw}$ aids in delineating the practically relevant range of shear rates (Azad et al., 2020; Boetker et al., 2016; Jackson and Dickens, 2021). Following the empirical measurement of the volumetric flow rate $\dot{Q}$ to equal 1.13 mm^3/s, value $\dot{\gamma}_{nw}$ was determined as follows with a nozzle radius r_n of 0.2 mm (Eq. (7)) (Azad et al., 2020; Boetker et al., 2016):

$$\dot{\gamma}_{nw} = \frac{4 \bullet \dot{Q}}{\pi \bullet r_n^3} = 180\,s^{-1} \quad (7)$$

The nozzle wall shear rate $\dot{\gamma}_{nw}$ was determined to be 180 s^{-1} for all three formulations at given 3DP parameters. This implies that formulation TPH-10 exhibits a viscosity of 143 Pa·s upon exiting the nozzle, while TPH-30 and TPH-50 display 119 Pa·s and 172 Pa·s, respectively. The values fall within a comparable regime.

The loss factor is also an important rheological parameter that needs to be understood at 3DP temperatures (see Fig. 2b). The loss factor is derived from the ratio of the loss modulus G'' to the storage modulus G' of individual components and is used to represent the viscous and elastic character of a polymer melt. As the loss factor converges low values, the mechanical behavior of the examined polymer approaches full elastic behavior, while at higher loss factors, the polymer entirely absorbs applied shear force. The viscous character of the formulations increases with the proportion of the active ingredient (see Fig. 2b). Additionally, the viscous character of the TPH-50 formulation exhibits a particularly high dependency on shear rate (see Fig. 2b).

3.4. Granule drug distribution homogeneity

It is imperative to ensure that during the granules manufacturing process, the active ingredient TPH is homogeneously distributed within the product. Only in this manner tablets can be printed that contain controlled and calculable quantities of active ingredients. As Table 4 demonstrates, the average true drug contents deviate by no more than 2.23 % from the target value in all three cases. As the drug content in the formulations increases, the relative standard deviation (RSD) of TPH contents also increases.

3.5. Physical pre-examinations of 3D printed oral dosage forms

For the generation of robust data, a printing process with small variations is crucial. The masses of the tablets and dimensions within a batch were recorded and are listed in Figs. 3 and 4. Low deviations in tablet dimensions and therefore tablet mass are closely associated with uniform drug contents, assuming homogeneous drug distribution within fed granules. Reproducible tablet dimensions, and therefore SFs, enable reliable evaluation of dissolution kinetics. During all 3DP processes, the tablets were individually examined for typical 3DP error phenomena such as unintentional free spaces, warping, sharp edges, under- or over-extrusion, offsets, stringing, and other undesirable effects. Six tablets of each batch ($n = 6$) were prepared and tested for in vitro dissolution.

Regarding target tablet dimensions, including radii (r) and heights (h), no deviations in a concerning range were obtained. Fig. 3 illustrates that very similar values in relation to the target dimensions were consistently achieved in every case. The result scattering exhibits low standard deviation around the target values. When deviations from the target values were observed, they leaned towards higher radii and heights. This indicates the typical 3DP phenomenon of over-extrusion, where slightly more polymer volume is extruded than what would actually be required for the creation of the object.

As depicted in Fig. 4a, tablet masses exhibited standard deviations

Table 4
Granules drug homogeneity ($n = 7$) of formulations TPH-10, TPH-30 and TPH-50 given by true drug contents and relative standard deviations (RSD).

Formulation	TPH-10	TPH-30	TPH-50
Expected drug content (wt.%)	10.00	30.00	50.00
True drug content (wt.%)	9.95	30.67	49.16
RSD (%)	± 2.14	± 3.35	± 3.99

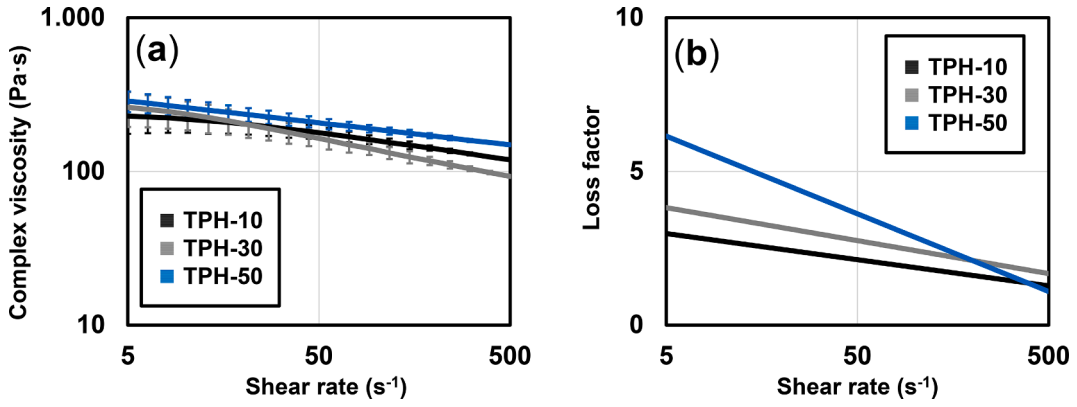

Fig. 2. Comparison of formulations TPH-10, TPH-30, TPH-50 regarding SAOS rheology results measured at respective printing temperatures: shear rate dependant (**a**) complex viscosity; (**b**) loss factor.

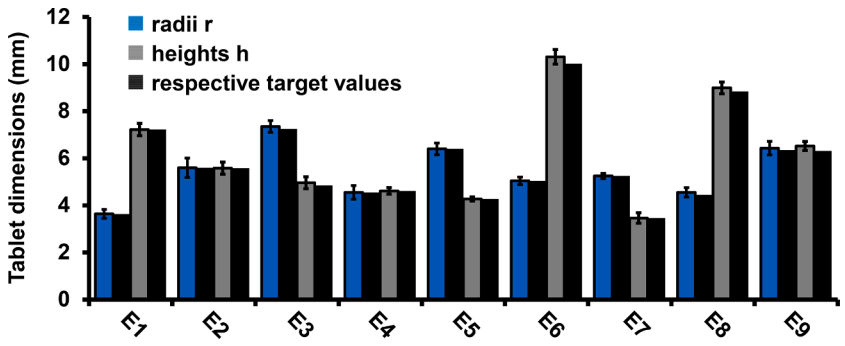

Fig. 3. Overview of the obtained tablet dimensions cylinder radius r (blue) and cylinder height h (grey) in comparison to their respective calculated target values (black). (For interpretation of the references to colour in this figure legend, the reader is referred to the web version of this article.)

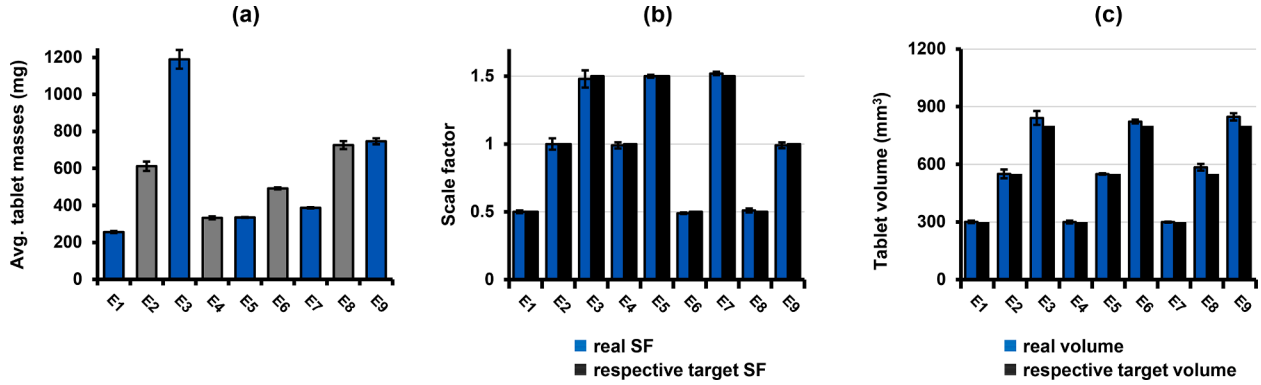

Fig. 4. Comparison of key physical tablet properties to assess physical homogeneity of the tablets in terms of (**a**) average tablet masses, (**b**) real scale factors, (**c**) and real volumes.

ranging from 0.75 % to 4.28 %. It is imperative to minimize deviations within a print set, as variance in mass also leads to variation in drug content. To ensure a robust statistical investigation, Fig. 4b compares the actual SFs with the expected SF values calculated from the obtained mean values of the tablet dimensions. Here, there were no noticeable deviations or trends concerning deviations from the target values. In the case of the actual tablet volumes, increased deviations from the target values are particularly evident for high tablet volumes and especially 800 mm^3, as illustrated in Fig. 4c. A longer printing process is consequently more susceptible to printing defects and inaccuracies. These values were also calculated from the measured radii and heights of the tablets. The suspicion of chronic slight over-extrusion intensifies, as here, too, only higher volumes than expected were obtained.

3.6. *In vitro release results and mathematical fitting*

The following Fig. 5 illustrates the in vitro dissolution results of all tablet designs E1 to E9 compared to the selected market product. The reference product is a dosage form labeled for dosing every twelve hours. The drug release profiles of tablets E1 to E9 exhibit a wide spectrum, ranging from relatively rapid and complete release within the examined time frame to incomplete, high prolongation release. Designs E5 and E6, with MDTs of 41 min and 40 min, respectively, display the fastest release and are thus not suitable for effective drug release prolongation (see Table 5). On the other hand, tablets E1 and E9 fall within a comparable range to the market product (see Table 5). These two designs also match the rate constants and diffusion exponents of the market product the most. The remaining tablet designs, E2, E3, E4, E7, and E8, demonstrate prolongation with all MDTs exceeding 398 min (see Table 5). Additionally, a direct comparison of the investigated release profiles with the chosen market product was pursued (see Table 5).

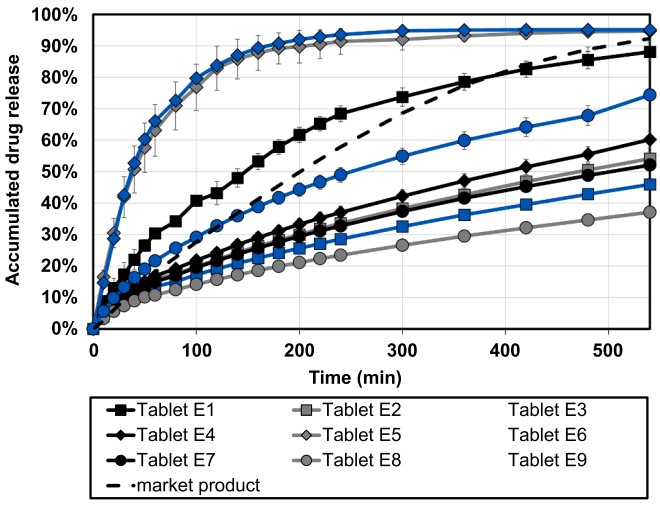

Fig. 5. In vitro dissolution results of selected tablet designs: (▬■▬) E1; (▬◆▬) E2; (▬●▬) E3; (▬□▬) E4; (▬◇▬) E5; (▬○▬) E6; (▬■▬) E7; (▬◆▬) E8; (▬○▬) E9; (▬ ▬) market product Theophyllin-retard ratiopharm®.

3.7. *Taguchi analysis*

3.7.1. *Statistical significance of factors*

The statistical significance of parameters is evaluated with the help of p-value tests. For this work, a parameter is considered statistically

Table 5
Summary of MDTs and application of the KP fit to drug release curves E1 to E9 with respective coefficient of determination, KP rate constants k and diffusion coefficients n.

Tablet	MDT (min)	R^2 of KP fit	KP rate constant k	KP diffusion exponent n	R^2 of PS fit	R^2 of QP fit
E1	154	0.9985	2.11×10^{-2}	0.6364	0.9905	0.8005
E2	474	0.9996	1.40×10^{-2}	0.5805	0.9997	0.9861
E3	630	0.9998	1.22×10^{-2}	0.5766	0.9997	0.9845
E4	398	0.9998	1.41×10^{-2}	0.5955	0.9998	0.9842
E5	41	0.9978	3.87×10^{-2}	0.6888	0.9206	0.5593
E6	40	0.9964	3.00×10^{-2}	0.7643	0.9094	0.5367
E7	506	0.9998	1.26×10^{-2}	0.5912	0.9997	0.9849
E8	918	0.9998	1.06×10^{-2}	0.5650	0.9998	0.9823
E9	252	0.9988	1.89×10^{-2}	0.5924	0.9982	0.8693
MP	201	0.9997	5.10×10^{-2}	0.8647	0.9996	0.9288

significant, without effect relationships, for p-values below 0.10. In the analyses, the mean MDTs were employed as the response variable. As summarized in Table 6, two factors exhibit high statistical significance, while the other two are considered insignificant. Therefore, influencing the MDT of a tablet design through the two factors, SF and V, is not statistically meaningful. The two statistically relevant parameters, DC and INF, have p-values below 0.10, with the factor INF exhibiting particularly high significance.

3.7.2. Factor effect size analysis

Subsequent Fig. 6a presents the mean main effect plots for the chosen response variable, MDT. Only the two factors assessed as statistically relevant, DC and INF, are further investigated. As expected, the results indicate that the MDT response increases with the INF value in an almost linear fashion. The carrier polymer ERL constitutes a polymer matrix that releases the drug primarily through diffusion and not erosion. The factor INF is closely correlated with the contact surface area available for potential drug diffusion between the formulation and the solvent. Kumar et al., Ibrić et al., and Qi et al. also observed this positive correlation in their work (McDonagh et al., 2022; Obeid et al., 2021; Sharma et al., 2021). Furthermore, the results indicate that the average responses strongly depend on the selected formulation and its DC. While TPH-10 and TPH-50 generate comparatively elevated average MDTs, TPH-30 results in reduced release prolongation. To ensure comparability, the excipient ratio was kept constant within each formulation. However, different parameters had to be selected for the 3D printing of each formulation due to processability considerations. The exact reason why formulation TPH-30 generates particularly low responses needs further investigation. Potential reasons may encompass supersaturation effects and hence, presence of API crystals.

In Fig. 6b, the four examined factors are graphically compared in terms of effect sizes. The effect size of a factor describes the maximum difference in the generated averaged responses, aiding in assessing the importance of a factor for the targeted control of the response variable. Both factors, V and SF have very little influence on the response variable, characterized by negligible effect sizes. By a significant margin, the most influential factor is INF, and the factor DC also plays a substantial role in controlling the response variable.

Table 6
Assessment of statistical factor significance by calculation of p-values.

Factor	p-value	Statistical interpretation
Drug content (DC)	0.06889	Significant
Body infill (INF)	0.00001	Significant
Scale factor (SF)	0.96042	Insignificant
Tablet volume (V)	0.62853	Insignificant

3.7.3. Standard deviation minimization

A statistical analysis using the Taguchi method also allows an assessment of the factors and their factor levels in terms of the generated relative SDs (see Fig. 7a). In tablet production, the respective factor levels should always be chosen to minimize standard deviations. Regarding the factor DC, SDs can be kept relatively low, especially for formulations TPH-10 and TPH-50. At factor level DC equal to 30 %, the relative SD within the generated response rises to over 9 %. For the factor INF, an increase in magnitude is associated with a significant decrease in SDs. The most uniform and reproducible response results were achieved at full tablet body infill. Even at an INF of 60 %, SDs were generated within an acceptable range for a stable process. Unlike high INF values, low INF values lead to process difficulties, and the tablet printing process becomes increasingly imprecise, resulting in heterogeneous drug release profiles for the obtained tablets.

3.7.4. Signal-to-noise ratio maximation

The S/N ratio is employed to pinpoint control factor configurations that reduce the impact of noise factors on variability (see Fig. 7b). For each level of every control factor, main factor S/N ratios were computed, and generally efforts should be directed towards achieving the highest possible S/N ratio values. Regarding the control factor DC, factor levels TPH-10 and TPH-50 exhibit desirable values once again, whereas factor level TPH-30 is associated with the highest degree of noise effects. In the case of factor INF, levels 60 % and 100 % consistently yield the most reproducible results, while an INF of 30 % is subject to high levels of noise. With complete infill, the effects of uncontrollable factors are minimized, allowing for maximized process robustness and minimized variability.

3.7.5. Interim summary for beneficial factors design

In summary, factors V and SF do not need be considered in the context of drug release design as they are statistically irrelevant factors. Nevertheless, in a final tablet design, factor levels should be chosen based on reproducibility. As Fig. 7 demonstrates, for both V and SF, the first or third factor level should be selected. For the DC factor, formulations akin to TPH-10 or TPH-50 should be adhered to in terms of process stability, while the focus for INF should lean towards higher factor levels, 60 % and especially 100 %.

The designed formulations in this study that exhibit release profiles comparable to the market product, E1 and E9, both exclusively meet the suitable factor levels required for process robustness.

3.8. Release profile kinetic modeling

Table 5 compares the coefficients of determination for the selected kinetic model fits to assess fit quality. The KP fit emerges as the most suitable fit for describing the release curves, which is why the release rate constant k and diffusion exponent n are provided for KP. The diffusion exponent ranges between 0.45 and 0.89 ($0.45 < n < 0.89$) for all investigated tablet designs, indicating anomalous transport with both Fickian diffusion and Case-II transport. The PS model also demonstrates the capability to describe anomalous transport and is therefore included additionally. A purely mathematical evaluation of the release profiles using QP plots proved to be the least successful.

3.9. Dose individualization considerations

After demonstrating that the fundamental proportional drug release strongly depends on the tablet design parameters, we consider the real

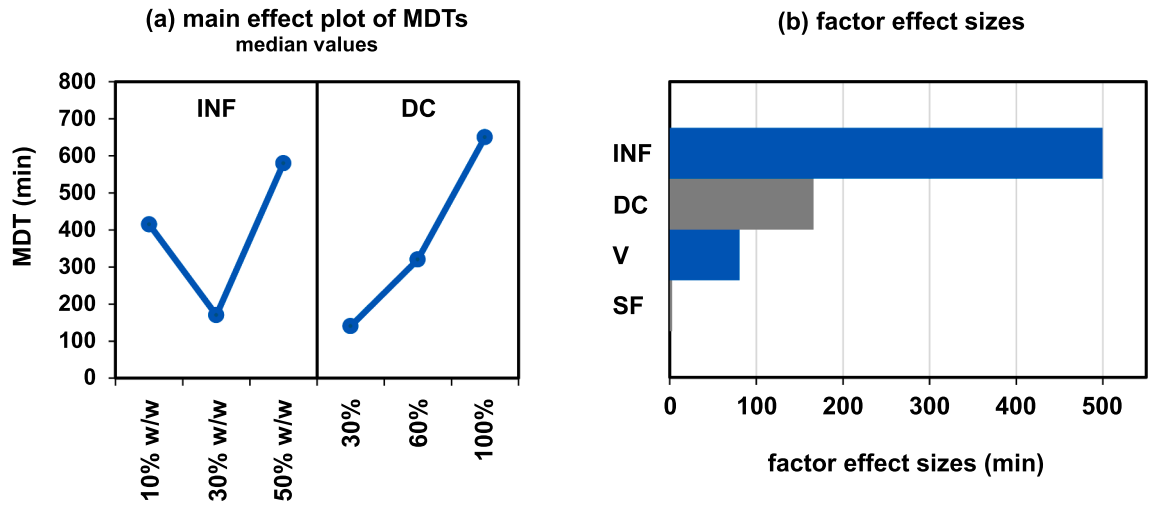

Fig. 6. Statistical analysis according to Taguchi: (**a**) statistically significant factors DC and INF mean main effect plots of response MDT; (**b**) factor effect size graphical illustration.

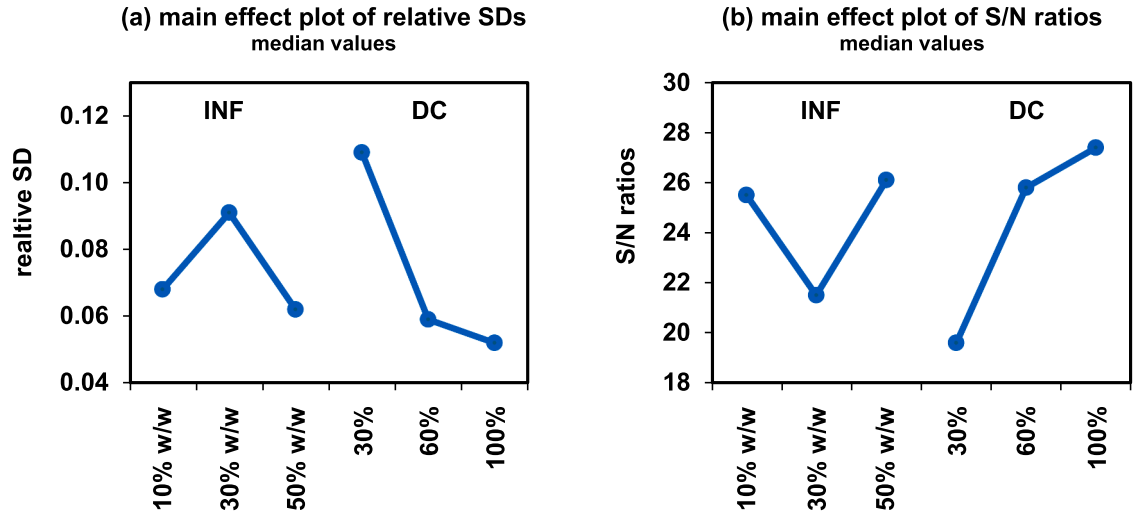

Fig. 7. Analysis of statistically significant factors DC and INF following Taguchi: (**a**) mean main effect plots of relative SDs; (**b**) mean main effect plots of S/N ratios.

printed TPH dose of the tablets for dosage customization. The real printed dose is neither an input nor an output parameter of the chosen DOE but rather a directly dependent combinatorial outcome of the parameters DC, V, and INF, excluding SF. It is crucial to comprehend that correcting dissolution profiles by modifying these parameters inevitably leads to alterations in the real printed doses. Once a tablet design with a suitable release is identified, the question arises as to whether it can be geometrically scaled for individualization while preserving the release profiles.

To address this research question, tablet design E4 was taken into consideration, as the greater drug release prolongation was expected to result in an improved drug blood level profile, maintaining the blood level between 1 and 5 μg/mL for an extended period. Although several tablet designs exhibit similar sustained drug release profiles (E2, E3, E4, E7, E8), only E4 was chosen for further examination due to its particularly beneficial design parameters within this group. In addition to the original E4 design derived from the DOE, six other real printed doses were produced and investigated for their drug release. These geometrically identical tablets, based on the E4 design, underwent isotropic scaling to cover real printed doses relevant for practical applications adhering to the low-dose TPH approach previously mentioned in between 163 mg and 322 mg TPH.

As Fig. 8 illustrates, the scaling of tablet design E4 indeed exerts a substantial influence on the drug release behavior. The trend reveals that as the tablet volume, and consequently the real printed dose, increases, the proportional drug release decreases, leading to a deceleration in the release profile (see Fig. 8a). This phenomenon is attributed to the declining ratio of tablet surface area to volume. Similar trends have been observed by other research groups in the context of 3DP solid dosage forms (El Aita et al., 2020; Windolf et al., 2021). Despite the proportional decrease in drug release with increasing dose strength of E4 (Fig. 8a), an opposite effect is observed in terms of the absolute amounts of released TPH (see Fig. 8b). With a higher E4 absolute drug content, the release rate of the absolute amount of TPH also increases. In an effort to understand the mentioned drug release phenomena for our specific case a linear regression study of MDTs and KP fit parameters was carried out. Table 7 summarizes the fit parameters obtained and certain trends are visible. While the MDT positively correlates with increasing real printed E4 doses, the KP release rate constant k decreases. The KP fits for the single release curves all show coefficients of determination of more than 0.9997. Fig. 9 depicts the MDTs and the KP release rate constants k for a set specific diffusion exponent n, along with the corresponding linear regression curves and their coefficients of determination versus printed doses. The obtained regression coefficients of determination,

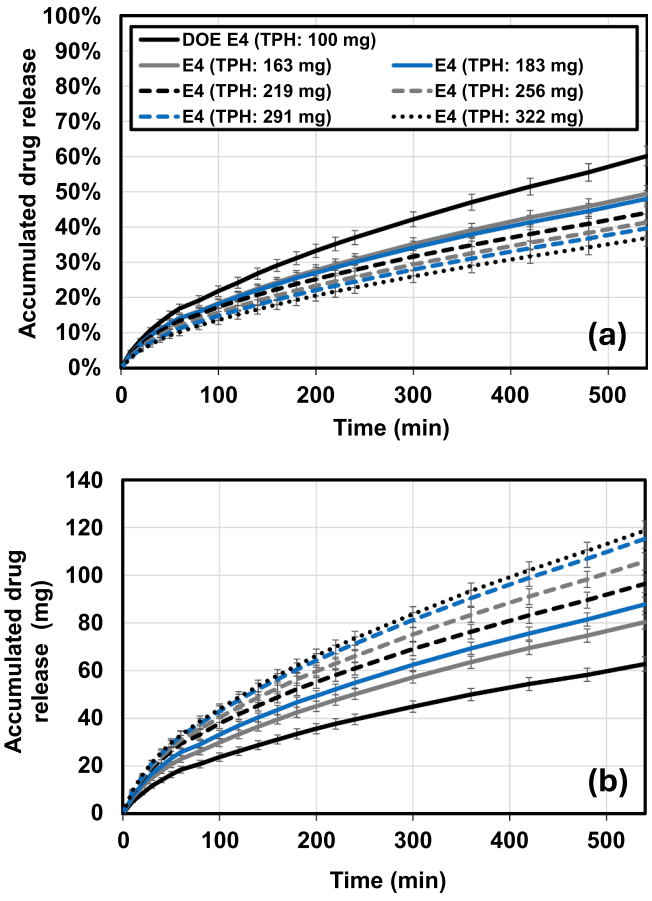

Fig. 8. In vitro dissolution results of selected E4 tablet designs: (**a**) proportional drug release regarding the real printed dose over time; (**b**) absolute released TPH over time.

Table 7
Summary of MDTs and application of the KP fit to drug release curves E1, E1-A, E1-B, E9, E9-A, E9-B and scaled E4 designs with respective coefficient of determination, KP rate constants k and diffusion coefficients n.

Tablet	INF	MDT (min)	R^2 of KP fit	Rate constant k	Diffusion exponent n
E4	100.0 %	355	0.9997	1.56×10^{-2}	0.5900
E4-163 mg	100.0 %	541	0.9999	1.22×10^{-2}	
E4-183 mg	100.0 %	559	0.9998	1.20×10^{-2}	
E4-219 mg	100.0 %	624	0.9999	1.13×10^{-2}	
E4-256 mg	100.0 %	718	0.9999	1.03×10^{-2}	
E4-291 mg	100.0 %	795	0.9999	9.72×10^{-3}	
E4-322 mg	100.0 %	904	0.9999	9.01×10^{-3}	
MP	-	201	0.9997	5.10×10^{-2}	0.8647

with values of $R^2 = 0.9809$ for the MDTs and $R^2 = 0.9959$ for k, suggest high linearity of the release result fits. These findings can contribute to making predictions for the drug releases of various E4-related real printed dose strengths.

3.10. IVIVC modeling of suitable E4-related dose strengths

As previously mentioned, finding suitable designs for a solid dosage form with sustained drug release, allowing for free dose individualization while maintaining proportional drug releases, is particularly challenging and extensive. This is especially true since any modification or scaling of a tablet design alters both the proportional release and the absolute drug content, as demonstrated. For our specific application, E4 drug releases were modelled in potential patient groups using PBPK modeling.

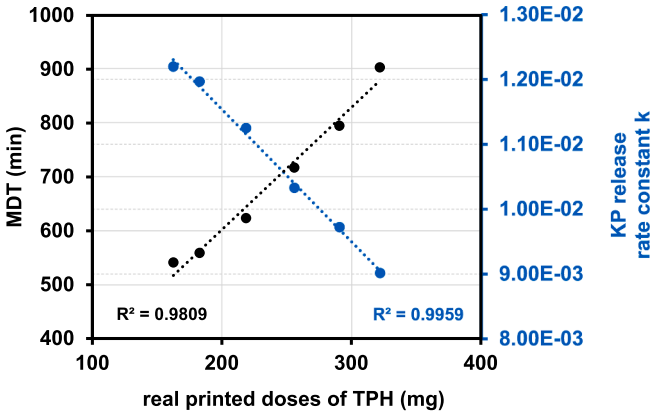

Fig. 9. Linear regression models for drug release of six selected E4-related tablet designs for MDTs and KP release rate constants k (for diffusion exponents n = 0.59).

Fig. 10 illustrates the in vivo profile of the MP in direct comparison to our developed 3DP dosage forms. The MP's data was extracted from the corresponding technical information data sheet. The results for tablets E4 with varying dose strengths of 163, 183, 219, 256 and 322 mg were simulated using patient groups according to the information provided in Fig. 10 and chapter 2.2.12. As the absolute drug release of the E4 tablet with a strength of 322 mg showed only marginal differences compared to that with 291 mg, it was excluded for the purpose of individualization due to redundancy. While the MP exceeds the targeted "low dose" TPH range with a spike, E4 exhibits a more pronounced prolongation in blood profile kinetics (Fig. 10). Recent pharmaceutical insights indicate that TPH blood serum concentrations between 1 and 5 μg/mL are effective in combating Covid-19 symptoms and other pulmonary diseases while minimizing side effects. This range is outlined in Fig. 10, and the investigated E4 dosage forms do not exceed the target range but maintain therapeutic blood levels for 34 h. Additionally, the MP reaches the timepoint of the maximum serum concentration (t_{max}) after 8 h, while dosage forms E4 achieve t_{max} further delayed after 10 h. Following the maximum serum concentration (c_{max}), the TPH concentration decreases with a less steep gradient for our 3DP tablet designs compared to the MP, as evident from the calculated elimination rate constants (k_{el}) (see Table 8). A more gradual decline in blood serum levels minimizes side effects for patients. Furthermore, the E4 tablets require only a single administration, whereas the technical data sheet of the MP indicates that intake is required up to six times a day. Less frequent administration potentially enhances patient compliance.

3.11. Discussion of results

The active ingredient TPH has already been printed using various 3DP technologies, such as filament fused deposition modeling printing or direct powder extrusion, in previous studies (Giri et al., 2020; Kuźmińska et al., 2021; Okwuosa et al., 2016; Tan et al., 2019). However, all these studies focused solely on technical proof of concept, the novelty of the applied printing technologies or formulation development. The printer employed in this investigation has been documented in literature only once (Pflieger et al., 2022). To our knowledge, the printing of low doses of TPH has not been reported previously. Furthermore, the utilization of PBPK modeling for printed TPH tablets,

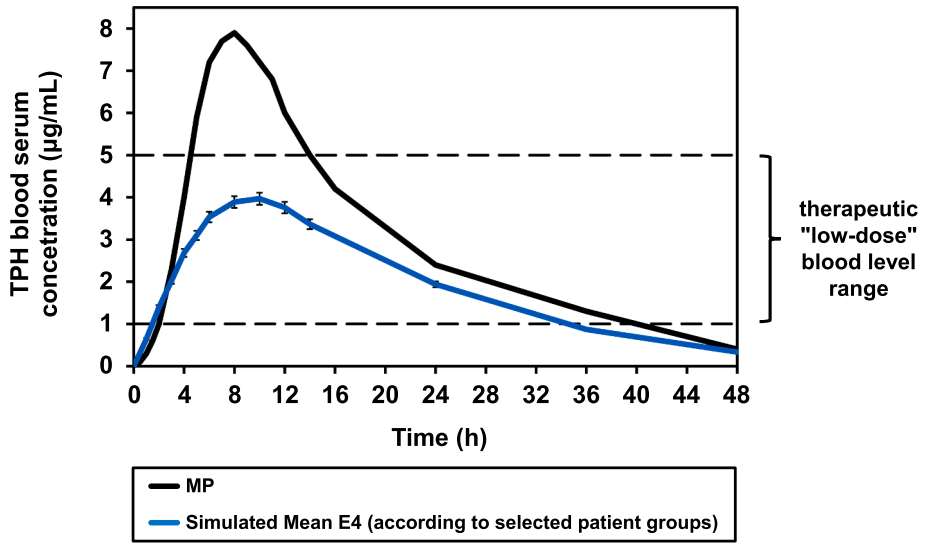

Fig. 10. Modelled TPH blood serum levels of 3DP E4 tablets according to individual patient populations in comparison to the MP.

Table 8
Comparison of blood profile parameters of the MP and the mean of 3DP E4 tablets including the maximum drug blood serum concentration (c_{max}), time-point of maximum blood serum concentration (t_{max}), area under curves (AUC) and elimination rate constants (k_{el}).

Tablet	c_{max} (µg/mL	t_{max} (h)	AUC (h · µg/ml)	k_{el} (h^{-1})
E4	3.97 ± 0.14	10	84.73 ± 2.98	6.66×10^{-2}
MP	8.26 ± 1.34	8	139.2 ± 35.94	10.5×10^{-2}

as well as its comparison to that of commercially available products, has not been documented in existing literature. A more detailed evaluation or investigation of the control of the real printed doses or release properties was also not conducted. Our work addresses this gap in the research field, providing a foundation for assessing critical design parameters for the control of drug release of 3D-printed TPH dosage forms. The freedom in tablet design and, consequently, the control of release properties represents a key strength of the pharmaceutical 3DP technology. A comprehensive understanding of the complex relationships between tablet design parameters and release properties is essential, for enabling a greater acceptance of this technology in real world application.

4. Conclusions

In this study, various 3D printed TPH dosage forms were investigated for their sustained drug release properties. An initial statistical DOE served as a first assessment of parameter effect sizes and helped to establish appropriate process parameter levels for a stable printing process. On top of that, the study illustrated the challenge of achieving freely scalable tablet designs, especially when considering sustained drug release in combination with tailored dosages. Our findings indicate that modifying the actual printed dose inevitably alters the drug release of the dosage form. Thus, individualized application must be further investigated and tailored for each individual case to find real world application. Additionally, it was observed that changes in the tablets' drug releases, as assessed by various metrics like the mathematical KP model fit or the MDT, demonstrate a linear correlation. This establishes a predictable connection between the actual printed dose of our tablet designs and their sustained drug release, which renders calculation of the exact dimensions and printing parameters for dose individualization possible.

CRediT authorship contribution statement

Thomas Pflieger: Conceptualization, Methodology, Validation, Investigation, Data curation, Writing – original draft preparation, Visualization. **Rakesh Venkatesh:** Conceptualization, Methodology, Writing–review and editing, Supervision. **Markus Dachtler:** Conceptualization, Writing–review and editing. **Karin Cooke:** Writing–review and editing. **Stefan Laufer:** Conceptualization, Methodology, Writing–review and editing, Supervision. **Dominique Lunter:** Conceptualization, Methodology, Writing–review and editing, Supervision.

Declaration of competing interest

The authors declare that they have no known competing financial interests or personal relationships that could have appeared to influence the work reported in this paper.

Data availability

The data that has been used is confidential.

Appendix A. Supplementary material

Fig. A.1. TGA results of: (a) single formualtion components; (b) formulation physical mixtures and (c) post-HME granules. Respecitve degradation temperatures are marked by outlined circles. Fig. A.2. Comparison of DSC measurements of: (a) TPH; (b) ERL; (c) PEG; (d) TPH-10 physical mixture; (e) TPH-10 granules; (f) TPH-30 physical mixture; (g) TPH-30 granules; (h) TPH-50 physical mixture; (i) TPH-50 granules. Supplementary data to this article can be found online at https://doi.org/10.1016/j.ijpharm.2024.124207.

References

Asmus, M.J., Weinberger, M.M., Milavetz, G., Marshik, P., Teresi, M.E., Hendeles, L., 1997. Apparent decrease in population clearance of theophylline: Implications for dosage. Clin. Pharmacol. Ther. 62, 483–489.
Azad, M.A., Olawuni, D., Kimbell, G., Badruddoza, A.Z.M., Hossain, M.S., Sultana, T., 2020. Polymers for extrusion-based 3D printing of pharmaceuticals: a holistic materials–process perspective. Pharmaceutics 12, 124.
Barnes, P.J., 2003. Theophylline: new perspectives for an old drug. Am. J. Respir. Crit. Care Med. 167, 813–818.
Boetker, J., Water, J.J., Aho, J., Arnfast, L., Bohr, A., Rantanen, J., 2016. Modifying release characteristics from 3D printed drug-eluting products. Eur. J. Pharm. Sci. 90, 47–52.

Chandekar, A., Mishra, D.K., Sharma, S., Saraogi, G.K., Gupta, U., Gupta, G., 2019. 3D printing technology: a new milestone in the development of pharmaceuticals. Curr. Pharm. Des. 25, 937–945.
Chen, G., Xu, Y., Kwok, P.C.L., Kang, L., 2020. Pharmaceutical applications of 3D printing. Addit. Manuf. 34, 101209.
Cosio, B.G., Iglesias, A., Rios, A., Noguera, A., Sala, E., Ito, K., Barnes, P.J., Agusti, A., 2009. Low-dose theophylline enhances the anti-inflammatory effects of steroids during exacerbations of COPD. Thorax 64, 424–429.
Dachtler, M., Huber, G., Pries, T., 2020. 2D & 3D-Print Technologien in der pharmazeutischen Industrie, Digitale Transformation von Dienstleistungen im Gesundheitswesen VII. Springer 53–66.
Dachtler, M., Eggenreich, K., Pflieger, T., 2021. Digital health - digital 2D/3D printing of personalized medication. In: Proceedings of the 4th International Symposium on Pharmaceutical Engineering Research (SPhERe), pp. 15–17.
Devereux, G., Cotton, S., Fielding, S., McMeekin, N., Barnes, P.J., Briggs, A., Burns, G., Chaudhuri, R., Chrystyn, H., Davies, L., 2019. Low-dose oral theophylline combined with inhaled corticosteroids for people with chronic obstructive pulmonary disease and high risk of exacerbations: a RCT. Health Technology Assessment (winchester, England) 23, 1.
Drumond, N., 2020. Future perspectives for patient-centric pharmaceutical drug product design with regard to solid oral dosage forms. J. Pharm. Innov. 15, 318–324.
El Aita, I., Rahman, J., Breitkreutz, J., Quodbach, J., 2020. 3D-Printing with precise layer-wise dose adjustments for paediatric use via pressure-assisted microsyringe printing. Eur. J. Pharm. Biopharm. 157, 59–65.
Giri, B.R., Song, E.S., Kwon, J., Lee, J.-H., Park, J.-B., Kim, D.W., 2020. Fabrication of intragastric floating, controlled release 3D printed theophylline tablets using hot-melt extrusion and fused deposition modeling. Pharmaceutics 12, 77.
Huber, G., Dachtler, M., Edinger, D., 2017. Digitalisierung in der Pharmaindustrie. Digitale Transformation von Dienstleistungen im Gesundheitswesen II: Impulse für das Management, 241-255.
Jackson, S., Dickens, T., 2021. Rheological and structural characterization of 3D-printable polymer electrolyte inks. Polym. Test. 104, 107377.
Jahromi, L.P., Ghazali, M., Ashrafi, H., Azadi, A., 2020. A comparison of models for the analysis of the kinetics of drug release from PLGA-based nanoparticles. Heliyon 6, e03451.
Karow, T., Lang-Roth, R., 2020. Allgemeine und spezielle Pharmakologie und Toxikologie: vorlesungsorientierte Darstellung und klinischer Leitfaden für Studium und Praxis: 2021. Dr. med Thomas Karow.
Klein, B., 2021. Versuchsplanung-Design of Experiments: Einführung in die Taguchi und Shainin-Methodik. Walter de Gruyter GmbH & Co KG.
Korsmeyer, R.W., Gurny, R., Doelker, E., Buri, P., Peppas, N.A., 1983. Mechanisms of solute release from porous hydrophilic polymers. Int. J. Pharm. 15, 25–35.
Kuźmińska, M., Pereira, B.C., Habashy, R., Peak, M., Isreb, M., Gough, T.D., Isreb, A., Alhnan, M.A., 2021. Solvent-free temperature-facilitated direct extrusion 3D printing for pharmaceuticals. Int. J. Pharm. 598, 120305.
McDonagh, T., Belton, P., Qi, S., 2022. An investigation into the effects of geometric scaling and pore structure on drug dose and release of 3D printed solid dosage forms. Eur. J. Pharm. Biopharm. 177, 113–125.
Menditto, E., Orlando, V., De Rosa, G., Minghetti, P., Musazzi, U.M., Cahir, C., Kurczewska-Michalak, M., Kardas, P., Costa, E., Sousa Lobo, J.M., 2020. Patient centric pharmaceutical drug product design—the impact on medication adherence. Pharmaceutics 12, 44.
Montaño, L.M., Sommer, B., Gomez-Verjan, J.C., Morales-Paoli, G.S., Ramírez-Salinas, G. L., Solís-Chagoyán, H., Sanchez-Florentino, Z.A., Calixto, E., Pérez-Figueroa, G.E., Carter, R., 2022. Theophylline: Old drug in a new light, application in COVID-19 through computational studies. Int. J. Mol. Sci. 23, 4167.
Obeid, S., Madžarević, M., Ibrić, S., 2021. Tailoring amlodipine release from 3D printed tablets: influence of infill patterns and wall thickness. Int. J. Pharm. 610, 121261.
Okwuosa, T.C., Stefaniak, D., Arafat, B., Isreb, A., Wan, K.-W., Alhnan, M.A., 2016. A lower temperature FDM 3D printing for the manufacture of patient-specific immediate release tablets. Pharm. Res. 33, 2704–2712.
Paloucek, F.P., Rodvold, K.A., 1988. Evaluation of theophylline overdoses and toxicities. Ann. Emerg. Med. 17, 135–144.
Pflieger, T., Venkatesh, R., Dachtler, M., Eggenreich, K., Laufer, S., Lunter, D., 2022. Novel approach to pharmaceutical 3D-printing omitting the need for filament—investigation of materials, process, and product characteristics. Pharmaceutics 14, 2488.
Pouya, F.D., Nemati, M., Asl, E.R., Rasmi, Y., 2020. The combination effects of theophylline and corticosteroids in COVID-19. Health Biotechnol Biopharma 4, 1–5.
Ramos, P., 2022. Application of thermal analysis to evaluate pharmaceutical preparations containing theophylline. Pharmaceuticals 15, 1268.
Ratiopharm, 2020. Fachinformation Theophyllin retard-ratiopharm 250 mg Hartkapseln.
Rizzuti, S., De Napoli, L., 2020. ANOVA applied to the taguchi method: a new interpretation, Design Tools and Methods in Industrial Engineering: Proceedings of the International Conference on Design Tools and Methods in Industrial Engineering, ADM 2019, September 9–10, 2019, Modena, Italy. Springer, pp. 342–351.
Robinson, J.H., Callister, L.C., Berry, J.A., Dearing, K.A., 2008. Patient-centered care and adherence: definitions and applications to improve outcomes. J. Am. Acad. Nurse Pract. 20, 600–607.
Roy, R.K., 2010. A Primer on the Taguchi Method. Society of Manufacturing Engineers.
Seoane-Viaño, I., Trenfield, S.J., Basit, A.W., Goyanes, A., 2021. Translating 3D printed pharmaceuticals: from hype to real-world clinical applications. Adv. Drug Deliv. Rev. 174, 553–575.
Sharma, V., Shaik, K.M., Choudhury, A., Kumar, P., Kala, P., Sultana, Y., Shukla, R., Kumar, D., 2021. Investigations of process parameters during dissolution studies of drug loaded 3D printed tablets. Proc. Inst. Mech. Eng. [H] 235, 523–529.
Siddharthan, T., Pollard, S.L., Jackson, P., Robertson, N.M., Wosu, A.C., Rahman, N., Padalkar, R., Sekitoleko, I., Namazzi, E., Alupo, P., 2021. Effectiveness of low-dose theophylline for the management of biomass-associated COPD (LODOT-BCOPD): study protocol for a randomized controlled trial. Trials 22, 1–9.
Souto, E.B., Campos, J., Filho, S., Teixeira, M., Martins-Gomes, C., Zielinska, A., Carbone, C., Silva, A., 2019. 3D printing in the design of pharmaceutical dosage forms. Pharm. Dev. Technol. 24, 1044–1053.
Tan, D.K., Maniruzzaman, M., Nokhodchi, A., 2019. Development and optimisation of novel polymeric compositions for sustained release theophylline caplets (PrintCap) via FDM 3D printing. Polymers 12, 27.
Tanigawara, Y., Yamaoka, K., Nakagawa, T., Uno, T., 1982. New method for the evaluation of in vitro dissolution time and disintegration time. Chem. Pharm. Bull. 30, 1088–1090.
Trivedi, M., Jee, J., Silva, S., Blomgren, C., Pontinha, V.M., Dixon, D.L., Van Tassel, B., Bortner, M.J., Williams, C., Gilmer, E., 2018. Additive manufacturing of pharmaceuticals for precision medicine applications: a review of the promises and perils in implementation. Addit. Manuf. 23, 319–328.
Trucillo, P., 2022. Drug carriers: a review on the most used mathematical models for drug release. Processes 10, 1094.
Usp, 2020. United States Pharmacopeia (USP): Theophylline Extended Release Capsules - Test 9. U.S. Food and Drug Administration.
Windolf, H., Chamberlain, R., Quodbach, J., 2021. Predicting drug release from 3D printed oral medicines based on the surface area to volume ratio of tablet geometry. Pharmaceutics 13, 1453.
Wishart, D.S., 2016. Emerging applications of metabolomics in drug discovery and precision medicine. Nat. Rev. Drug Discov. 15, 473–484.

5. An Investigation of the Drug Release Kinetics of 3D-Printed Two Compartment Theophylline and Prednisolone Tablets

Thomas Pflieger[1,4], Rakesh Venkatesh[1], Markus Dachtler[1],
Stefan Laufer[2], Dominique Lunter[3,*]

[1] DiHeSys Digital Health Systems GmbH, 73529 Schwäbisch Gmünd, Germany

[2] Pharmaceutical Chemistry, Eberhard Karls University, 72074 Tübingen, Germany

[3] Pharmaceutical Technology, Eberhard Karls University, 72074 Tübingen, Germany

* Corresponding author

SSRN

Year 2024, Preprint 4932428
DOI: https://doi.org/10.2139/ssrn.4932428

An Investigation of the Drug Release Kinetics of 3D-Printed Two Compartment Theophylline and Prednisolone Tablets

Thomas Pflieger [1,3], Rakesh Venkatesh [1], Markus Dachtler [1], Stefan Laufer [2], Dominique Lunter [3,*]

[1] DiHeSys Digital Health Systems GmbH (Dihesys), Marie-Curie-Strasse 19, 73529 Schwaebisch Gmuend, Germany, info@dihesys.com

[2] Chair of Pharmaceutical Chemistry, Eberhard Karls University, Auf der Morgenstelle 8, 72074 Tuebingen, Germany

[3] Chair of Pharmaceutical Technology, Eberhard Karls University, Auf der Morgenstelle 8, 72074 Tuebingen, Germany

* Corresponding author: dominique.lunter@uni-tuebingen.de

University of Tuebingen, Chair of Pharmaceutical Technology, Auf der Morgenstelle 8, 72076 Tuebingen, Germany

Tel.: +49-7071-2974558

Abstract

Pharmaceutical 3D printing (3DP) not only offers the possibility of dose personalization but also the co-administration of multiple active pharmaceutical ingredients (APIs) in one combination tablet. In this study, Theophylline (TPH) and Prednisolone (PSL) were printed as bi-layered tablets, which are single tablets with two distinct separate compartments. New findings show that the combination therapy of TPH with systemic corticosteroids shows a highly synergistic effect in the treatment of pulmonary diseases. For TPH, a drug with a narrow therapeutic window (NTW), precise sustained release requirements are mandatory, while PSL requires immediate drug release and is individually administered in doses specifically tied to the treatment progression. The study aims to understand the extent to which the combination of two tablet compartments influences the individual drug dissolution kinetics of the respective single compartments. Utilizing a full factorial statistical experimental design, various practically relevant doses were produced, investigated for their drug release, analyzed using different mathematical model fits, and compared with respective mono-tablets. The results show that the sustained drug release of TPH is not significantly influenced by the addition of a second compartment in relationship to respective doses. Individualization of bi-layered tablet doses while maintaining similar release profiles is possible with the given design setup, as release curves still show high similarity. In all tablet designs, PSL release occurred sufficiently fast, with the release rate correlating to the surface area-to-volume ratio (SA/V) as the main determining parameter.

Keywords

pharmaceutical 3D printing; solid oral dosage forms; patient-centered therapy; drug coadministration; theophylline; prednisolone

1. Introduction

3D printing (3DP) introduces the possibility of unprecedented therapy precision and adaptability to the production of dosage forms [1-5]. This advanced technology allows the individual production of solid oral dosage forms tailored to unique patient requirements on-demand and on-site [1-7]. Beyond dose personalization, pharmaceutical 3DP facilitates the production of complex tablet structures, including multi-drug combinations [1,4,6-10]. By simplifying intricate medication regimens into a single, precisely formulated dosage form, the burden of multiple tablet intake is reduced for the patient [4,6,8-10]. This way, a strong enhancement of patient compliance is achieved [4,6,8-10].

In the subsequent study, the examined objects referred to as bi-layered tablets, abbreviated bi-tablets, represent multi-drug combination oral dosage forms, consisting of two separate tablet compartments containing distinct active pharmaceutical ingredients (APIs) [11-14]. Specifically, these are Theophylline (TPH) and Prednisolone (PSL), employed in combination for the treatment of pulmonary diseases like chronic obstructive pulmonary disease (COPD), asthma and exacerbations of Covid-19 [15-22]. Patients suffering from pulmonary diseases benefit from dosage forms administered orally, as opposed to typically prescribed inhaled medications. Patients often suffer from compromised lung function, difficulty in coordinating inhalation, or general inadequate response to inhaled therapies [23-25]. Systemic drug delivery ensures absorption and therefore reproducible therapy success for patients [23-25]. Recent studies investigating bronchodilator TPH document a synergy in combination with corticosteroids like PSL, especially when applied at low blood plasma levels of 1 to 5 µg/mL [5,15,16,18,19,21]. TPH directly impacts histone deacetylase (HDAC) activity, leading to the suppression of inflammatory genes and amplification of the anti-inflammatory effects of the corticosteroid [15-17,20].

Both the active substances, TPH and PSL, are particularly suitable for personalized medicine and delivery through pharmaceutical 3DP. TPH, a drug with a narrow therapeutic window (NTW), is individually administered based on the patient's body weight (BW) [15,22]. Incorrect dosing of NTW drugs risks severe side effects or even toxicity, which is why there is a special need for precision and vigilant monitoring [5,15,22,26]. On the other hand, PSL is administered with a high initial dose, promptly followed by reduction to a maintenance dose that is tapered off towards therapy finalization in accordance with the patients' treatment progression [27,28]. By means of 3DP, one can closely accompany this administration protocol.

The 3D printer utilized in this publication is the FlexDose™ Printer developed by Dihesys [5,29-32]. This screw extrusion-based printer conveys granules that hold APIs, with controlled polymer melt volume flow emerging from a heated nozzle [2,3,5,29-32]. By moving in three-dimensional directions and incrementally printing individual horizontal layers, it produces objects that were previously digitally modeled [5,29-34]. The printer has the capability to mount up to four independently functional print heads [5,29-32]. In our specific application, one TPH print head and one PSL print head were employed for the consecutive production of the bi-tablets.

This study aims to contribute to understanding the extent to which the combination of two tablet compartments influences the drug dissolution of each respective single compartment. Employing a statistical experimental design, various practically relevant doses were investigated and compared with their respective mono-tablets. The data provides insights into whether the requirements for the drug release of both compartments are maintained in combination. In addition to release studies, a comprehensive solid-state characterization was conducted. The thermal events of both formulations were examined using differential scanning calorimetry (DSC), while suitable 3DP and processing temperatures of the formulation components were recorded through thermogravimetric analysis (TGA) and small amplitude oscillatory shear (SAOS) rheology measurements.

2. Materials and Methods

2.1 Materials

The drugs Theophylline (TPH) and Prednisolone (PSL) were supplied by Thermo Fisher Scientific Inc., Waltham, USA and Caesar & Loretz GmbH, Hilden, Germany, respectively. The polymers Eudragit® RL (ERL) and Eudragit® E PO (EPO), along with the flow agent Aerosil® R972 (R972), were provided by Evonik AG in Essen, Germany. The polyethylene glycol plasticizer Lipoxol® 6000 MED (PEG) was received from Sasol Chemicals LLC, Houston, USA. All chemicals used were of analytical grade and used as received.

2.2 Methods

2.2.1 Abbreviation and notation system

In this work, a notation system is employed to clearly distinguish between active substances, formulations, mono- and bi-layered tablets. The subsequent Table 1 provides an overview of the utilized notation with specific examples.

2.2.2 Preparation of granules

For the production of the selected mono- and bi-tablets, the two formulations TPH-50 and PSL-12 were employed. The respective formulation compositions can be found in Table 2. The blends represent the final formulations that were used for the production of granules. The blend components were pre-weighed and geometrically mixed in three steps at 49 rpm for 15 min in a Turbula® T2F tumble mixer from WAB Group AG, Muttenz, Switzerland. All manufactured powder blends were further processed on the same day.

The prepared physical mixtures were transferred to twin-screw hot melt extrusion (HME) using the laboratory-scale extruder ZE HM9 from Three Tec GmbH, Seon, Switzerland. The hardware configuration included co-rotating screw elements with a nozzle diameter of 2.0 mm. The extrusion temperatures for formulations TPH-50 and PSL-12 are detailed in Table 2. The extrusion process involved four temperature zones, starting with a feeding zone held at room temperature and three consecutive uniformly heated zones. The extrusion screws served solely as conveying screws without additional kneading elements. The filament diameter of the extrudates was not monitored as it is irrelevant for granule production due to subsequent downsizing into granules.

After cooling to room temperature the extruded strands were immediately processed into granules through rasp sieve milling employing a U5 Comil® from Quadro Engineering Corp., Waterloo, Canada, operating at 250 rpm. Granules with a maximum diameter of 1.3 mm were obtained, and particles smaller than 0.6 mm were separated using a stack sieve. To prevent moisture sorption or potential alterations due to light exposure, the products were stored in sealed and tinted containers.

2.2.3 Feasibility considerations for reasonable application

Before generating a statistical experimental design, it is essential to assess the feasibility of the selected formulations for production of practically relevant bi-tablets. With regard to a rapidly adaptable and patient-centered therapy model, a certain dosage range must be covered for both TPH and PSL. It is crucial to carefully consider the drug content and composition of the formulation to ensure that 3DP of chosen tablet designs is technically feasible and selected tablet volumes are suitable for ingestion. Prior research indicated that a daily dose of 3.2 mg TPH/kg patient BW is appropriate to achieve beneficial blood levels following a "low-dose" approach with given in-vitro drug release [5,15,16,18,21]. The selected dosage steps of 135, 205 and 275 mg therefore cover a broad, relevant patient spectrum. PSL is typically administered with an elevated initial dose of 40 mg, which is then reduced to lower maintenance doses of 25 mg or 10 mg in the course of further treatment. As shown in Table 3, the smallest and largest bi-tablets are represented by the designs T135-P10 and T275-P40, containing 10 and 40 mg PSLThese tabletsdo not only achieve the required absolute doses but also ensure feasible administration due to sizes suitable for ingestion.

2.2.4 3D printing process and printlet design

The printlets were modeleld by computer aided design (CAD) to take the form of cylinders, as depicted in Figure 1. The respective printlet models were sliced into g-code (.gcode) with Ultimaker® Cura 4.10.0 by Ultimaker B.V., Utrecht, Netherlands. All CAD models were sliced with full body infill. Mono- and bi-layered tablets were fabricated by fused deposition modeling (FDM) applying the pharmaceutical 3D printer FlexDose™ supplied by DiHeSys Digital Health Systems GmbH, Schwaebisch Gmuend, Germany. This printer features multiple independently controllable printheads, each designated for extrusion of one respective drug-containing formulation, either TPH-50 or PSL-12. Regarding the production of bi-tablets, for all tablet designs, initially a series of TPH compartments (n = 6) were printed sequentially onto the printing bed. Subsequent to the retraction of the TPH printhead, the printing process proceeded with PSL compartments (n = 6) utilizing the second printhead. The 3DP process of the mono-tablets (n = 6) was accomplished utilizing the respective single printheads only. 3DP and g-code generation included standardized settings as follows for both printheads: fine resolution slicing; extrusion factor 1.2 mm^3/s; nozzle speed factor 25 mm/s; single layer height 240 µm; three wall circumnavigations; no base brim, supports or rafts; build plate bed and nozzle printing temperatures respective to Table 2. A body infill of 30% was selected for the TPH compartment, while the PSL compartment was 100% body infill. The infill grades were implemented this way for both the mono- and all bi-layered tablets. Across all tablet sets, there were no differences in the cylinder radius, but in the number of horizontal layers to implement dose individualization.

2.2.4.1 Calculation of individualized doses

Estimating a dose pre-print poses a significant challenge, particularly for tablet designs with porous body infills. When examining a g-code file, it comprises simple non-extrusion movement commands and extrusion commands. An empirical correlation between the total extrusion travel distance (TETD) and the printed dose can be determined for each formulation and g-code file, provided that process parameters and the extrusion flow are kept constant. To analyze the TETD, the open-source tool G-Code Analyser by Cyber Fabrication, San Francisco, USA, was used. Before the actual printing of the mono- and bi-layered tablets, the printed dose per distance (PDPD) was empirically determined for both formulations under relevant printing parameters (n = 9 each). The respective values are depicted in Table 2. Through back-calculation (Eq. 1), the tablet designs described in the following paragraph were sliced to achieve the desired printed doses. The required $TETD_{req.}$ for a sliced g-code to achieve the dose m_{API} of the respective API is calculated as follows:

$$TETD_{req.} = \frac{m_{API}}{PDPD_{API}} \qquad \text{Eq. 1}$$

2.2.5 Design of experiments

A full-factorial statistical experimental design was employed to design selected bi-layered tablets. The design comprises of two three-level main factors and therefore nine experimental runs with three repetitions each. Table 3 shows the two factors chosen and observed with according factor levels: dose of TPH (m_{TPH}) and dose of PSL (m_{PSL}). To enable direct comparison without interaction effects, identical single compartments were also manufactured in form of mono-tablets. The mean dissolution times (MDTs) and timepoints of 70% drug release ($t_{70\%}$s) were considered as the system responses. The calculation of both responses is described in Chapter 2.2.11.

2.2.6 Physical characterization of tablets

The mass of all printed mono-tablets and bi-tablets (n = 6 each) was promptly assessed post-production using the analytical balance Talent TE214S from Sartorius AG, Goettingen, Germany. The dimensions of 3D printed tablets (n = 6 each) were measured by a digital caliper.

2.2.7 Differential scanning calorimetry (DSC)

DSC experiments were conducted utilizing a DSC 1 from Mettler Toledo, Columbus, USA. Sample preparation included 100 µL aluminum crucibles, and each crucible contained 10 to 20 mg of sample, with duplicates for each measurement. Working conditions covered a range of 30 °C to a maximum of 230 °C with a heating rate of

5 °C/min. The DSC measurements were performed under nitrogen atmosphere, with a flow rate of 30 mL/min. Physical state transformations and thermal events were observed in between processing steps, by analyzing physical mixtures and pre-print granules.

2.2.8 Thermogravimetric analysis (TGA)

The proportional weight loss was determined by a STA 409 PC/PG Luxx from Netzsch GmbH, Selb, Germany, in nitrogen atmosphere (flowrate 20 mL/min) from 50 °C to 230 °C with a heating rate of 5 °C/min. For the selection of suitable processing and 3DP temperatures without thermal degradation effects, duplicate tests on single components and excipients, physical mixtures, and granules were conducted. All samples were measured no later than one day after production.

2.2.9 Rheology: small amplitude oscillatory shear (SAOS)

The SAOS tests were performed with a Physica MCR301 Rheometer from Anton Paar GmbH, Graz, Austria, in oscillation mode with parallel plate configuration. Rheological measurements exclusively involved extruded blends. Samples were placed on a pre-heated Peltier plate, molten and compressed to a 1.0 mm gap by a 25 mm diameter stainless-steel plate. The measurements were performed within the linear viscoelastic region (LVR), established by strain sweeps executed at the minimal processing temperature. Strain sweeps were conducted from 0.01% to 10.0% strain at 10 rad/s angular frequency. Consequently, frequency sweeps were performed at decreasing angular frequencies from 500 to 1 rad/s as to determine material viscoelastic behavior in relation to time and frequency. The rheological evaluations were carried out in duplicates.

2.2.10 Determination of granules drug loading and in-vitro dissolution

To evaluate homogenous drug content (DC) distribution within granules of both formulation batches TPH-50 and PSL-12, 14 samples were weighed in total, and transferred to 250 mL volumetric flasks containing pH 6.8 phosphate buffer and 0.1 M hydrochloric acid, respectively. The flasks were exposed to 24 h of magnetic stirring to ensure full drug dissolution. API concentrations were measured at 271 nm for TPH and 254 nm for PSL ($n = 7$; sample mass 100 mg each), utilizing 0.1 cm cells in a HP 8453 UV-Vis Spectrophotometer from Agilent Technologies Inc., Santa Clara, USA.

The in-vitro dissolution measurements were performed using the United States Pharmacopoeia (USP) type I dissolution apparatus Sotax AT7 from Sotax AG, Basel, Switzerland, in 900 mL of pH 1.2 simulated gastric fluid for the first hour and pH 6.0 phosphate buffer for the remaining seven hours. These parameters correspond to the USP monograph “Theophylline Extended-Release Capsules: Test 9” [35]. In the case of PSL, exclusively 0.1 M hydrochloric acid was used, as only

immediate drug release was studied. The rotation speed was set to 50 rpm at a constant measurement temperature of 37 ± 0.5 °C and studies were performed in triplicates (*n* = 3). The average proportional accumulated drug releases were plotted as functions of time. Drug quantification of TPH and PSL was assessed using a HP 8453 UV-Vis Spectrophotometer from Agilent Technologies Inc., Santa Clara, USA, at resepctive wavelengths of 271 nm and 254 nm in a 0.1 cm cell.

For TPH, the applied calibration range for the first hour was in between 2.8 and 111 mg/L (R^2 = 0.9999; LOD = 2.8 mg/L; LOQ = 8.3 mg/L), while 5.5 to 220 mg/L (R^2 = 0.9999; LOD = 5.5 mg/L; LOQ = 16.7 mg/L) after the pH change. For PSL, the calibration range lies in between 0.6 and 55.6 mg/L (R^2 = 0.9999; LOD = 0.6 mg/L; LOQ = 1.6 mg/L).

2.2.11 Mathematical fitting and comparison of dissolution curves

Our bi-layered tablets represent a dosage form containing two active substances with individual drug release. While TPH is administered in a sustained-release fashion, PSL is released with immediate-release kinetics. For TPH, the Higuchi model was employed to mathematically analyze and characterize the drug release curves. The Higuchi model describes the amount of active substance M_t released at time t in relation to the maximum release amount M_{max} according to the principle of Fickian diffusion for non-erodible matrixes (see Eq. 2) [36,37]. The Higuchi constant k_H provides insights into the underlying drug release rates [37].

$$\frac{M_t}{M_{max}} = k_H \cdot t^{0.5} \qquad \text{Eq. 2}$$

The mean dissolution time (MDT) serves as a parameter for evaluating the release retardation efficacy of a pharmaceutical formulation [38]. In units of minutes, it expresses the average time it takes for a drug molecule to dissolve in a dissolution medium (see Eq. 3) [38]. In Eq. 3, ABC stands for the area between the curves and is calculated via the trapezoidal equation with c as the concentration of the API released over time t and c_{max} as the maximum or final drug concentration.

$$MDT = \frac{ABC}{c_{max}} = \frac{\sum_{i=0}^{\infty}\left[((c_{max} - c_{i+1}) + (c_{max} - c_i)) \cdot \left(\frac{t_{i+1} - t_i}{2}\right)\right]}{c_{max}} \qquad \text{Eq. 3}$$

To evaluate the immediate release properties of PSL, the parameter $t_{70\%}$ is used. This parameter is defined as the timepoint at which 70% of the nominal content of the dosage form is reached and given in minutes. The value derives from the 70% drug release intersection of respective 2nd degree polynomial equations that fitted the

experimental data (see Eq. 4). The polynomial fit was determined under minimization of the coefficient of determination R^2 using linear regression and solved for $t_{70\%}$ applying a modified quadratic equation (see Eq. 4).

$$2^{nd} \text{ degree polynomial function: } \frac{M_t}{M_{max}} = at^2 + bt + c; \qquad \text{Eq. 4}$$

$$70\% \text{ drug release intercept: } t_{70\%} = \frac{-b \pm \sqrt{b^2 - 4a \cdot (c - 0.7)}}{2a}$$

2.2.12 Statistics

One-sample t-tests were used both for the evaluation of granule drug distribution and for the assessment of PSL drug releases in specific applications. For the calculation of the respective means (M), standard deviations (SDs), standard errors of the mean (SEM), t-values, p-values, degrees of freedom (df), and the boundaries of the confidence interval (CI) for alpha values $\alpha < 0.05$, the software Minitab® version 21 by Minitab GmbH, Munich, Germany, was used.

For the application in the case of granule drug distribution, a two-tailed test was conducted asspecific target values were stated for the granule drug contents, whereby this test determines whether these values deviate significantly from the hypothesized means.

For the assessment of PSL drug release, a one-tailed test, particularly a left-tailed one, was conducted. In this case, the entire significance level is placed in one tail of the distribution, allowing for testing if the test value is significantly lower than the hypothesized mean value. This is useful for investigating the PSL drug release, as according to the USP monograph "Prednisolone Tablets", a dosage form is considered immediate release if at least 70% of the labeled drug content is released within 30 min [39].

2.2.13 In vitro/In vivo correlation and PBPK prediction

PBPK modeling was conducted utilizing the PK-sim® software within OSP Suite version 11, provided by Open Systems Pharmacology Inc., Boston, USA. Drug TPH's physico-chemical properties and information about the processes of absorption, distribution, metabolism, and excretion were predominantly taken from the PK-Sim® database. TPH is a substance showing complete absorption and considered a Biopharmaceutics Classification System (BCS) class I drug [40]. The corresponding average population models were generated based on PK-Sim® data sets. For the simulation of blood profiles of the obtained 3DP bi-tablets, the following average population was utilized: group size of $n = 24$, individuals aged 20 - 25, male, of Caucasian ethnicity, non-smokers, and otherwise in good health, with BWs falling

within a range deviating by a maximum of 10% from their ideal BW. A single administration of 3.2 mg TPH/kg patient BW was chosen as the administration regimen. Accordingly, a total of three simulations were performed for three TPH dose strengths of 135, 205, and 275 mg, with corresponding population BWs of 42, 64, and 86 kg, and the results were averaged. Furthermore, the previously reported systematic model-building approach was closely tied to with and retrospectively validated against published literature regarding IVIVC.

3. Results

3.1 Thermogravimetric analysis

TGA assists in determining suitable process temperatures for both thermally intensive process steps: table-top HME during granules production and the actual 3DP. The process temperatures must be thoughtfully selected to ensure that no formulation component is at risk of thermal degradation. The results from the TGA investigations are summarized in Figure 2. This includes the TGA curves of both the TPH-50 and PSL-12 single formulation components (see Figure 2a, b). The intermediates of both formulations, such as physical powder mixtures and post-HME granules, are also depicted (see Figure 2c, d). Thermal stability of samples was assumed up to a 1.00% accumulated mass loss after deduction of the water desorption plateau.

The obtained data reveal that the active ingredient TPH is a completely anhydrous product with a degradation temperature of 225 °C (see Figure 2a). The utilized plasticizer PEG shows no thermal degradation across the entire examined temperature range, in regard to the criteria mentioned earlier. The water content of PEG was determined to be 0.25 wt.% (see Figure 2a). Among all the single formulation components of TPH-50, polymer ERL emerges as the limiting component since it exhibits the lowest degradation temperature of 195 °C (see Figure 2a). ERL also depicts a relatively high amount of adsorbed water at 1.10 wt.%. Thus, all individual fractions of formulation TPH-50 are processed during HME and 3DP at 120 °C and 180 °C well below the minimal observed degradation temperature.

The main polymer EPO in formulation PSL-12 shows a content of 0.60 wt.% of adsorbed water and shows no thermal degradation within the examined temperature range (see Figure 2b). The same applies to PSL, with the difference that there is no absorbed water (see Figure 2b).

In Figure 2c, the two process intermediates of the TPH-50 formulation, namely powder physical mixture (p.m.) and granules, are compared. Both the physical mixture and granules contain higher water amounts than their individual components, 1.53% and 1.87%, respectively. Both, the process step of preparing the powder blends and table-top HME expose the formulations to humidity leading to some water adsorption. The corresponding respective degradation temperatures are 205 °C and 212 °C, which are sufficiently higher than subsequent process temperatures of 180 °C.

Generally, the intermediates of PSL absorb less water than those of TPH, with water contents of 0.36% and 0.48% for powder and granules, respectively (see Figure 2d). In contrast to the individual components of formulation PSL-12, both intermediates exhibit onset degradation temperatures within the studied range. These are 221 °C and 223 °C, which do not risk thermal decomposition at given processing conditions (120 °C and 160 °C °C).

3.2 Differential scanning calorimetry (DSC)

Figure 3 summarizes the results of all DSC measurements. The active ingredient TPH and the polymer ERL do not exhibit clear endothermic events within the examined temperature range (see Figure 3a, b). In the literature, an onset melting point of over 355 °C has been demonstrated for polymer ERL [41,42], while this value for TPH is reported to be 271 °C [43]. The melting point of plasticizer PEG is indicated by a distinct endothermic peak with an onset at 67 °C (see Figure 3c). The physical mixture of formulation TPH-50 further retains this endothermic peak, but to a lower extent as the PEG content is decreased in the mixture (see Figure 3d). This peak further decreased after the table-top HME, as shown by the granules sample (see Figure 3e). The peak decline suggests partial and incomplete solution of PEG in the polymer matrix. Both single formulation components that form PSL-12, as well as the two respective intermediate forms, show no thermal events (see Figure 3f-i). The melting point of PSL is outside the investigated temperature range, i.e. at 240 °C (see Figure 3f) [44].

3.3 Small amplitude oscillatory shear rheology

The assessment of rheological properties of polymer blends, like the complex viscosity |η*| and the loss factor tan(δ), plays a crucial role due to their direct impact on 3DP feasibility, process and quality. The following paragraph is dedicated to the evaluation of rheological properties concerning absolute viscosity levels and, consequently, the printability of samples at apparent nozzle wall shear rate $\dot{\gamma}_{nw}$ and printing temperature.

In a previous study, also utilizing the FlexDose™ 3D printer, a rheological target regime for the printability of polymer blends was successfully established [2]. In particular, this comprises complex viscosity levels between 90 and 290 Pa·s at apparent shear rates, as well as tan(δ) values between 0.8 and 5.5. Deviating from this range leads to phenomena hindering 3DP known as "clogging" or "polymer melt backflow" [2]. Figure 4a illustrates that post-HME granule samples from both formulations fall into the required viscosity regime at relevant printing temperatures. Therefore, both previously described obstructing extrusion effects can be ruled out. At an apparent nozzle wall shear rate of 180 s^{-1} [2,5], determined semi-empirically for the utilized printing geometry, both formulations exhibit highly similar viscosity properties. Specifically, it is 119 Pa·s for TPH-50 and 108 Pa·s for PSL-12. Both formulations also demonstrate a comparable shear rate dependency regarding their complex viscosity.

Additionally, the loss factors of both formulations were recorded, as summarized in Figure 4b. The loss factor is defined as the ratio of the viscous modulus, G‘‘ or loss modulus, to the elastic modulus, G‘ or storage modulus, of a sample. Thus, elevated absolute values of the dimensionless loss factor indicate a highly viscous behavior of the respective polymer melt. Formulation TPH-50 exhibits a tan(δ) of 2.15 and formulation PSL-12 possesses a tan(δ) of 2.77 at apparent printing temperatures and nozzle wall shear rates. Translated to the respective polymer characteristics, formulation PSL-12 extrudes more viscously from the nozzle and, therefore, was chosen as the secondary tablet compartment in the bi-layered tablets. Our experience

indicates that arranging the printing process like this is advisable, as it leads to improved adhesion of the secondary tablet compartment onto the primary one. This observation aligns with the findings of Thumsorn and Supaphorn et al., who investigated multi-material layer adhesion in FDM 3DP rheologically. Their work indicates that polymers with a higher tan(δ), and therefore stronger viscous character, possess a higher adhesion factor [45].

3.4 Granules drug loading homogeneity

Ensuring uniform distribution of TPH and PSL throughout the granules as the feeding material for 3DP is crucial as drug content uniformity is essential for printing tablets with precise and predictable doses. Within the samples tested, the relative standard deviation (RSD) in drug content of both batches was determined to amount to 3.99% and 3.57%, respectively (see Table 4). Results from Table 4 show, that the sample means do not significantly deviate from the expected values. The applied two-tailed one-sample t-tests show that H_0 can be rejected with high probability for both formulations.

3.5 Physical characterization of tablets and print evaluation

To ensure the generation of reliable data, it is imperative to produce tablets with minimal variations in terms of mass, volume, dimensions and surface area. Maintaining low deviations in tablet dimensions and, consequently, tablet mass is linked to achieving consistent drug contents. The recorded masses and dimensions of bi-layered and mono-tablets within a given batch are presented in Figure 5. In the case of mono-layered tablets, precise determination of tablet dimensions and masses was achievable. For bi-layered tablets, only the total dimensions and total mass values, comprising both compartments, can be provided. Characterizing individual compartments within the bi-tablets is not feasible, as the printing process occurs consecutively, and the tablet can only be retrieved from the print bed after 3DP of the second compartment is completed. Splitting the two compartments after printing is also not feasible due to excellent layer adhesion. Furthermore, each tablet underwent individual scrutiny for common 3DP error phenomena, such as hollow areas, warping, sharp edges, under- or over-extrusion, offsets, stringing, and other undesirable effects. Out of a total of 90 tablets none had any defects or caused excessive deviations in the PSL mono-tablets or bi-tablets. One of the 18 TPH mono-tablets and three of the 54 bi-tablets showed 3DP defects. In all four defective prints, the printing of TPH led to stringing-related defects. While the cylinder walls of the tablets were error-free in all cases, there were minor under-extrusion phases in the infill. As a result, the extrusion strand could not properly adhere to the missing infill spots, causing the infill to become stringy within the tablet body. It was assumed that the targeted drug release could no longer be achieved, and the tablets were not used for dissolution. Relevant deviations in mass and outer dimensions were not detected. The correct extrusion mass was present but without the correct internal geometry. Such effects were not observed in

the PSL mono-tablets, as a geometry with 100% infill can compensate for a short under-extrusion period without significant geometric impairment. This effect was already demonstrated in one of our previous works, where tablets with comparable infills, formulations and print parameters were produced [5]. Here too, the print accuracy decreased with lower infills, while high and complete infills led to fewer 3DP deviations.

Figure 5 summarizes the results of the physical characterization of tablets within the sample groups. Regarding the tablet masses, it is noticeable that the SDs are generally higher for TPH mono-tablets compared to PSL mono-tablets (see Figure 5a). This indicates that the 3DP process is fundamentally more stable and consistent for PSL compartments than for TPH compartments. Generally, low SDs were obtained for the tablet masses as well as the heights and radii, which are within a reasonably low range (see Figure 5).

3.6 In-vitro dissolution evaluation

3.6.1 Theophylline release from mono-layered tablets

The mono-tablets examined in Figure 6a are identical to the individual tablet compartments later included in the bi-tablets. Firstly, three similar release curves were obtained that show full drug release in a sustained fashion over a period of seven hours (see Figure 6a). The standard deviations within the sets of all three mono-tablet curves are low and results are therefore close to the mean. This indicates that the 3DP process with formulation TPH-50 is sufficiently precise in terms of generating consistent release behaviors.

The polymer ERL used in TPH-50 is designed for extrusion applications such as 3DP and primarily releases the drug through the mechanism of diffusion. The polymer matrix swells but does not erode and remains intact throughout the release process. The Higuchi drug release model describes the drug release from a solid matrix as a diffusion process based on Fick's law [36]. The Higuchi constant k_H is a parameter in the model that quantifies the rate of drug release [36]. The coefficients of determination (R^2) in Table 5 indicate that the Higuchi fit is an appropriate model for describing the sustained drug release of TPH mono- and bi-tablets. For our TPH mono-tablets, the k_H results for the highest and lowest relevant doses range between 3.710×10^{-2} and 3.986×10^{-2}, while the MDTs range between 43.94 and 47.89 min (see Table 5). Both parameters are only minimally influenced by the tablet dose, and the release rates k_H and the MDTs, remain within a similar range despite dose scaling. Considering a total release duration of 7 h, MDT differences of less than four minutes are not relevant.

3.6.2 Theophylline release from bi-layered tablets

As seen in Figure 6b-e, the in-vitro drug release of TPH from each of the bi-tablets in Table 3 was also recorded. Identically to the mono-tablets, the bi-tablets also release more than 80% of their nominal drug content in a sustained manner within 7 h. The curves' standard deviations are all low and depicted in Figure 6b-e. Generally, it is

noticeable that the obtained drug release curves of all nine bi-tablets shown in Figure 6b, despite significantly different combinations and dose strengths, are highly similar to each other.

Figure 6c-e compares the in-vitro dissolution within selected bi-tablet sets and their TPH single-compartment equivalents. In the case of T135-related bi-tablets (see Figure 6c) all three release curves of TPH (T135-P10, T135-P25 and T135-P40) align and no relevant difference in MDTs or k_Hs was found. The exact data can be found in Table 5, and in the case of MDTs, they differ by less than a single minute. As k_Hs values showed almost no deviations, a trend analysis was not pursued. The same applies to the tablet set consisting of T205-P10, T205-P25 and T205-P40 from Figure 6d. Similarly, for the T275-related bi-tablets in Figure 6e, there is no difference between the individual bi-tablet releases during the first 5 h, with only minor significant but not relevant differences in total release observed in the final two hours of the release study. Expressed in terms of the MDT, this can also be confirmed as the difference within the group amounts to less than 2 min. In conclusion, the TPH compartments within the bi-tablets release TPH independently of the dose and volume of the second PSL tablet compartment, and sustained release is maintained.

3.6.3 Prednisolone release from mono-layered tablets

In this study, in addition to the TPH drug release, the drug release of PSL was also investigated. To enable the comparison of release rates and trends, all PSL mono-tablets analyzed were also used as top compartments in the bi-tablets. The dose strengths were 10, 25, and 40 mg PSL and unlike TPH, immediate release is aimed for with PSL. This follows the USP monograph "Prednisolone Tablets", which specifies that under the conditions used, not less than 70% of the labeled amount should dissolve within 30 min [39]. Therefore, instead of MDT, $t_{70\%}$ was introduced and calculated for all PSL tablets (see Table 5). This parameter is particularly informative as it indicates when the crucial requirement for successful immediate release is met and whether this value falls within the targeted 30 min (see Table 5). Higuchi fitting was omitted because it is typically unsuitable for erosion-based immediate release products.

As shown in Figure 6f, all three PSL mono-tablets reach the required 70% drug release within 30 min but with significantly differing release rates. P10 meets the requirement the fastest, followed by P25 and P40. This finding is in line with the results shown in Table 5, where it is fundamentally evident that $t_{70\%}$s of PSL mono-tablets positively correlate with an increase in dose. To quantify this effect, a linear regression fit was applied to the $t_{70\%}$ results versus PSL doses (see Table 6). A regression line with a high $R^2 = 0.9620$ was found, demonstrating with its positive slope that a higher dose is associated with a higher $t_{70\%}$ value (see Table 6).

Unlike TPH, PSL tablets do not exhibit any infill or porosities. EPO is a polymer that is soluble in acidic dissolution media conditions, which leads to drug release by gradual erosion of the polymer matrix. This means that the tablets surface area to volume

(SA/V) ratios are a key factor controlling the release. The research groups Quodbach et al. and Goyanes et al. demonstrated in four projects that the drug release from 3DP tablets can be predicted and controlled using only a single parameter, the SA/V ratio [46-49]. For this reason and to assess the influence of the SA/V ratio on $t_{70\%}$, further linear regression calculations were conducted, also detailed in Table 6. Utilizing the SA/V ratio, a linear correlation could be established, and an even more accurate fit with $R^2 = 0.9778$ was found (see Table 6). The negative value of the slope of the regression line suggests that a high SA/V ratio correlates with rapid release (see Table 6). This general trend aligns with those reported in the literature [46-49].

3.6.4 Prednisolone release from bi-layered tablets

The PSL release curves of the nine different bi-tablets are reported as $t_{70\%}$ values in Table 5. The obtained $t_{70\%}$ values range from 13.36 to 30.37 min. They all meet the criterium of min. 70% release within 30 min as evidenced by the one-tailed one-sample t-test results given in Table 4. The $t_{70\%}$ values found do not differ from the expected value of ≤ 30 min, indicating that the deviations are caused by statistical variation. The obtained p-values are well above the chosen α-value of 0.05, which strongly supports the accuracy of this assumption. Therefore, immediate release is still achieved with all bi tablets.

To assess the extent to which the dose and consequently the size of the TPH compartment influence the release of PSL, the $t_{70\%}$ results were plotted against TPH content in Figure 7a. The three PSL doses are presented in separate groups, and linear regression lines were fitted. Linear correlations with high R^2 values of 0.9941, 0.9783, and 0.9670, respectively, were obtained for all three groups (see Figure 7a), indicating that the size of the TPH compartment has a linear impact on $t_{70\%}$ of PSL. Moreover, Figure 7a shows that PSL compartments with larger doses generally release more slowly than those with smaller doses. This finding aligns with the results from PSL mono-tablets, regardless of the influence of the second TPH compartment.

Another interesting finding and trend can be observed when comparing the slopes of the regression lines for each group in Figure 7a. Firstly, positive slopes were obtained for all three groups, indicating that $t_{70\%}$ of PSL increases with increasing TPH dose. This phenomenon can again be explained by the primary parameter SA/V, which is responsible for the release of PSL as shown in previous evaluations. Unlike in the case of mono-tablets, a reasonable modification of parameter SA/V for PSL in bi-tablets is SA_{bi}/V (see Eq. *5*). Here, it is assumed that one of the two cylinder cap surfaces of the tablet compartment is covered by the second compartment and does not contribute to the total surface area (see Eq. *5*).

$$SA_{bi}/V = \frac{2\pi r h_{PSL} + \pi r^2}{\pi r^2 h_{PSL}} \qquad \text{Eq. 5}$$

Table 6 summarizes the calculated values of SA_{bi}/V and compares them directly to the corresponding SA/V ratios. As with the mono-tablets, the SA_{bi}/V decreases with increasing PSL dose in the bi-tablets. In Figure 7b, the means of the $t_{70\%}$ results for P10, P25, and P40 from bi-tablets, were plotted against the corresponding SA_{bi}/V ratios. The extremely high R^2 value of 0.9991 demonstrates that the means are significantly controlled by SA_{bi}/V and that our assumption is correct.

Interestingly, the magnitude of the slopes shows that the TPH compartment dose impacts PSL release and that this effect decreases with increasing PSL dose. In simpler terms, higher PSL doses are less affected by the TPH doses, and the magnitude of the slope approaches zero from P10 to P40. This may be a result of the boundary layer between the two compartments being at least partially available for contact with the receptor medium. The TPH compartments were printed with low infill, thus leaving voids between the printed strands into which the dissolution medium may diffuse. In the case of higher dose TPH compartments, the diffusion pathlength is increased as the height of the TPH compartment is increased. Thus, the diffusion of release medium and PSL within the voids is slowed down and release is slowed down as a consequence. In the case of P40 compartments, release by erosion is already slow enough for the TPH compartment not to show an effect anymore.

3.7 Theophylline blood level modeling

As previously mentioned, the drug TPH is not only an NTW drug forcing specific requirements for sustained drug release, but it is also a substance for which we are targeting a novel therapeutic “low-dose” blood serum range in patients. This range is between 1 - 5 µg/mL, and recent research has shown it to be particularly beneficial in combination with systemic corticosteroids like PSL for treating pulmonary diseases and exacerbations [5,15,16,18,19,21]. Additionally, this therapeutic target range should be maintained over an extended period with a single administration of the corresponding bi-tablet. Our bi-tablet designs enable the realization of various absolute doses through a "layer adaptation" approach, ensuring that the proportional in-vitro release profile remains consistent regardless of the absolute dose. This means that our bi-tablet designs can provide a wide range of patients with individualized doses of TPH and generate reproducible and consistent in-vivo blood concentrations provided a certain dosing approach is stuck to. We determined that an administration approach of 3.2 mg TPH/kg patient BW (corresponding to 135-275 mg) is adequate for the given simulated population.

Three patient populations with body weights corresponding to this regimen for the intake of the respective bi-tablets 135, 205 and 275 mg were simulated and represented as an averaged curve in Figure 8. Firstly, the bi-tablets reach the maximum serum concentration timepoint t_{max} after 8 h with a maximum serum concentration c_{max} of 3.66 ± 0.12 µg/mL. The lower therapeutic limit (1.00 µg/mL) is exceeded after 24 h while the upper therapeutic limit of 5.00 µg/mL is never exceeded. Additionally, our dosage forms are capable of maintaining the therapeutic “low dose” range over 24 h, meaning that a single daily administration is sufficient. This results in

increased patient compliance. The drug PSL was not simulated since the IR requirements were met by each bi-tablet combination, and matching specific kinetics is not relevant for therapy in this case.

4. Discussion of results

The subsequent discussion covers several thematic areas in detail and from various perspectives.

Currently, we are facing a lack of suitable dosage forms on the market offering a "low dose" TPH approach for patients. As previously mentioned, TPH is a drug that has long been established in therapy but is less frequently used [15,22,23,50-53]. This trend is due to the fact that traditional administration still recommends and targets blood serum concentrations of up to 20 µg/mL [15,22,52]. These concentrations are likely to cause adverse effects, and physicians often prefer inhaled beta-2 sympathomimetics [51,53,54]. However, patients with lung diseases often suffer from limited lung function and prefer the intake of oral dosage forms [22,55,56]. Our newly developed dosage forms aim to facilitate the latest “low dose” research findings [5,15,16,18,19,21,22].

Furthermore, there market provides insufficient dose increments and the correct range for true personalized TPH therapy is not covered. As shown in previous work, a dosage regimen of 3.2 mg TPH/kg patient BW is required for "low dose" administration [5]. Traditionally, 5.5 - 6.5 mg TPH/kg patient BW is targeted, and market medications have dose increments in steps of at least 125 mg, corresponding to roughly 20 kg BW increments [57,58]. The available products are granulate-filled hard capsules that are not splittable [57,58]. Between the lowest relevant TPH dose of 135 mg and the highest of 275 mg in our bi-tablet design, there are twelve printed layers that allow for on-demand personalization through layer number adaptation. This represents a much finer increment than the 125 mg steps of market products, allowing for patient fine-tuning in 10.4 mg (or 3.25 kg BW) steps. With these values, a truly personalized therapy can be offered that substantially reduces adverse effects.

TPH/PSL combination dosage forms are not available on the market. New research has shown that the combination of TPH with systemic corticosteroids like PSL leads to synergistic and highly beneficial therapeutic effects [5,15,16,18,19,21]. For the first time as of now, we developed a combination dosage form of these APIs that is also dose individualizable. Combining two drugs in a bi-layered tablet increases patient adherence, as only a single dosage form needs to be taken once daily as in-vivo simulations showed. Compared to conventional market products, the technical data sheets indicate that up to six tablets must be taken per day alternatively just to cover TPH therapy [57,58]. If PSL is tapered off towards the end of therapy or one of the two drug doses is adjusted during therapy, our 3DP design allows this to be done on-demand.

We show development of 3DP TPH and PSL dosage forms beyond superficial proof-of-concept towards the real-world application. Both TPH and PSL have been printed using various 3DP technologies in previous studies. However, for TPH, the focus has been solely on technical proof of concept or solid-state characterization during formulation development [59-63]. The development of a dosage form for relevant application, with appropriate drug loadings for personalization or concepts for personalization, has not been achieved yet [59-63]. The same applies to PSL, where

previous research has mainly focused on the development of suppositories and medical implants, not oral dosage forms [64-68].

We introduce a “layer adaption” dose personalization concept that maintains drug release integrity and improves previously developed TPH dosage forms. The research group Alhnan et al. reached the same conclusion in their project on the development extended-release 3DP tablets as we did in our last study on controlling the sustained release of TPH from 3DP tablets [5,68]. In both cases, the layer adaptation approach for dose individualization was unsuitable because changing the number of layers also led to a drastic change in proportional sustained drug releases [5,68]. In this bi-tablet TPH compartment design, several improvements have been made that now allow for broad dose personalization through layer adaptation while maintaining drug release kinetics. In comparison to previous designs [5], a lower infill value was successfully used to make the drug release of the tablets less dependent on their external surface areas. This is also beneficial for the later addition of a second compartment as the covered TPH area is minimized and to reach full TPH drug release over 7 h [5]. To ensure this effect is sufficient, preliminary studies helped modifying the base layer so that, in conjunction with the correct infill value, the target release could be achieved [5]. Since the introduction of infill also reduces the printed polymer mass, the drug content in the current formulation design was increased to still realize relevant doses still considering the targeted drug release [5]. Besides these essential improvements in TPH release and compartment design, a second compartment was successfully added. Unlike in our earlier work, which was monolithic and where drug release was heavily controlled by the SA/V ratio, the addition of the second compartment in the current design did not influence TPH release [5]. This is because the lower infill results in a lower impact of dose scaling on SA/V-ratio. Proportionally less surface area is covered by the second compartment again keeping the SA/V-value more constant. Additionally, the PSL formulation is an IR formulation that dissolves in less than 30 min in all cases. During the dissolution process of the PSL compartment, the covered surface of the first compartment is already gradually exposed to the dissolution medium and the whole area is available for dissolution after a maximum of 30 min. This means that, for TPH release lasting over 7 h, only a small portion of the surface is covered for a rather short time. Once the PSL compartment dissolved completely, the bi-tablet behaves identically to the corresponding TPH mono-tablet in terms of release characteristics.

5. Conclusion

The aim of this work was to develop dose-independently customizable bi-compartmental 3DP tablets that allow for personalized administration of the drugs TPH and PSL under preservation of similar drug release profiles. This dosage form aligns with new scientific insights that advocate for a “low dose” administration of TPH in combination with a corticosteroid. To this end, nine different 3DP bi-tablets with clinically relevant doses were designed and manufactured according to a full factorial DOE, followed by solid-state characterization and statistical evaluation of the in-vitro dissolution results. Through the simulation of the averaged TPH blood concentration profiles over time, it was shown that the developed bi-tablets are capable of maintaining the desired "low dose" range with a single administration over a 24 h period. The combined administration of TPH and PSL is a promising new therapy strategy for treating pulmonary conditions. However, implementing this with traditional pharmaceuticals would be highly challenging and would not provide sufficient flexibility for dose adjustments. The bi-tablets presented in this work could, in the future, help tailor treatments to patients with pulmonary diseases, improving their treatment outcomes, adherence, and overall quality of life. According to the current state of knowledge, pharmaceutical 3DP often lacks genuine personalization strategies, with research in the field mostly focusing on proof-of-concept. This applies not only to TPH and PSL but to the technology in general. To develop a personalization strategy for an API, a multitude of complex factors must be considered and balanced. This includes creating a chemically and thermally stable, printable, rheologically suitable pharmaceutical formulation with practically relevant drug loadings, along with a concept for calculating individualized doses, a print strategy for these doses, and validation of the release properties. The results of this work contribute valuable insights that can help this technology transition further into real-world applications, which ultimately benefits patients and the health care sector as a whole.

Thomas Pflieger: conceptualization, methodology, validation, investigation, data curation, writing—original draft preparation, visualization. **Rakesh Venkatesh**: conceptualization, methodology, writing—review and editing, supervision. **Markus Dachtler**: conceptualization, writing—review and editing. **Stefan Laufer**: conceptualization, methodology, writing—review and editing, supervision. **Dominique Lunter**: conceptualization, methodology, writing—review and editing, supervision. All authors have read and agreed to the published version of the manuscript.

Conflicts of Interest: The authors declare no conflict of interest. The company had no role in the design of the study, in the collection, analyses, or interpretation of data, in the writing of the manuscript, and in the decision to publish the results.

References

1. Dachtler, M.; Eggenreich, K.; Pflieger, T. Digital health-digital 2D/3D printing of personalized medication. In Proceedings of the Proceedings of the 4th International Symposium on Pharmaceutical Engineering Research (SPhERe), Online, 2021; pp. 15-17.
2. Pflieger, T.; Venkatesh, R.; Dachtler, M.; Eggenreich, K.; Laufer, S.; Lunter, D. Novel Approach to Pharmaceutical 3D-Printing Omitting the Need for Filament—Investigation of Materials, Process, and Product Characteristics. *Pharmaceutics* **2022**, *14*, 2488.
3. Pflieger, T.; Venkatesh, R.; Eggenreich, K.; Dachtler, M.; Laufer, S.; Lunter, D. Granule-Fed 3D Printing for Personalized Pharmaceuticals — A Comprehensive Investigation of Material Characteristics from Physical Mixture to Final Product. *Annual Meeting of the German Pharmaceutical Society - DPhG* **2023**, doi:10.13140/RG.2.2.17769.06244.
4. Tracy, T.; Wu, L.; Liu, X.; Cheng, S.; Li, X. 3D printing: Innovative solutions for patients and pharmaceutical industry. *International Journal of Pharmaceutics* **2023**, *631*, 122480.
5. Pflieger, T.; Venkatesh, R.; Dachtler, M.; Cooke, K.; Laufer, S.; Lunter, D. Influence of design parameters on sustained drug release properties of 3D-printed theophylline tablets. *International Journal of Pharmaceutics* **2024**, 124207.
6. Dachtler, M.; Huber, G.; Pries, T. 2D & 3D-Print-Technologien in der pharmazeutischen Industrie. *Digitale Transformation von Dienstleistungen im Gesundheitswesen VII: Impulse für die Pharmaindustrie* **2020**, 53-66.
7. Huber, G.; Dachtler, M.; Edinger, D. Digitalisierung in der Pharmaindustrie. *Digitale Transformation von Dienstleistungen im Gesundheitswesen II: Impulse für das Management* **2017**, 241-255.
8. Goh, W.J.; Tan, S.X.; Pastorin, G.; Ho, P.C.L.; Hu, J.; Lim, S.H. 3D printing of four-in-one oral polypill with multiple release profiles for personalized delivery of caffeine and vitamin B analogues. *International Journal of Pharmaceutics* **2021**, *598*, 120360.
9. Khaled, S.A.; Burley, J.C.; Alexander, M.R.; Yang, J.; Roberts, C.J. 3D printing of five-in-one dose combination polypill with defined immediate and sustained release profiles. *Journal of controlled release* **2015**, *217*, 308-314.
10. Pereira, B.C.; Isreb, A.; Forbes, R.T.; Dores, F.; Habashy, R.; Petit, J.-B.; Alhnan, M.A.; Oga, E.F. 'Temporary Plasticiser': A novel solution to fabricate 3D printed patient-centred cardiovascular 'Polypill'architectures. *European Journal of Pharmaceutics and Biopharmaceutics* **2019**, *135*, 94-103.
11. Macedo, J.; Marques, R.; Vervaet, C.; Pinto, J.F. Production of bi-compartmental tablets by FDM 3D printing for the withdrawal of diazepam. *Pharmaceutics* **2023**, *15*, 538.
12. Zhang, P.; Xu, P.; Chung, S.; Bandari, S.; Repka, M.A. Fabrication of bilayer tablets using hot melt extrusion-based dual-nozzle fused deposition modeling 3D printing. *International Journal of Pharmaceutics* **2022**, *624*, 121972.
13. Tabriz, A.G.; Nandi, U.; Hurt, A.P.; Hui, H.-W.; Karki, S.; Gong, Y.; Kumar, S.; Douroumis, D. 3D printed bilayer tablet with dual controlled drug release for tuberculosis treatment. *International journal of pharmaceutics* **2021**, *593*, 120147.
14. Crișan, A.G.; Porfire, A.; Iurian, S.; Rus, L.M.; Lucăcel Ciceo, R.; Turza, A.; Tomuță, I. Development of a Bilayer Tablet by Fused Deposition Modeling as a Sustained-Release Drug Delivery System. *Pharmaceuticals* **2023**, *16*, 1321.
15. Barnes, P.J. Theophylline: new perspectives for an old drug. *American journal of respiratory and critical care medicine* **2003**, *167*, 813-818.
16. Cosio, B.G.; Iglesias, A.; Rios, A.; Noguera, A.; Sala, E.; Ito, K.; Barnes, P.J.; Agusti, A. Low-dose theophylline enhances the anti-inflammatory effects of steroids during exacerbations of COPD. *Thorax* **2009**, *64*, 424-429.
17. Markham, A.; Faulds, D. Theophylline: a review of its potential steroid sparing effects in asthma. *Drugs* **1998**, *56*, 1081-1091.
18. Ford, P.A.; Durham, A.L.; Russell, R.E.; Gordon, F.; Adcock, I.M.; Barnes, P.J. Treatment effects of low-dose theophylline combined with an inhaled corticosteroid in COPD. *Chest* **2010**, *137*, 1338-1344.
19. Monserrat Villatoro, J.; Mejia-Abril, G.; Diaz Garcia, L.; Zubiaur, P.; Jimenez Gonzalez, M.; Fernandez Jimenez, G.; Cancio, I.; Arribas, J.R.; Suarez Fernandez, C.; Mingorance, J. A case-control of patients with COVID-19 to explore the association of previous hospitalisation use of medication on the mortality of COVID-19 disease: a propensity score matching analysis. *Pharmaceuticals* **2022**, *15*, 78.

20. Devereux, G.; Cotton, S.; Fielding, S.; McMeekin, N.; Barnes, P.J.; Briggs, A.; Burns, G.; Chaudhuri, R.; Chrystyn, H.; Davies, L. Effect of theophylline as adjunct to inhaled corticosteroids on exacerbations in patients with COPD: a randomized clinical trial. *Jama* **2018**, *320*, 1548-1559.
21. Sullivan, P.; Jaffar, Z.; Page, C.; Costello, J.; Bekir, S.; Jeffery, P. Anti-inflammatory effects of low-dose oral theophylline in atopic asthma. *The Lancet* **1994**, *343*, 1006-1008.
22. Barnes, P.J. Theophylline. *American journal of respiratory and critical care medicine* **2013**, *188*, 901-906.
23. Barnes, P.J. Inhaled glucocorticoids for asthma. *New England Journal of Medicine* **1995**, *332*, 868-875.
24. Labiris, N.R.; Dolovich, M.B. Pulmonary drug delivery. Part II: the role of inhalant delivery devices and drug formulations in therapeutic effectiveness of aerosolized medications. *British journal of clinical pharmacology* **2003**, *56*, 600-612.
25. Ruge, C.A.; Kirch, J.; Lehr, C.-M. Pulmonary drug delivery: from generating aerosols to overcoming biological barriers—therapeutic possibilities and technological challenges. *The lancet Respiratory medicine* **2013**, *1*, 402-413.
26. Burns, M. Management of narrow therapeutic index drugs. *Journal of thrombosis and thrombolysis* **1999**, *7*, 137-143.
27. Liu, D.; Ahmet, A.; Ward, L.; Krishnamoorthy, P.; Mandelcorn, E.D.; Leigh, R.; Brown, J.P.; Cohen, A.; Kim, H. A practical guide to the monitoring and management of the complications of systemic corticosteroid therapy. *Allergy, asthma & clinical immunology* **2013**, *9*, 1-25.
28. Stanbury, R.M.; Graham, E.M. Systemic corticosteroid therapy—side effects and their management. *British Journal of Ophthalmology* **1998**, *82*, 704-708.
29. Druckvorrichtung für additive Fertigungsverfahren mit Schraubenvorrichtung zur Materialzuführung. 2022.
30. Druckvorrichtung und additive Fertigungsverfahren mit automatischer Positionskalibrierung (WO2023094565A1). 2021.
31. Verfahren zur Herstellung patientenoptimierter Darreichungsformen (WO2022135919A1). 2021.
32. Additives Verfahren zum dreidimensionalen Druck wirkstoffhaltiger Objekte (EP3975986A1). 2020.
33. Long, J.; Gholizadeh, H.; Lu, J.; Bunt, C.; Seyfoddin, A. Application of fused deposition modelling (FDM) method of 3D printing in drug delivery. *Current pharmaceutical design* **2017**, *23*, 433-439.
34. Mwema, F.M.; Akinlabi, E.T.; Mwema, F.M.; Akinlabi, E.T. Basics of fused deposition modelling (FDM). *Fused deposition modeling: strategies for quality enhancement* **2020**, 1-15.
35. USP. United States Pharmacopoeia (USP) Volume 29: monograph "Theophylline Extended-Release Capsules: Test 9". *U.S. Food and Drug Administration* **2005**.
36. Siepmann, J.; Peppas, N.A. Higuchi equation: Derivation, applications, use and misuse. *International journal of pharmaceutics* **2011**, *418*, 6-12.
37. Korsmeyer, R.W.; Gurny, R.; Doelker, E.; Buri, P.; Peppas, N.A. Mechanisms of solute release from porous hydrophilic polymers. *International journal of pharmaceutics* **1983**, *15*, 25-35.
38. Tanigawara, Y.; Yamaoka, K.; Nakagawa, T.; Uno, T. New method for the evaluation of in vitro dissolution time and disintegration time. *Chemical and Pharmaceutical Bulletin* **1982**, *30*, 1088-1090.
39. USP. United States Pharmacopoeia (USP) Volume 29: monograph "Prednisolone Tablets". *U.S. Food and Drug Administration* **2005**.
40. Hasan, N.M.; Khaleel, M.A.; Altwairqi, A.S.; Alqurashi, A.G.; Altwairqi, A.H. Effect of Self-Microemulsifying Lipid Formulations on the Dissolution and Compaction Profiles of Tablets Containing Theophylline; A BCS Class I Compound. *Journal of Applied Pharmaceutical Science* **2018**, *8*, 030-038.
41. Amin, S.; Mir, S.R.; Kohli, K.; Ali, A. Novel Polymeric Matrix Films for Transdermal Delivery of Metoclopramide. *International journal of frontier in pharmaceutical research* **2012**, *2*, 48-60.
42. Eraga, S.; Eichie, F.; Nnadozie, J.; Obinokwara, H.; Cash-Torunarigha, O. Influence of mode of incorporation of Pleurotus tuber-regium powder on the release characteristics of acetaminophen tablets formed with some acrylate methacrylate copolymer binders. **2018**.
43. Cohen, J.L. Theophylline. In *Analytical profiles of drug substances*; Elsevier: 1975; Volume 4, pp. 466-493.
44. Technical Data Sheet Prednisolone - Thermo Fisher UK **2024**.
45. Thumsorn, S.; Prasong, W.; Kurose, T.; Ishigami, A.; Kobayashi, Y.; Ito, H. Rheological behavior and dynamic mechanical properties for interpretation of layer adhesion in FDM 3D printing. *Polymers* **2022**, *14*, 2721.

46. Windolf, H.; Chamberlain, R.; Quodbach, J. Predicting drug release from 3D printed oral medicines based on the surface area to volume ratio of tablet geometry. *Pharmaceutics* **2021**, *13*, 1453.
47. Mazur, H.; Erbrich, L.; Quodbach, J. Investigations into the use of machine learning to predict drug dosage form design to obtain desired release profiles for 3D printed oral medicines. *Pharmaceutical Development and Technology* **2023**, *28*, 219-231.
48. El Aita, I.; Rahman, J.; Breitkreutz, J.; Quodbach, J. 3D-Printing with precise layer-wise dose adjustments for paediatric use via pressure-assisted microsyringe printing. *European Journal of Pharmaceutics and Biopharmaceutics* **2020**, *157*, 59-65.
49. Goyanes, A.; Martinez, P.R.; Buanz, A.; Basit, A.W.; Gaisford, S. Effect of geometry on drug release from 3D printed tablets. *International journal of pharmaceutics* **2015**, *494*, 657-663.
50. Barnes, P.J. Therapy of chronic obstructive pulmonary disease. *Pharmacology & therapeutics* **2003**, *97*, 87-94.
51. Clark, T. Inhaled corticosteroid therapy: a substitute for theophylline as well as prednisolone? *Journal of Allergy and Clinical Immunology* **1985**, *76*, 330-334.
52. Milgrom, H.; Bender, B. Current issues in the use of theophylline. *American Review of Respiratory Disease* **1993**, *147*, S33-S33.
53. Boylan, P.M.; Abdalla, M.; Bissell, B.; Malesker, M.A.; Santibanez, M.; Smith, Z. Theophylline for the management of respiratory disorders in adults in the 21st century: A scoping review from the American College of Clinical Pharmacy Pulmonary Practice and Research Network. *Pharmacotherapy: The Journal of Human Pharmacology and Drug Therapy* **2023**, *43*, 963-990.
54. Wilson, A.; Gibson, P.; Coughlan, J. Long acting beta-agonists versus theophylline for maintenance treatment of asthma. *The Cochrane database of systematic reviews* **2000**, CD001281-CD001281.
55. Vanfleteren, L.E.; Spruit, M.A.; Wouters, E.F.; Franssen, F.M. Management of chronic obstructive pulmonary disease beyond the lungs. *The Lancet Respiratory Medicine* **2016**, *4*, 911-924.
56. Miravitlles, M.; Vogelmeier, C.; Roche, N.; Halpin, D.; Cardoso, J.; Chuchalin, A.G.; Kankaanranta, H.; Sandström, T.; Śliwiński, P.; Zatloukal, J. A review of national guidelines for management of COPD in Europe. *European Respiratory Journal* **2016**, *47*, 625-637.
57. Ratiopharm. Fachinformation Theophyllin retard-ratiopharm 250 mg Hartkapseln. **2020**.
58. Pharma, G. Bronchoretard® 350 Fachinformation. **2018**.
59. Isreb, A.; Baj, K.; Wojsz, M.; Isreb, M.; Peak, M.; Alhnan, M.A. 3D printed oral theophylline doses with innovative 'radiator-like'design: Impact of polyethylene oxide (PEO) molecular weight. *International journal of pharmaceutics* **2019**, *564*, 98-105.
60. Nashed, N.; Lam, M.; Ghafourian, T.; Pausas, L.; Jiri, M.; Majumder, M.; Nokhodchi, A. An insight into the impact of thermal process on dissolution profile and physical characteristics of theophylline tablets made through 3D printing compared to conventional methods. *Biomedicines* **2022**, *10*, 1335.
61. Tan, D.K.; Maniruzzaman, M.; Nokhodchi, A. Development and optimisation of novel polymeric compositions for sustained release theophylline caplets (PrintCap) via FDM 3D printing. *Polymers* **2019**, *12*, 27.
62. Giri, B.; Song, E.; Kwon, J.; Lee, J.; Park, J.; Kim, D. Fabrication of intragastric floating, controlled release 3D printed theophylline tablets using hot-melt extrusion and fused deposition modeling. Pharmaceutics 2020; 12.
63. Kuźmińska, M.; Pereira, B.C.; Habashy, R.; Peak, M.; Isreb, M.; Gough, T.D.; Isreb, A.; Alhnan, M.A. Solvent-free temperature-facilitated direct extrusion 3D printing for pharmaceuticals. *International Journal of Pharmaceutics* **2021**, *598*, 120305.
64. Holländer, J.; Hakala, R.; Suominen, J.; Moritz, N.; Yliruusi, J.; Sandler, N. 3D printed UV light cured polydimethylsiloxane devices for drug delivery. *International journal of pharmaceutics* **2018**, *544*, 433-442.
65. Koopaie, M.; Nassar, D.H.M.A.; Shokrolahi, M. Three-dimensional bioprinting of mucoadhesive scaffolds for the treatment of oral mucosal lesions; an in vitro study. *3D Printing in Medicine* **2022**, *8*, 30.
66. Farto-Vaamonde, X.; Auriemma, G.; Aquino, R.P.; Concheiro, A.; Alvarez-Lorenzo, C. Post-manufacture loading of filaments and 3D printed PLA scaffolds with prednisolone and dexamethasone for tissue regeneration applications. *European Journal of Pharmaceutics and Biopharmaceutics* **2019**, *141*, 100-110.
67. Kocabas, L.; Ayyoubi, S.; Tajqurishi, M.; Quodbach, J.; Vermonden, T.; Kok, R. 3D-printed prednisolone phosphate suppositories with tunable dose and rapid release for the treatment of inflammatory bowel disease. *International Journal of Pharmaceutics* **2024**, *649*, 123639.

68. Skowyra, J.; Pietrzak, K.; Alhnan, M.A. Fabrication of extended-release patient-tailored prednisolone tablets via fused deposition modelling (FDM) 3D printing. *European Journal of Pharmaceutical Sciences* **2015**, *68*, 11-17.

Table 1. Notation system distinguishing between active substances, formulations, and mono- and bi-layered 3DP tablets.

	notation	notation derivation	example(s)
formulation component	-	three letter abbreviation.	TPH, PSL, ERL, PEG
formulation	TPH-n, PSL-n	three letter abbreviation of API, hyphen, respective drug content in % *w/w*.	TPH-30; PSL-12
mono-tablet	Tn, Pn	single letter abbreviation of API, respective dose in mg.	T275; P40
bi-tablet	Tm-Pn	dose of TPH m in mg, hyphen, dose of PSL n in mg.	T275-P40

Table 2. Composition of formulations TPH-50 and PSL-12 alongside HME, 3DP and printed dose per distance (PDPD) parameters.

		TPH-50	PSL-12
formulation components	TPH (% *w/w*)	50.0	-
	PSL (% *w/w*)	-	12.0
	ERL (% *w/w*)	40.0	-
	EPO (% *w/w*)	-	87.5
	PEG (% *w/w*)	9.50	-
	R972 (% *w/w*)	0.50	0.50
HME	Extrusion T. (°C)	120	120
	Screw speed (rpm)	100	100
3DP	Nozzle T. (°C)	180	160
	Print bed T. (°C)	90	70
PDPD	PDPD (mg/cm)	1.04	0.13

Table 3. Summary of design parameters for selected cylindrical bi- and mono-tablets, including the height of the TPH compartment h_{TPH}, the height of the PSL compartment h_{PSL}, the radius r and total height h of respective tablets.

notation	m_{TPH} (mg)	m_{PSL} (mg)	h_{TPH} (mm)	h_{PSL} (mm)	r (mm)	total h (mm)
T135-P10	135	10	3.12	0.72		3.84
T135-P25	135	25	3.12	1.92		5.04
T135-P40	135	40	3.12	3.12		6.24
T205-P10	205	10	4.56	0.72		5.28
T205-P25	205	25	4.56	1.92	6.36	6.48
T205-P40	205	40	4.56	3.12		7.68
T275-P10	275	10	6.00	0.72		6.72
T275-P25	275	25	6.00	1.92		7.92
T275-P40	275	40	6.00	3.12		9.12
T135	135	-	3.12	-		3.12
T205	205	-	4.56	-	6.36	4.56
T275	275	-	6.00	-		6.00
P10	-	10	-	0.72		0.72
P25	-	25	-	1.92	6.36	1.92
P40	-	40	-	3.12		3.12

Table 4. One-sample t-test results and statistical evaluation regarding drug content uniformity of granules and $t_{70\%}$s values from PSL bi-tablet release.

application	**granules' DC**		**Bi-tablet PSL release: t_{70s} (min)**	
	TPH-50	PSL-12	T205-P40	T275-P40
n	7	7	3	3
df	6	6	2	2
target M	0.500	0.120	≤ 30.00	≤ 30.00
actual M	0.485	0.118	30.20	30.37
SD	0.193	0.042	0.670	0.460
RSD	3.99%	3.57%	2.22%	1.51%
SEM	7.31×10^{-3}	1.59×10^{-3}	0.387	0.266
CI bottom border	-3.34×10^{-2}	-6.08×10^{-3}	n/a	n/a
CI upper border	2.38×10^{-3}	1.69×10^{-3}	31.33	31.15
t-value	2.121	1.385	0.520	1.390
p-value	0.078	0.215	0.672	0.851
H_0 evaluation	insignificant	insignificant	insignificant	insignificant

Table 5. Evaluation of in-vitro drug releases by calculation of MDT, $t_{70\%}$ and application of the Higuchi fit including coefficients of determination (R^2) and Higuchi release rate constant k_H.

	TPH evaluation			**PSL evaluation**
notation	**MDT (min)**	**R^2 of Higuchi fit**	**k_H ($min^{-1/2}$)**	**$t_{70\%}$ (min)**
T135-P10	47.74 ± 0.46	0.9792	3.975×10^{-2}	13.36 ± 0.69
T135-P25	47.49 ± 1.47	0.9793	3.957×10^{-2}	25.89 ± 0.55
T135-P40	47.14 ± 1.20	0.9794	3.927×10^{-2}	29.87 ± 0.56
T205-P10	46.22 ± 1.25	0.9805	3.935×10^{-2}	15.23 ± 0.96
T205-P25	45.80 ± 0.57	0.9808	3.901×10^{-2}	26.89 ± 0.65
T205-P40	44.89 ± 0.50	0.9825	3.836×10^{-2}	30.20 ± 0.67
T275-P10	42.94 ± 1.03	0.9846	3.645×10^{-2}	16.66 ± 0.97
T275-P25	42.69 ± 1.25	0.9848	3.596×10^{-2}	27.48 ± 0.76
T275-P40	41.35 ± 1.22	0.9851	3.536×10^{-2}	30.37 ± 0.46
T135	47.89 ± 0.40	0.9788	3.986×10^{-2}	-
T205	46.47 ± 0.98	0.9795	3.950×10^{-2}	-
T275	43.94 ± 1.12	0.9825	3.710×10^{-2}	-
P10	-	-	-	9.56 ± 0.62
P25	-	-	-	21.02 ± 0.40
P40	-	-	-	26.61 ± 0.12

Table 6. Comparison of linear regression fits within the group of PSL mono-tablets including the time of 70% drug release $t_{70\%}$, dose and the surface area to volume ratio SA/V and evaluation of modified SA/V ratios for bi-tablet PSL compartments SA_{bi}/V.

		linear regression fits with R^2 of fit		
tablet group	**notation**	**$t_{70\%}$ (min) vs. dose (mg)**	**$t_{70\%}$ (min) vs. SA/V (mm^{-1})**	
PSL mono-tablets	P10 P25 P40	y = 0.5685x + 4.8502 R^2 = 0.9620	y = -7.5944x + 32.758 R^2 = 0.9778	
		SA/V (mm^{-1})	**SA_{bi}/V (mm^{-1})**	**SA_{bi}/SA**
PSL bi-tablets	Txxx-P10	3.09	1.70	55.0%
	Txxx-P25	1.36	0.84	61.7%
	Txxx-P40	0.96	0.63	65.6%

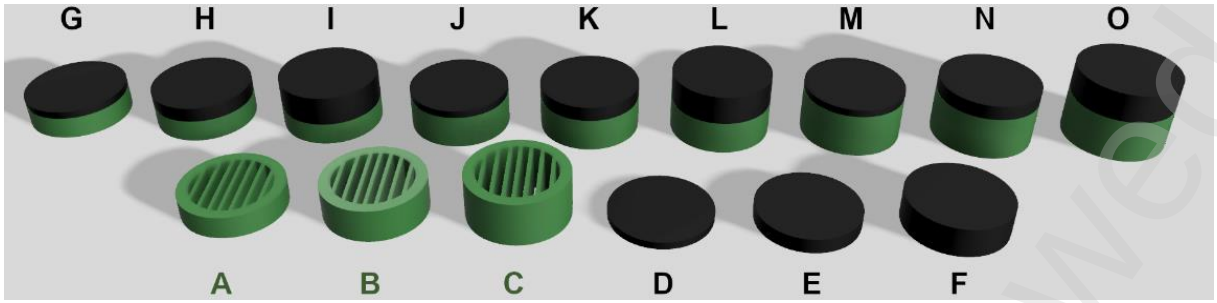

Figure 1. Selected tablet designs consisting of TPH compartments (green) and PSL compartments (black) with regarding notations: (**a**) T135, (**b**) T205, (**c**) T275, (**d**) P10, (**e**) P25, (**f**) P40, (**g**) T135-P10, (**h**) T135-P25, (**i**) T135-P40, (**j**) T205-P10, (**k**) T205-P25, (**l**) T205-P40, (**m**) T275-P10, (**n**) T275-P25, (**o**) T275-P40.

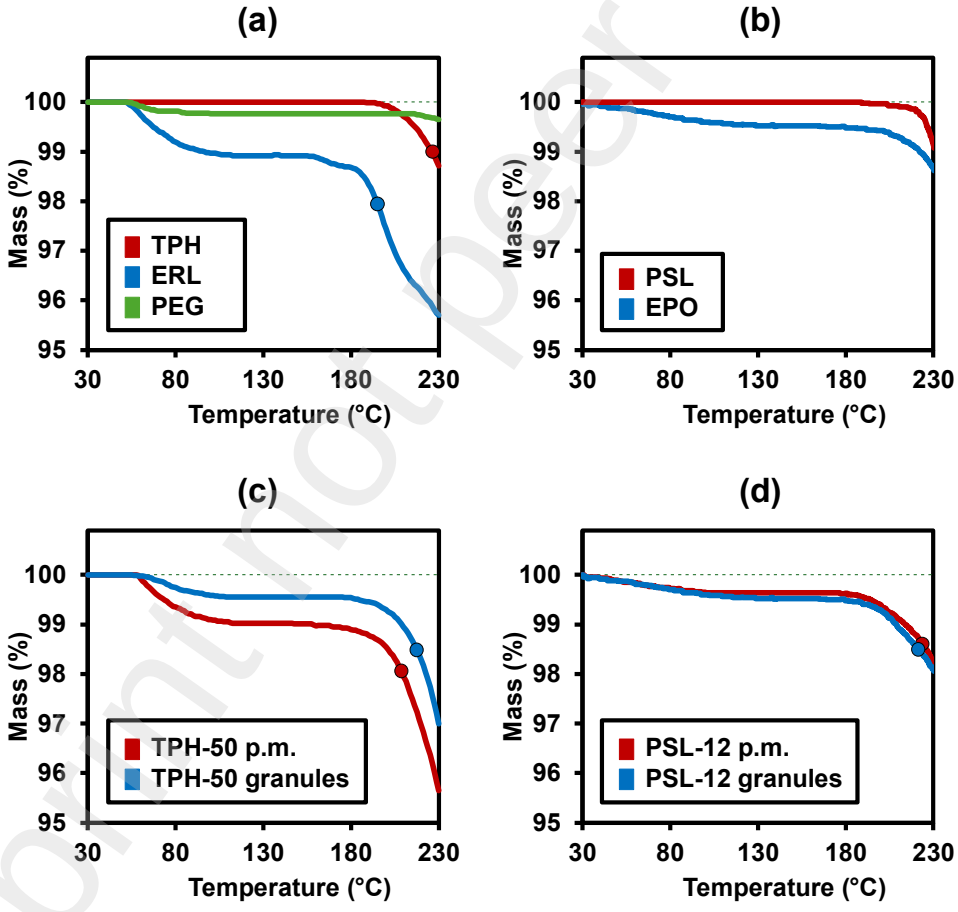

Figure 2. Results of TGA measurements regarding formulation single components, physical mixtures (p.m.) and granules: (**a**) TPH-50 single formulation components; (**b**) PSL-12 single formulation components; (**c**) TPH-50 formulation intermediates; (**d**) PSL-12 formulation intermediates.

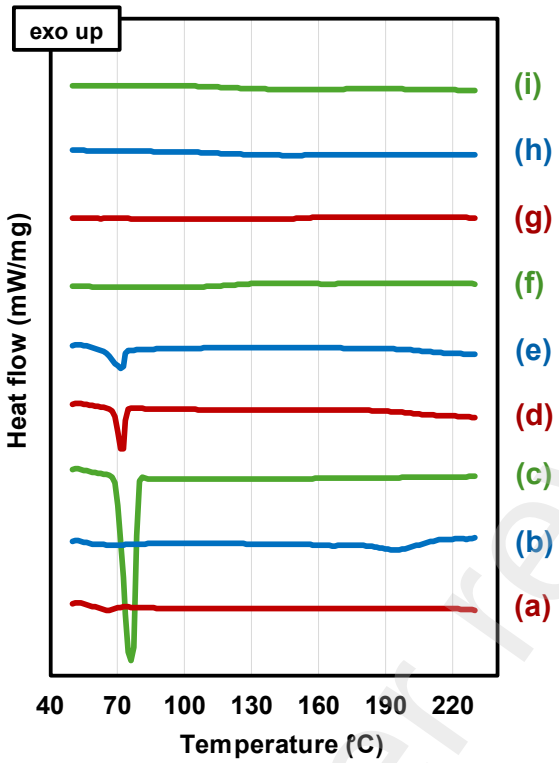

Figure 3. DSC thermograms regarding formulation single components, physical mixtures (p.m.) and granules: (**a**) TPH; (**b**) ERL; (**c**) PEG; (**d**) TPH-50 p.m.; (**e**) TPH-50 granules; (**f**) PSL; (**g**) EPO; (**h**) PSL-12 p.m.; (**i**) PSL-12 granules.

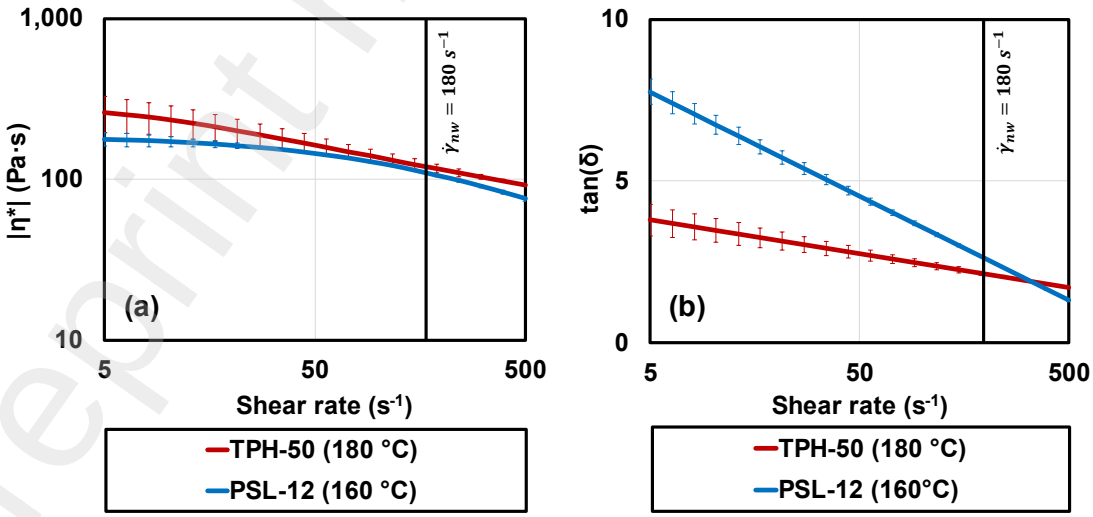

Figure 4. Rheology results of post-HME granules samples of formulations TPH-50 and PSL-12 at apparent printing temperatures: (**a**) shear rate dependent complex viscosities |η*|; (**b**) shear rate dependent loss factors tan(δ).

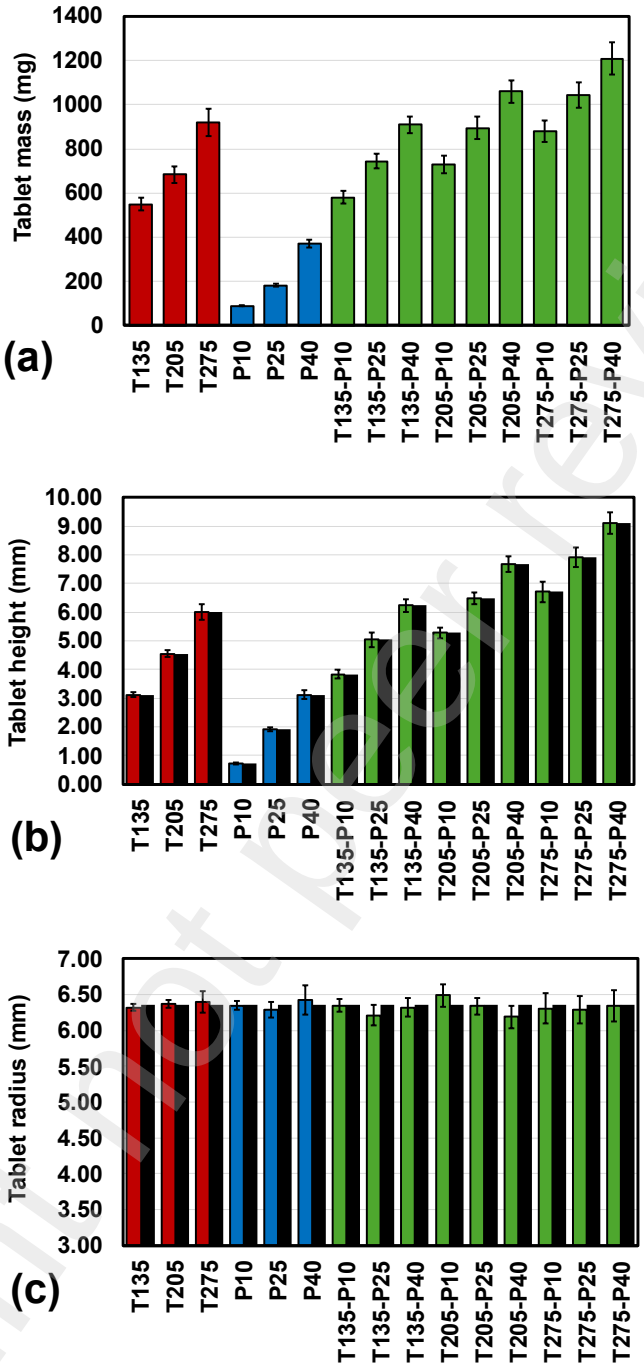

Figure 5. Comparison of physical characterization parameters for selected bi- and mono-tablets with absolute and relative standard deviations within the batch: (**a**) tablet masses m, (**b**) total tablet heights h, (**c**) tablet radius. Specific RSDs are depicted as grouped orange-colored lines, while solid black columns represent respective target values.

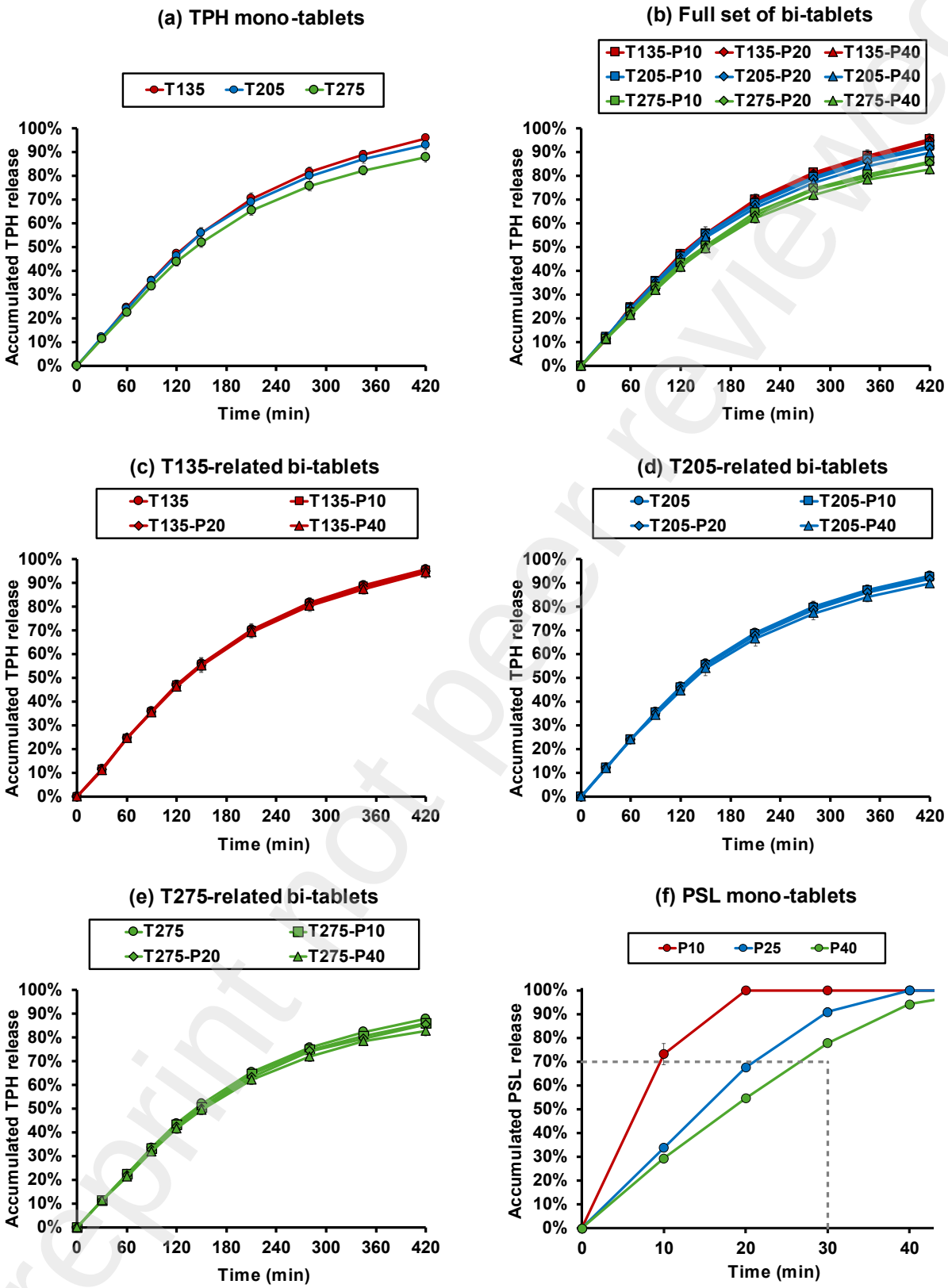

Figure 6. Comparison of in vitro dissolution results of selected mono- and bi-tablet designs: (**a**) TPH mono-tablets, (**b**) full DoE set of bi-tablets, (**c**) T135-related mono- and bi-tablets, (**d**) T205-related mono- and bi-tablets, (**e**) T275-related mono- and bi-tablets, (**f**) PSL mono-tablets.

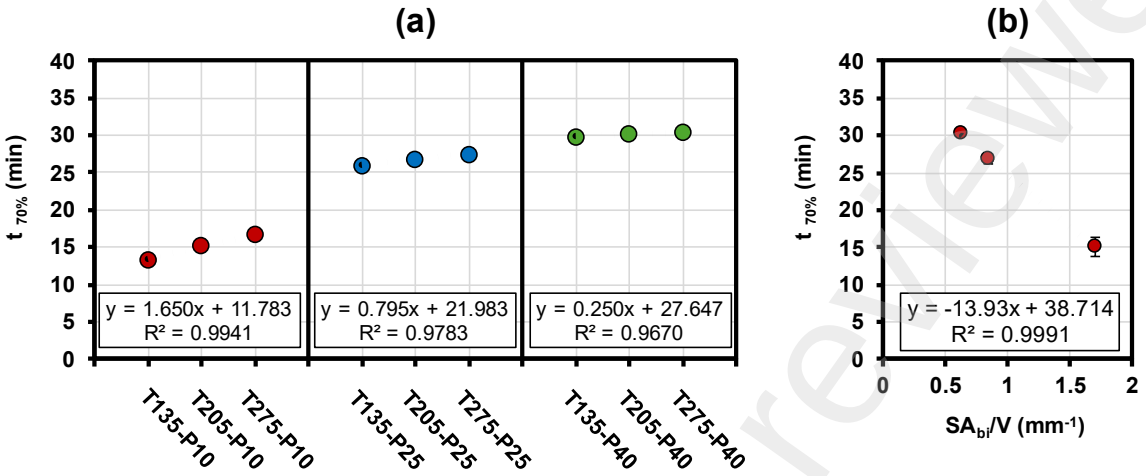

Figure 7. Comparison of in-vitro dissolution parameter $t_{70\%}$ results of 3DP PSL bi-tablets fitted with linear regression: (**a**) grouped bi-tablets according to PSL dose strengths, (**b**) mean $t_{70\%}$s versus according SA_{bi}/V ratios.

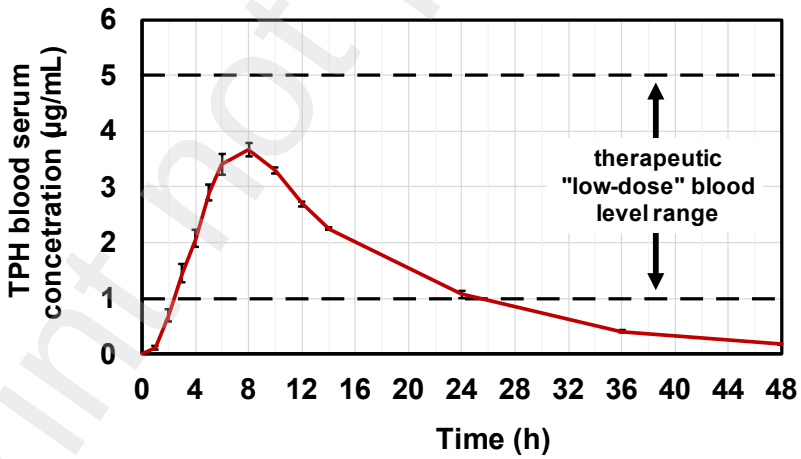

Figure 8. Averaged modelled TPH blood serum levels after single administration of our bi-tablets for a selected patient group dosed 3.2 mg TPH/kg patient BW.